DELETION OF BRANCHED-CHAIN AMINO ACID CATABOLIC GENE PPM1K INDUCES ADIPOSE TISSUE DYSFUNCTION IN MOUSE MODEL

SHAMA MANSOORI

PhD

The Hong Kong Polytechnic University

2024

The Hong Kong Polytechnic University

Department of Health Technology and Informatics

Deletion of Branched-chain Amino Acid Catabolic Gene PPM1K Induces Adipose Tissue Dysfunction in Mouse Model

Shama Mansoori

A thesis submitted in partial fulfilment of the requirements for the degree of Doctor of Philosophy

August 2023

CERTIFICATE OF ORIGINALITY

I hereby declare that this thesis is my own work and that, to the best of my knowledge and belief, it reproduces no material previously published or written, nor material that has been accepted for the award of any other degree or diploma, except where due acknowledgment has been made in the text.

_____

SHAMA MANSOORI
Date- 31st August 2023

DEDICATION

Dedicated to almighty Allah, my beloved family, and my friend Murtaza.

Abstract

Obesity and type 2 diabetes (T2D) are featured by dysfunctional adipose tissue and increased circulatory branched-chain amino acids (BCAAs). White and brown adipose tissues (WAT and BAT) play a crucial role in maintaining systemic BCAA homeostasis. On the other hand, adipocytes utilise BCAAs for various metabolic functions such as lipogenesis and energy expenditure. Interestingly, an altered expression of BCAA catabolic genes was reported in adipose tissue of *db/db* mice. However, the involvement of impaired BCAA pathway in the development of adipose tissue dysfunction within the context of metabolic disorders remains elusive. Thus, we hypothesize that aberrant BCAA metabolism contributes to adipose tissue dysfunctions, thereby inducing or exacerbating obesity/T2D. The current study is focused on delineating the role of Protein phosphatase 1K (PPM1K), a key regulatory enzyme that controls BCAA catabolism, in the regulation of adipose tissue function. To investigate the hypothesis, two mouse models of global PPM1K knockout (KO) and adipocyte-specific PPM1K knockout (A-KO) were employed.

As anticipated, the defective BCAA catabolism is observed in global KO mice evidenced by higher circulatory/tissue levels of BCAA and its downstream metabolites. PPM1K deletion had a modest impact on energy balance, glucose tolerance, and insulin sensitivity, while significantly increasing adipose tissue fibrosis and inflammation. Supporting this observation, a negative correlation between PPM1K and pro-fibrotic genes was found in datasets from Gene expression omnibus (GEO) database in obese human subjects. Subsequent analysis of WAT fractions revealed an upregulated fibrotic response in the stromal vascular fraction (SVF), while no changes were observed in the adipocyte fraction of PPM1K KO mice compared to wild-type controls. Fibrosis in WAT was accompanied by the induction of *Hif-1α* coinciding with pro-fibrotic and

inflammatory gene markers. This observation suggests that activation of HIF-1α pathway may contribute to the induction of fibrosis, although it warrants further investigation.

In the A-KO model, metabolic characterisation revealed significant impairments in glucose, lipid, and energy metabolism. Interestingly, deficiency of adipocyte PPM1K increased the circulatory BCKA levels. These defects were accompanied by fibrosis in different fat depots including WAT and BAT and increased M1 macrophage infiltration in WAT. Additionally, heightened cellular senescence was observed in adipose tissue of A-KO mice, highlighting the role of PPM1K in aging alongside its conventional involvement in BCAA catabolism. Deletion of adipocyte PPM1K also led to impaired TCA cycle and mitochondrial respiration in eWAT, indicating cellular respiration defects. RNA sequencing data implicated the Rho GTPase pathway as a potential contributor to adipose tissue dysfunction, requiring further investigation for a detailed understanding of the mechanism. Furthermore, adipocyte PPM1K deletion altered the liver function leading to increased fibrosis, inflammation, and steatosis in addition to inducing adipose tissue dysfunction.

Overall, this study investigated the unprecedented role of PPM1K in regulation of adipose tissue functions.

.

Conferences/symposiums and publications:

1) Shama, Dr. LIN Huige, and Dr. Kenneth CHENG K.Y. Defective BCAA metabolism impairs Glucose Stimulated Insulin Secretion (GSIS) in pancreatic β cells by interrupting glucose metabolism. Advances in Diabetes and Metabolism organised by Hong Kong Society of Endocrinology, Metabolism, and Reproduction Limited (HKSEMR), HK.
2) Shama, Dr. LIN Huige, and Dr. Kenneth CHENG K.Y. Defective BCAA catabolism induced by deletion of PPM1K causes adipose tissue fibrosis in a mouse model. 3rd ABCT Research post-graduate symposium in biology discipline, 2022
3) Shama, and Dr. Kenneth CHENG K.Y. Defective BCAA catabolism induced by deletion of PPM1K causes adipose tissue fibrosis in a mouse model. PolyU Research Student Conference (PRSC)-2023
4) Shama Mansoori, Dr. LIN Huige, and Dr. Kenneth CHENG K.Y. Deletion of BCAA catabolic gene PPM1K causes adipose tissue dysfunction in mice. Australasian Diabetes Congress 2023, August 2023.
5) The interplay between muscle and liver in the regulation of glucolipid metabolism. Cheng Chen, Liping Xie, Mingliang Zhang, **Shama,** Kenneth King-yip Cheng* and Weiping Jia* (Journal of Molecular Cell Biology, mjad073).
6) Branched-chain amino acid metabolism: pathophysiological mechanism and therapeutic intervention in metabolic diseases. **Shama Mansoori,** Melody Yuen-man Ho, Kelvin Kwun-wang Ng, Kenneth King-yip Cheng* (under review in OBESITY reviews).
7) Deletion of BCAA catabolic gene PPM1K induces adipose tissue dysfunction. **Shama Mansoori,** Kenneth King-yip Cheng* (manuscript under preparation).

Acknowledgments:

Firstly, I would like to express my heartfelt gratitude to my chief supervisor Dr. Kenneth K.Y. Cheng, who gave me the opportunity to explore research questions at a doctoral level, guided me patiently and provided me with timely feedback throughout my project. All the knowledge I gained from him in the past three years are priceless treasure. I also acknowledge my co-supervisor Dr. CM Wong for providing me an opportunity to commence my study, and my senior lab colleague Dr Huige Lin, and Dr. Kelvin Wu for providing me valuable suggestions and help.

I would like to further extend my gratitude to all faculty members, general, and technical staff (especially Dr. Raymond) of the Department of Health Technology and Informatics for helping me with various processes throughout the study period, and University Research Facility in Life Sciences staff (Dr. Ryan Chow, Dr. So Pui-kin, and Dr. Alan Leung) for their support to perform the flow cytometry, mass spectrometry, and metabolic cage experiments respectively. I am thankful to the Centralised Animal Facilities (CAF) staff for their timely support and for taking good care of experimental mouse models.

I will take this chance to wholeheartedly acknowledge the Research Grant Council, for providing me generous support through HKPFS, and the travel grants for attending the international conference, and the Department of Health Technology and Informatics, Graduate school, and PolyU for embracing me an opportunity to pursue PhD study. Further, my wholehearted thanks to the Croucher Foundation for their munificent support starting from application to attending the most prestigious 72nd Lindau Nobel Laureate meeting, in Germany during my PhD study.

Second, a big thanks to all my colleagues (some have already moved to other places) K.K, Chen Xi, Becca, Joy, Joseph, Thashma, Moinul, Tongxi, Una, Yumei, Melody, Abebe, and Chala for all your support and help in the PhD project and life. A special thanks to Thashma Ganapathy for keeping me grounded, motivated, and for supporting me unconditionally at my most vulnerable moments, and Moinul Hoque for helping me to perform different bioinformatics analyses, and for adding an extra layer of knowledge.

I am extremely grateful to my friends- Murtaza, Ashish, Deepa, Pallavi, Arka, Gufran, Harman, Alex, Ayesha, Riham, and Aamir for encouraging me through my study and for supporting me emotionally and to my 12^{th}-grade mentors Chintamani Sir and Kalpana Seth Ma'am for trusting my potential to pursue higher education. Thank you Murtaza and Ashish for your unfailing support, keeping me motivated and patience through all ups and downs. A heartfelt thanks to Arka, for helping me starting from my application for HKPFS, settling down in HK, and for countless support in the fragile period during the PhD journey.

Last but not least, incalculable gratitude to my parents (Mehmooda Khatoon, and Riyazuddin) for all the sacrifices they made for me, their moral support, hard work, and despite all odds allowing me to pursue higher education, and my sisters Rizwana and Neha, and brother Rihan and Rizwan for their love and unwavering support in all ups and downs, and keeping me motivated. I am deeply grateful to almighty Allah for his abundant grace, for everything and every situation.

Table of content

List of figures:

List of abbreviations:

ATM	Ataxia-telangiectasia mutated (ATM)
ATMs	Adipose tissue macrophages
ATR	Ataxia telangiectasia and Rad3-related protein
BAT	Brown adipose tissue
BCAAs	Branched-chain amino acids
BCKAs	Branched-chain keto acids
BCKDH	Alpha-keto acid dehydrogenase
BMP	Bone morphogenetic proteins
CEBP	CCAAT/enhancer-binding proteins
CVD	Cardiovascular disease
DAPI	4, 6- diamidino-2-phenylindole
ECM	Extracellular matrix
eWAT	Epididymal white adipose tissue
FFA	Free fatty acid
GDF	Growth differentiation factor
G-3-P	Glycerol-3-phosphate
GTT	Glucose tolerance test
HIBCH	3-Hydroxyisobutyryl-CoA Hydrolase
HIF-1A	Hypoxia-inducible factor 1A
HFHC	High fat high cholesterol
HSL	Hormone-sensitive lipase
IF	Immunofluorescence
IR	Insulin resistance
IL	Interleukin
ITT	Insulin tolerance test
KO	Knockout

LPL	Lipoprotein lipase
MCP1	Monocyte chemoattractant protein-1
mmBCFA	Monomethyl branched-chain fatty acid
MHL	Metabolically healthy lean
MIF1	Macrophage inflammation factor 1
MHO	Metabolically healthy obese
MUO	Metabolically unhealthy obese
NADH	Nicotinamide adenine dinucleotide
NAFLD	Non-alcoholic fatty liver disease
NASH	Non-alcoholic steatohepatitis
PPAR	Peroxisome proliferator-activated receptor
PPM1K	Protein phosphatase 1K (mitochondrial)
qPCR	Quantitative polymerase chain reaction
SEM	Standard error of the mean
SNP	Single nucleotide polymorphism
siRNA	Small interfering RNA
STC	Standard chow diet
SVF	Stromal vascular fraction
sWAT	Subcutaneous white adipose tissue
TAG	Triacyl glycerides
TCA	Tricarboxylic acid
T2D	Type 2 diabetes
TG	Triglyceride
TG-VLDL	Triglycerides very low-density protein
UCPI	Uncoupling protein 1
WAT	White adipose tissue
WHO	World health organization

WT	Wild type

List of tables:

Chapter 1: Introduction

1.1 Obesity/ type 2 diabetes (T2D): An expanding pandemic

World Health Organization (WHO) defines obesity as an "abnormal or excessive fat accumulation that may impair health. As per WHO, a body mass index (BMI) greater than or equal to 30, is considered obese which may vary among different ethnic groups[1]. Globally more than one billion people are suffering from obesity and their number is expanding at an alarming rate. Obesity is linked to an elevated risk of developing diabetes, chronic kidney disease, cardiovascular diseases (CVD), cancer, and hypertension (Figure 1.1) [2]. Recently, during the COVID outbreak obesity has emerged as one of the risk factors for developing severe COVID-19 infection [3]. In Hong Kong (HK), diabetes is the leading cause of morbidity and mortality (10th common cause of death) as per data from the centre for health protection (CHP), HK.

The way white adipose tissue (WAT) expands and remodels has a direct impact on the risk of developing metabolic syndrome in obese people and the importance of healthy fat tissue is revealed by transgenic animal models expressing glucose transporter (GLUT) 4, and adiponectin (AdipoQ) [4].

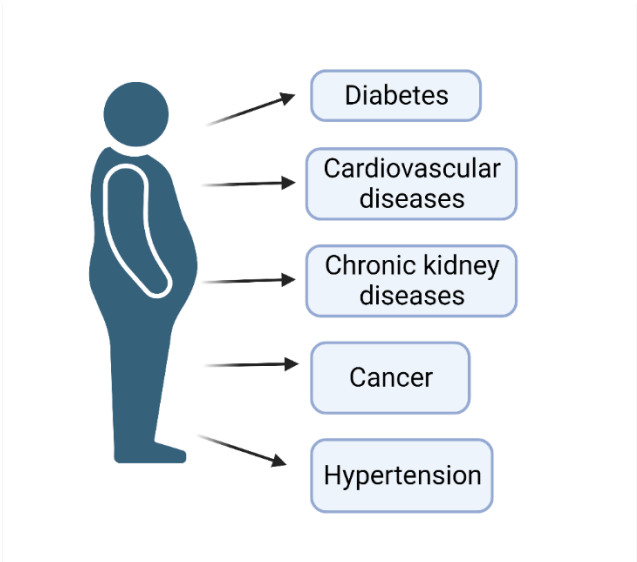

Figure 1.1: Obesity is linked to a high risk of developing various metabolic diseases and cancer. Obesity is associated with a higher incidence of several diseases including diabetes, CVD, chronic kidney diseases, hypertension, and cancer.

1.2 Physiological functions of Adipose tissue:

Adipose tissue serves as an important regulator of energy homeostasis and acts as a caloric reservoir. Adipose tissue performs a plethora of functions including nutrient transport, appetite and energy balance, lipid metabolism, and glucose homeostasis (Figure 1.2). The adipose tissue is dispersed throughout the body and categorised into WAT and brown adipose tissue (BAT). These two tissues differ in their morphology and functional characteristics. WAT occupies the largest volume in fat depots and is vital for maintaining energy reservoir, endocrine functions, and insulin signaling. On the other hand, BAT is crucial in non-shivering thermogenesis and thus important for maintaining core body temperature [5].

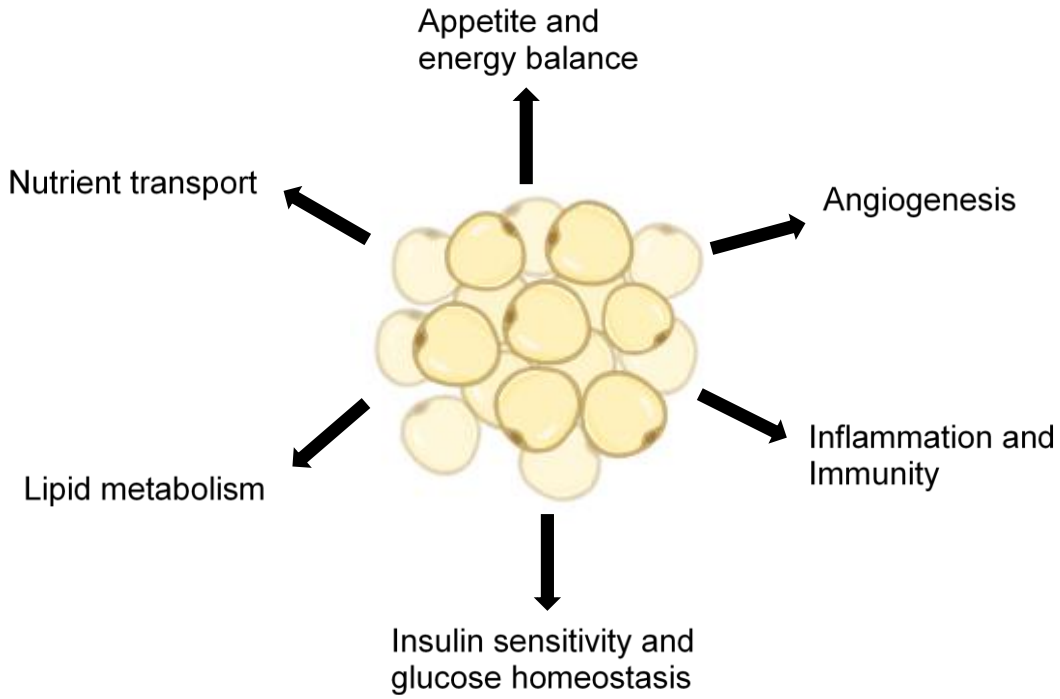

Figure 1.2: A diverse range of functions performed by adipose tissue. Adipose tissue performs a plethora of functions ranging from glucose and lipid metabolism to energy homeostasis and immunity.

1.2.1 Adipose tissue acts as an energy reservoir

Adipose tissue has the capability to expand (remodel) to store surplus energy in the form of triglycerides (TG). WAT consists of two key depots including subcutaneous WAT (sWAT) and epididymal WAT (eWAT) [6]. The adipose tissue stores surplus resources in the form of lipids under nutrient-excess conditions (Lipogenesis), whereas delivers nutrients to peripheral tissues through lipolysis under nutrient-deficient conditions (4). Under the fed state, the lipids storage in adipocytes occurs via two processes (as described in Figure 1.3). During the first process, the free fatty acids (FFA) are generated from the chylomicron or very low-density protein (VLDL)-TG in circulation by the enzyme lipoprotein lipase (LPL) [7]. These FFAs enter into adipocytes through the fatty acid transporter CD36. The glucose up taken by adipocytes can be converted into acetyl Co-A and glycerol-3-phosphate (G-3-P), and G-3-P can be utilised as a backbone for the esterification of fatty acids. It leads to the generation of TG, which can be added to the TG reserve [5]. In the second process, the acetyl-CoA generated from glucose is utilised for fatty acid synthesis (*de novo* lipogenesis) and combined with glycerol to generate TG [8]. On the other hand, during fasting, adipocytes deliver nutrients to other tissues such as muscle and liver tissue via mobilising its TG pool through lipolysis. Thus, the balance between lipogenesis and lipolysis is crucial to maintain whole-energy homeostasis.

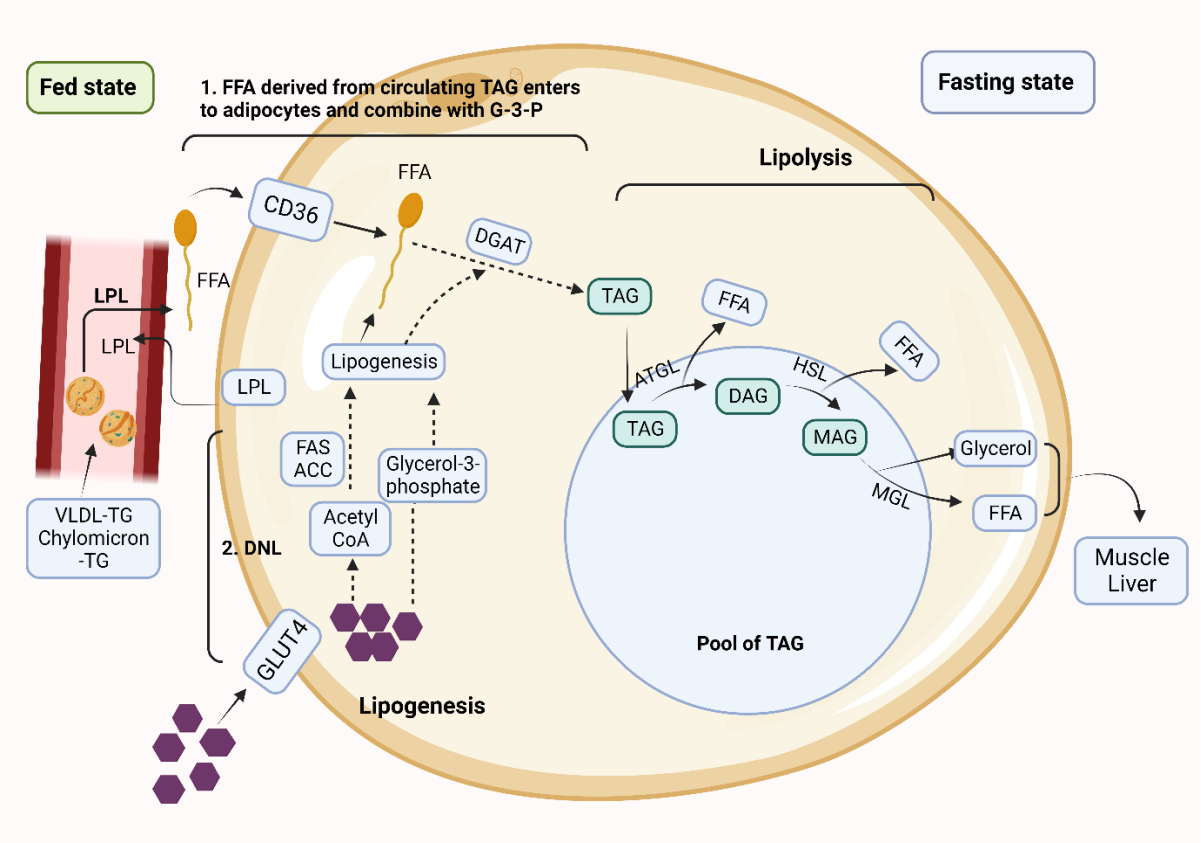

Figure 1.3: Adipose tissue in maintaining whole-body energy balance. In adipocytes, the balance between lipolysis and lipogenesis process is crucial for the maintenance of energy homeostasis. The lipogenesis occurs through two different processes (labeled as 1 and 2 in the figure). Adipocytes, on the other hand, supply nutrients to other tissues including muscle and liver tissue during fasting by mobilizing their TG or triacyl glycerides (TAG) pool through lipolysis.

1.2.2 Adipose tissue functions as an endocrine organ

Adipose tissue not only acts as a passive energy reservoir but also secretes an array of bioactive molecules designated as "adipokines" such as hormones, cytokines, and peptides [9]. In adipose tissue, adipokines are secreted mainly by adipocytes or by other cell types such as adipose tissue macrophage, endothelial cells, fibroblast, and precursor cells [10]. Adipokines can mediate their effect through autocrine, endocrine, or paracrine signaling and establish a cross-talk between adipose tissue and other organs. They play a crucial role in regulating food intake

and appetite, insulin release and sensitivity, immune response, and energy homeostasis [11,12]. Furthermore, adipokines also regulate the process of adipogenesis and adipocyte metabolism. Based on their expression and ability to induce inflammation, adipokines can be categorized into pro-inflammatory and anti-inflammatory cytokines (Figure 1.4). Most of the pro-inflammatory cytokines are increased in obese conditions including leptin, interleukin (IL) -6, IL-18, tumor necrosis factor (TNF), CXC-chemokine ligand 5 (CXCL5), retinol-binding protein 4 (RBP4), lipocalin 2, and CC-chemokine ligand 2 (CCL2). On the other hand, anti-inflammatory adipokines including secreted frizzled-related protein 5 (SFRP5) and adiponectin levels decrease in the obese state [13].

Leptin was the first adipokine discovered in 1994 by Friedman *et al;* and is the most extensively studied adipokine. Leptin is secreted from the adipose tissue in response to food intake and suppresses appetite by modulating neural circuits in the hypothalamus. Circulatory leptin directly correlates with the size of adipose tissue. Both the expression and circulatory levels of leptin are subjected to regulation by nutritional status. The level of plasma leptin decreases during fasting whereas feeding or obese condition leads to an increase in leptin [14]. Resistin is secreted by adipocytes in rodents and its level increases during obesity. It induces insulin resistance and inflammation through the secretion of IL-6 and TNF from macrophages [13]. TNF, IL6, IL-18, and CCL2 levels increased in obese state and are well known for inducing adipose tissue inflammation [13].

Adiponectin is secreted by adipocytes and functions as a regulator of lipid metabolism, glucose homeostasis, and insulin sensitivity and also known for its anti-inflammatory, and anti-fibrotic effect [15]. Adiponectin supports healthy adipose tissue expansion and rescues ectopic lipid deposition by adipocyte lipid storage in rodent models [16,17]. The genetic variation

of the adiponectin gene is reported to be associated with an elevated risk of developing T2D in the Japanese population [18]. SFRP5 is an anti-inflammatory adipokine secreted by adipocytes and suppresses pro-inflammatory through canonical and non-canonical WNT signaling [19].

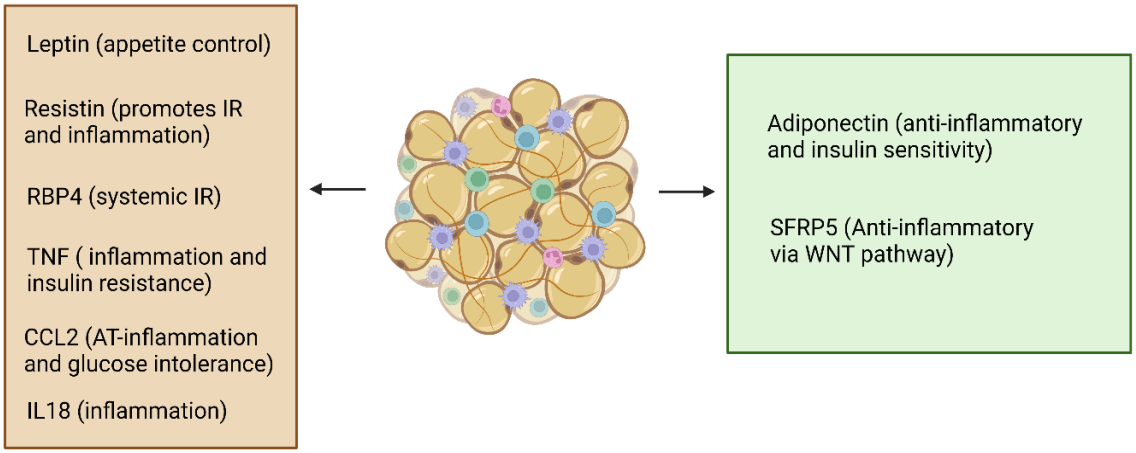

Figure 1.4: Function of adipose tissue as an endocrine organ. Adipose tissue serves as an endocrine organ, producing and secreting a variety of hormones, known as adipokines. These adipokines can be categorised into pro-inflammatory and anti-inflammatory based on their ability to induce inflammatory status. The pro-inflammatory cytokines secreted by adipose tissue include leptin, resistin, TNF, CCL2, and IL8, and they are known to induce inflammation and systemic insulin resistance. Conversely, adiponectin and SFRP5 are examples of anti-inflammatory adipokines that have been shown to enhance insulin sensitivity. IR: insulin resistance, AT: adipose tissue, RBP4: Retinol binding protein 4.

1.2.3 Adipose tissue as a temperature regulator

BAT is vital for the process of thermal homeostasis (non-shivering) and aids in maintaining the core body temperature. Unlike WAT, BAT contains multilocular lipid droplets, a central nucleus, copious mitochondria, and uncoupling protein 1 (UCP1) expression [20]. Under cold conditions, the UCP1 expression in BAT allows the uncoupling of oxidative phosphorylation and ATP production to release energy in the form of heat. Sympathetic nerves, which are enriched in BAT, directly regulate the process of thermogenesis. In brief, under cold

conditions, the release of norepinephrine from the sympathetic nerve terminal binds to β-adrenergic receptors and subsequently activates adenylate cyclase and hormone-sensitive lipase (HSL). The HSL-mediated hydrolysis of intracellular TG releases FFA and activates UCP1. This allows the release of chemical energy in the form of heat. Additionally, adrenergic signaling also stimulates the peroxisome proliferator-activated receptor coactivator 1 (PGC-1) expression, which in turn induces UCP1 and mitochondrial gene expression [21].

1.3 Different cell types in adipose tissue

Upon collagenase digestion, adipose tissue yields two fractions including a floating upper layer of mature adipocytes and pellet as stromal vascular fraction (SVF) (Figure 1.5). SVF mainly contains preadipocytes, fibroblasts, and endothelial cells from the vasculature, progenitor cells, and immune cells, participating in a cross-talk with adipocytes[22]. Endothelial cells account for about 30% of SVF, and fibroblasts may account for up to 50%. CD34 is a marker for endothelial cells.

Mesenchymal stem cells (MSCs) give rise to an early precursor of adipocytes and under appropriate stimulatory conditions they differentiate into mature adipocytes. The transition from preadipocytes to adipocytes involves distinct stages, including growth arrest, clonal expansion, early differentiation, and terminal differentiation [23]. The different phases of adipocyte differentiation are controlled by transcription factors such as peroxisome proliferator-activated receptors (PPARγ) and members of the CCAAT-enhancer binding protein (CEBP) family [24]. PPARγ plays a vital role in adipogenesis since it is required for adipocyte differentiation and the maintenance of adipocytes in their terminal differentiated state.

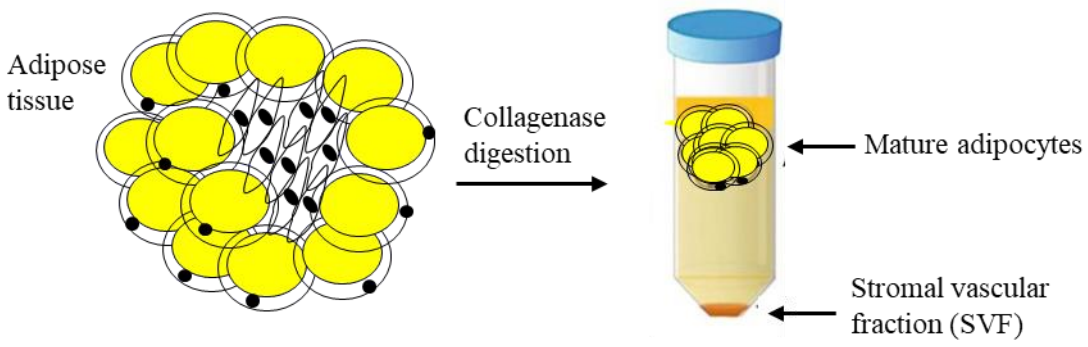

Figure 1.5: Fractionation of adipose tissue into stromal vascular fraction and mature adipocytes. Upon collagenase digestion, the adipose tissue gives rise to two different components such as the upper layer of floating mature adipocytes and SVF at the bottom (in the form of pellet) following centrifugation.

In a pivotal research Berry *et al;* showed that adipogenic progenitor cells (APCs) are generated from the Lin lineage and express the array of surface markers including Cd34+, Cd29+, Cd24+, Sca1+, and these markers can be utilised for the enrichment of the adipogenic population [25]. Single-cell RNA sequencing (scRNAseq) analysis performed on platelet-derived growth factor receptor (PDGFR) β+ cells within the stromal vascular fraction (SVF) derived from eWAT (of mice) revealed the presence of two distinct cell populations. The first population was identified as PDGFRβ+/LY6C-/CD9-, indicating highly adipogenic APCs, while the second population expressed LY6C (LY6C+/PDGFRβ+), which were referred to as Fibro-inflammatory progenitors (FIPs) due to their pro-fibrogenic/pro-inflammatory phenotype and lack of adipogenic potential [26].

1.4 Overview of BCAA catabolism

BCAAs, leucine, isoleucine, and valine are three out of nine essential amino acids. BCAAs account for about 20% of total protein intake in the human diet [27,28]. Unlike other amino acid oxidation, which occurs largely in the liver, BCAA absorption and oxidation occur in a variety

of tissues due to hepatocytes' low transaminase (BCAT) activity [29]. However, because BCAT is present in non-hepatocytes of the liver, some transamination may occur in the liver [30].

Adipose tissues, liver, skeletal muscle, kidney, pancreas, and heart are the major sites for BCAA metabolism [31]. Once within the cell, BCAAs can serve different purposes such as mitochondrial oxidation, protein synthesis, and stocking for the amino acid pool [28]. BCAAs can also act as nitrogen donors, transferring nitrogen from amino acid oxidation (muscle) to the liver for the synthesis of urea as alanine and glutamine [32]. Furthermore, they serve as an important nitrogen donor for the synthesis of neurotransmitters such as amino butyric acid (GABA) and glutamate in the brain [33]. BCAAs can also be used as a sterol and glucose biosynthetic precursor.

As per the *in vivo* isotope tracing experiment, skeletal muscle largely contributes to whole-body BCAA oxidation whereas skeletal muscle, the liver, and the pancreas contribute to the disposal of BCAAs for protein synthesis [31]. The reversible transamination of BCAA into their corresponding branched-chain keto acids (BCKAs) commences BCAA degradation and is catalyzed by the mitochondrial enzyme BCAT. Furthermore, BCKA undergoes oxidative decarboxylation and is catalyzed by an enzyme complex alpha-keto acid dehydrogenase (BCKDH) and leads to the formation of acyl-CoA derivatives and nicotinamide adenine dinucleotide (NADH) [34]. The acyl-CoA derivatives go through several metabolic events to generate acetyl-CoA and succinyl-CoA, which then enter the tricarboxylic acid (TCA) cycle (Figure 1.6) [31,35]. Acetyl-CoA and succinyl-CoA (end products) can be utilised as substrates for anaplerotic processes, while acetyl CoA can also be used as a substrate for lipogenesis.

The rate-limiting enzyme BCKDH is comprised of three subunits: E1, E2, and E3 [36]. BCKDH activity is regulated by covalent modification, namely phosphorylation and dephosphorylation

at serine 293 (Ser^{293}) on the E1 subunit [37]. BCKDH is positively controlled by the mitochondrial protein phosphatase 1K (PPM1K) via dephosphorylation at Ser^{293} on the E1 subunit [37] whereas inactivation of BCKDH complex is mediated by branched-chain ketoacid dehydrogenase kinase (BCKDK) by phosphorylating it at the same site [38]. The nutritional status of cells plays an important role in post-translational regulation by protein BCKDK and PPM1K [37]. Aside from post-translational modification, the activity of the BCKDH complex is influenced by transcription factors CEBP and PPAR family [28].

BCAAs and their metabolites, participate in crosstalk with other nutrients and metabolic pathways. Valine and its metabolite 3-hydroxybutyrate (3-HIB), increases endothelial FFA transport and their oxidation in skeletal muscles of MCK-alpha mice model and creates lipotoxicity [39]. ATP citrate lyase (ACL) stimulates lipogenesis in hepatocytes via activation of fatty acid synthase. The enzyme ACL is regulated by BCAA catabolic genes PPM1K and BCKDK in obese and insulin-resistant states. Consequently, it connects lipogenesis to BCAA catabolism [40]**.** BCAA is shown to suppress glucose oxidation in heart tissue by blocking the pyruvate dehydrogenase (PDH) complex in PPM1K KO mice, thus linking BCAA to glucose metabolism [41].

Besides, BCAA and its metabolites are known to activate molecular pathways such as mammalian target of rapamycin complex 1 (mTORC1), general control nonderepressible (GCN) 2, and AMP-activated protein kinase (AMPK) [32,42–45].

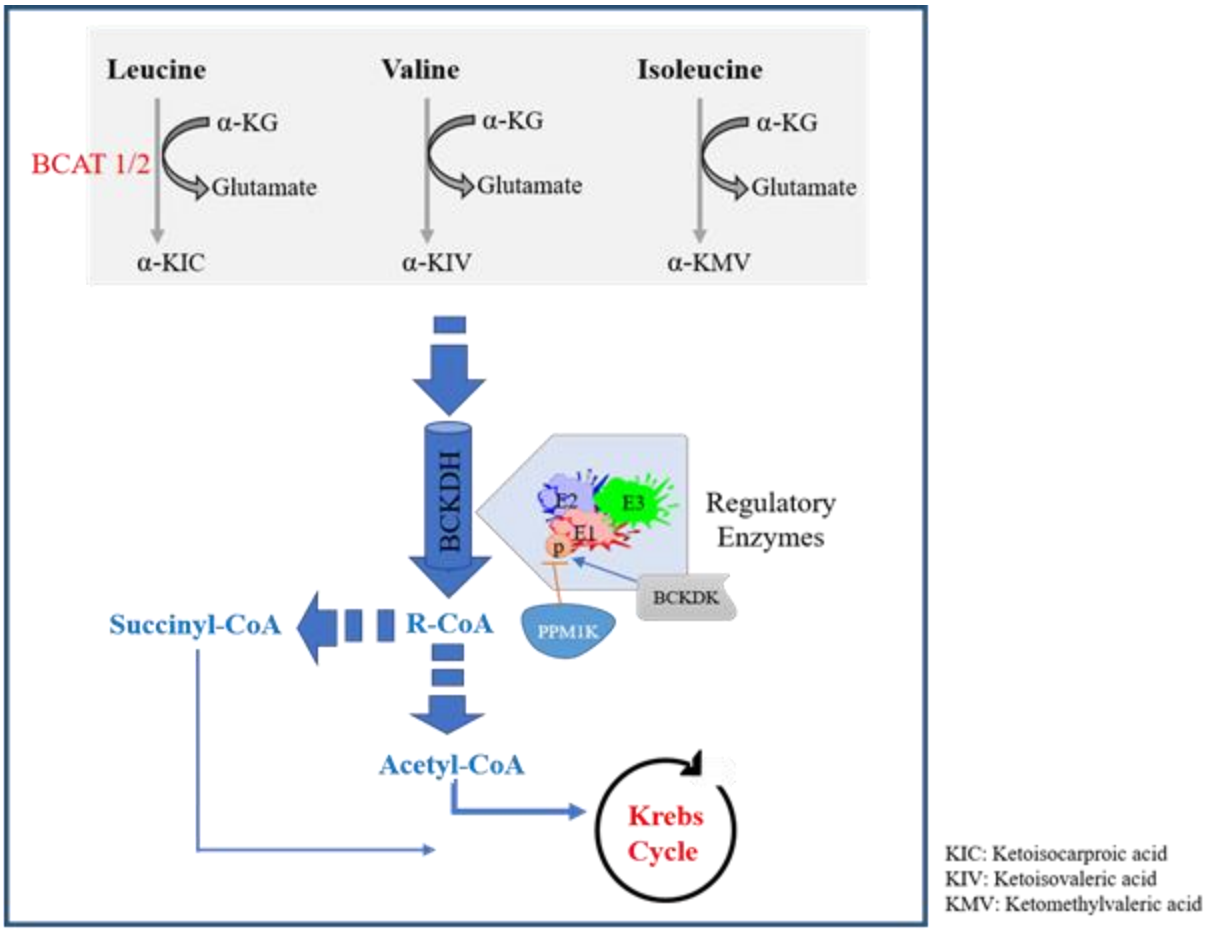

Figure 1.6: Overview of BCAA catabolic pathway. BCAAs are catabolised by a series of biochemical reactions. It initiates with the transamination of BCAAs to BCKAs by transaminase enzyme (BCAT). Further, BCKAs are converted to acyl-CoA in an irreversible reaction catalysed by multienzyme complex BCKDH (rate-limiting step). This enzyme is subjected to regulation by PPM1K and BCKDK. The generated acyl-CoA can either form acetyl CoA or succinyl CoA, which can eventually enter into the TCA cycle.

1.5 Association of BCAAs and its downstream metabolites with metabolic diseases

BCAAs can be used as a risk biomarker for a number of disorders, such as obesity, T2D [42,46], cardiovascular disease (CVD) [47,48], and several kinds of cancer. The higher level of circulating BCAA in obese/diabetic people has been observed for decades [42,49,50]. A positive association between levels of plasma BCAAs and obesity/T2D has been established in human subjects

and different obese/diabetic rodent models, like diet-induced obesity (DIO) rats, ob/ob mice, and Zucker rats [51–53]. In addition, genetic variants of BCAA catabolic genes affect circulatory BCAA levels and are associated with metabolic disorders [54,55]. PPM1K rs1440581 allele C is linked with higher serum BCAA levels and an increased risk of developing non-alcoholic fatty liver disease (NAFLD) [55,56]. Of note, the presence of both BCAT2 and BCKDH SNPs is linked to metabolic changes such as higher body weight and BMI, hyperglycemia, hypertension, and higher circulatory amino acids such as proline, methionine, and isoleucine [54].

In addition to BCAA, plasma BCKA levels have been linked to obesity/T2D and non-alcoholic steatohepatitis (NASH) [51,57,58]. More precisely, α-ketoisovalerate (KIV) and the ratio of BCKA/BCAA have shown a positive association with steatosis and NASH [57]. Steatosis grade was associated with a higher BCKA/BCAA ratio [57]. In a human cohort study (EPIC-Norfolk, United Kingdom) circulating 3-HIB levels have shown a positive association with the incidence of T2D and insulin resistance [59,60]. Increased levels of 3-HIB in skeletal muscle were detected under diabetic conditions in both mice (*db/db* animals) and human subjects [39,59]. The enzyme *3-Hydroxyisobutyryl-CoA Hydrolase* (HIBCH) catalyses the synthesis of 3-HIB. The hepatic *HIBCH* expression has shown a positive association with BMI, area of visceral fat, and NASH score and a negative association with serum adiponectin [61].

The involvement of higher BCAA levels in contributing to obesity/T2D was also supported by the studies using a BCAA-restricted diet. It has been reported that limiting the consumption of dietary BCAAs can lead to improvement in metabolic health including glycaemic control, body composition, and metabolic changes in adipose tissue in mouse model [62–64].

There are two proposed mechanisms of how BCAA is linked to T2D/obesity including persistent activation of mTORC1 and BCAA dysmetabolism [53]. The crosstalk between amino

acids and insulin is mediated through the mTOR signaling [65]. According to different theories, increased plasma leucine levels and insulin activate the mTORC1 and S6K1. The continuous activation of the mTORC1 and S6K1 can result in phosphorylation at the serine residue of insulin receptor substrate (1RS)-1 and IRS-2 [65]. This phosphorylation event might target the IRS-1 to the proteasomal degradation pathway and interfere with insulin signaling. A study by Zhou *et al;* (2019) has shown that similar to BCAA, BCKAs also have the potential to suppress insulin signaling and increase insulin-stimulated mTORC1 activity. Moreover, in the absence of BCAAs in culture media, BCKAs showed increased activity of mTORC1 and attenuated AKT phosphorylation [66]. The attenuated activity of AKT was abolished when treated with the mTORC1 inhibitor rapamycin, suggesting the mTORC1-dependent activity [66]. The second hypothetical mechanism is BCAA dysmetabolism which suggests that dysregulated BCAA metabolism could lead to the build-up of toxic BCAA downstream metabolites which can further contribute to β-cell mitochondrial dysfunction, β-cell apoptosis, and ultimately the progression towards T2D [53].

Recently, elevated circulatory BCAA levels have been observed in aged mice [67]. Using different model organisms (which include C. elegans, zebrafish, and mice), a study has identified the involvement of *Bcat1* in the regulation of physiological aging [68]. BCAA-restriction in progeroid Lamin A/C-deficient (Lmna−/−) mouse model, leads to improvement in lifespan and effects are dependent on the sex and age of the mice when dietary intervention is initiated [69]. Expression of *Bckdha, Bckdhb, Pcca, and Pccb* and protein levels of BCAT2, and BCKDHB involved in BCAA catabolism is reduced in aging adipose tissue in mouse model [67]. Thus, these findings suggest the role of BCAA catabolic machinery in aging.

1.6 BCAA metabolism in the physiology of adipose tissue

By serving as a caloric reservoir, adipose tissue acts as a crucial regulator of systemic energy homeostasis. The adipose tissue stores excess resources in neutral lipids form under surplus nutrient conditions, whereas it delivers nutrients to the peripheral through lipolysis under nutrient-deficient conditions [70–72]. The uptake of BCAAs into adipocytes is mediated through transporters *Slc1a, Slc3a2,* and *Slc7a5*. The direct transport of BCAA is facilitated through *Slc1a5* while a heterodimeric plasma membrane complex formed by *Slc3a2* and *Slc7a5* allows the exchange of internal glutamine and asparagine for external BCAA [73–76]. BCAAs are metabolized via a series of biochemical reactions in mitochondria to form acetyl-CoA and succinyl CoA (anaplerotic intermediates). The acyl Co-A derived from the BCAA catabolism can be used for the biosynthesis of monomethyl branched-chain fatty acids (mmBCFA) and this process is facilitated by carnitine acetyltransferase and fatty acid synthase [77].

Although the role of adipose tissue in glucose and lipid metabolism is well understood, its role in amino acid metabolism requires more exploration. There are several pieces of evidence from *in vitro* and *ex vivo* studies that indicate adipose tissue is capable of metabolizing a large amount of BCAA [78–80]. Further, adipose tissue is also reported to modulate the circulating BCAA levels [78]. It was observed that BCAAs are important for the differentiation of pre-adipocytes to mature adipocytes as the consumption of BCAAs increases during the differentiation process (Figure 1.7) [81]. Using a metabolic tracing experiment (using labeled BCAA), it was found that nitrogen derived from BCAAs contributes to the synthesis of amino acids in differentiated adipocytes [81]. Under the BCKDHA knockdown condition decrease in expression of adipogenic genes including *Pparg, Glut4, Plin4, Adipoq*, and *Lep,* and

attenuated lipid droplet formation was reported by *Green et al.* These findings give the impression about the role of BCAA catabolism during adipogenesis [81].

The process of thermogenesis takes place mainly in BAT and is mediated by UCP1 (also known as thermogenin) [82]. Thermogenesis can be induced by cold exposure and in response to adrenergic compounds. The main metabolic substrates utilized during thermogenesis are fatty acids and glucose [83]. However, recent findings by Yoneshiro *et al;* unprecedentedly reported the correlation between plasma BCAA and thermogenesis in BAT [84]. BAT in mice and humans actively consumes BCAA for thermogenesis and enhances systemic BCAA clearance when exposed to cold [84]. Further, inhibition of BCAA catabolism in BAT leads to reduced thermogenesis and BCAA clearance [84]. So, these finding highlights the potential of BCAA as a metabolic substrate for thermogenesis.

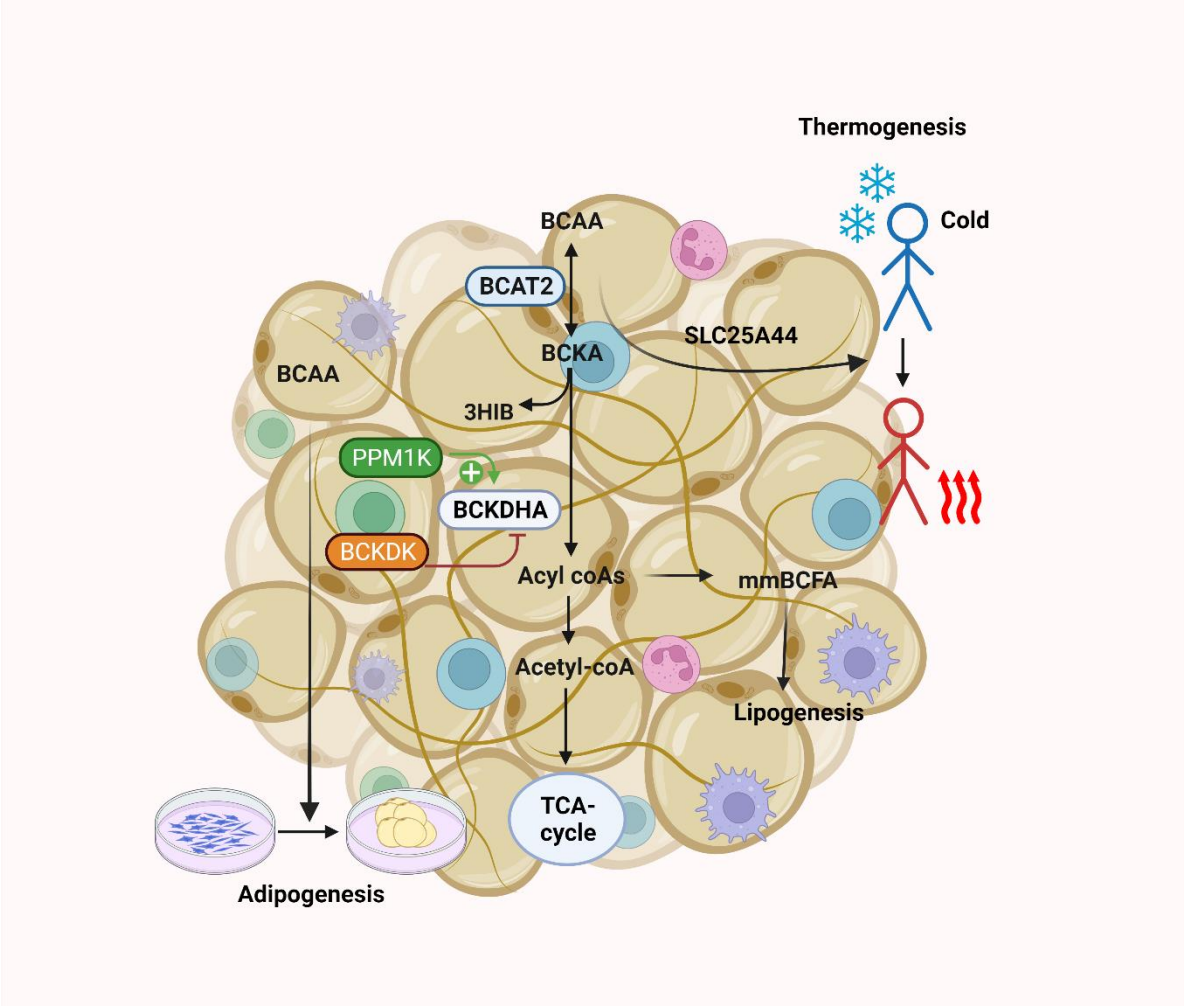

Figure 1.7: BCAA metabolism in maintaining adipose tissue physiological functions. BCAAs are utilised as substrates for adipogenesis, lipogenesis, and thermogenesis. The mmBCFA generated from the acyl CoA (derived from BCAA catabolism) is used for lipogenesis. In BAT, the BCAAs are utilized for thermogenesis under cold exposure. These BCAAs are transported via the newly characterized transporter SLC25A44 in BAT.

1.6.1 Factors regulating BCAA catabolism in adipose tissue

Adiponectin is secreted from adipose tissue and regulates lipid and glucose homeostasis [85,86]. From the shreds of evidence, a negative association has been found between obesity/T2D and adiponectin [85,87,88]. Lian *et al*; reported in diabetic adipose tissue the protein expression of PPM1K has reduced significantly while increasing BCKDK expression [89]. A decrease in

PPM1K expression can lead to a change in BCKDH activity. The positive effects of adiponectin on altered BCAA metabolism (induced by HFD) were reported in muscle tissue [90]. In adipose tissue, the activity of BCKDH is also rescued by adiponectin [89]. These findings suggest the role of adiponectin signaling in altered BCAA metabolism.

PPARγ belongs to the family of nuclear hormone receptors and is important for adipocyte development and regulation of glucose metabolism [91]. Pharmacological activation of PPARγ using thiazolidinediones acts as a therapeutic target for T2D intervention [92]. Moreover, in obese Zucker rats, administration of PPAR-γ agonists upregulated the expression of genes related to BCAA catabolism [93]. The insulin-sensitizing capability of PPAR ligands is strongly linked to adipose tissue alteration of the BCAA metabolic pathway [93]. Consistently, adipocyte-specific deletion of PPARγ in mice resulted in elevated serum BCAA and decreased incorporation of BCAA into triacylglycerol in WAT and BAT. Also, decreased expression of BCAA catabolic genes *Bcat2* and *Bckdh* [94].

In adipose tissue, hypoxia is identified as a crucial regulator of BCAA metabolism [95]. Hypoxia not only causes inflammation but also contributes to angiogenesis and tissue fibrosis [96]. Hypoxia was identified as a suppressor of BCAA catabolism in obese adipose tissue, limiting BCAA absorption in adipocytes and fuelling towards lipogenesis [77]. Under hypoxic conditions, the rate of BCAA consumption is attenuated, which impacts the process of *de novo* lipogenesis in adipocytes [95]. In adipocytes, higher utilisation of glutamine was partly used as a compensatory mechanism for the reduced BCAA catabolism. However, it was not sufficient enough to entirely reverse the effect of attenuated BCAA catabolism on lipogenesis [95].

1.7 BCAA metabolism in adipose tissue under pathophysiological conditions

A defect in BCAA catabolic machinery (*Bckdha knockdown*) impairs adipocyte differentiation and expression of *Adipoq, Leptin, Plin4, and Pparg* [81]. The altered protein expression of BCAA genes PPM1K (decreased) and BCKDK (increased) in adipose tissue is reported in *ob/ob* and diabetic mice models [89]. Unresolved inflammation, improper ECM remodeling (fibrosis), and insufficient angiogenic potential are the three major factors in the pathophysiology of dysfunctional adipose tissue in obesity or T2D [97], thus adipose tissue cannot expand appropriately. It has been reported hypoxia is negatively associated with the expression of several BCAA catabolic genes (such as BCKDHB, HIBDH, *MMUT*, etc.) and positively correlated with pro-fibrosis genes in obese human subjects [98]. Acetyl Co-A derived from BCKA can acetylate the PR domain-containing protein 16 (PRDM16), a master regulator of beiging, thus blocking the binding of PRDM16 with PPARγ and suppresses WAT browning [99,100].

Defective BCAA metabolism has been shown to influence macrophage polarization, implicating it in adipose tissue-resident macrophage functions. As per Zhao et al; [101] an elevation in BCAA levels stimulates the production of high mobility group box 1 (HMGB1) nuclear protein, an inducer of M1 macrophage polarization [102]. In *db/db* diabetic mice, an increase in BCKAs levels following BCAA supplementation induces macrophage hyperactivation. Furthermore, the BCKAs treatment leads to elevated pro-inflammatory cytokines production via induction of oxidative stress in bone marrow-derived macrophage (BMDM)[103]. Pro-inflammatory cytokines have also been shown to influence BCAA transport, catabolism, and lipogenesis in adipocytes [73]. Thus, the BCAA metabolism and inflammation share a reciprocal relationship in adipose tissue.

1.8 Changes in adipose tissue during obesity/T2D

As a key endocrine organ, adipose tissue engages in communication with various organs including the brain, liver, muscle, and pancreas to maintain energy balance. Adipose tissue is considered to be the key site for the onset and progression of obesity and T2D. Obesity induces alteration in adipose tissue that predisposes to metabolic dysregulation. Pro-inflammatory M1 macrophage infiltration, fibrosis, low lipid turnover, and ectopic lipid deposition are the adverse changes in adipose tissue associated with obesity [104]. In addition, the onset of obesity is associated with a higher burden of senescent cells in adipose tissue [105].

1.8.1 Adipose tissue as the origin of chronic low-grade inflammation during obesity

Obesity is associated with chronic low-grade inflammation and plays a central role in linking various tissue/organ functions collectively contributing to metabolic syndrome. Indeed, high calorie intake and obesity lineate with the activation of the immune system and inflammatory diseases. Expansion of adipose tissue occurs either through hyperplasia or hypertrophy. Hypertrophic adipocytes exhibit increased lipolysis and display distinct expression of cytokines and chemokines. This is important because several mechanisms implicated in the initiation of adipose tissue inflammation begin with adipocyte hypertrophy in obese conditions [106]. To note, hypertrophy is associated with an increase in fat mass and weight loss decreases the adipocyte volume. Thus, understanding the causes and the underlying pathological outcomes in terms of inflammation during obesity is an important issue to address.

Adipose tissue remodelling is a continuous process and the residing cells are supported mechanically by an extracellular matrix (ECM). During the fat expansion, the process intensifies and the upregulation of ECM-associated genes occurs. The accumulation of lipid droplets during obesity in adipocytes increases its size, but the surrounding ECM in excess

exerts sheer stress on the cell membrane of expanding cells. This activates inflammatory pathways by inducing the expression of various pro-inflammatory genes [107,108]. Due to hypertrophic cells in obese conditions, poor vasculature occurs and thus the cells get poorly oxygenated. This creates hypoxia resulting in an inflammatory reaction [109,110]. Further, in order to process the overflow of nutrients, trafficking inside the endoplasm reticulum (ER) occurs dictating the proper protein folding. However, the capacity of the ER may go beyond aberrant energy influx leading to ER stress [111]. Obese individuals are characterized by high circulating FFA due to ectopic lipid spillage. FFA inhibits the antilipolytic action of insulin thereby increasing the FFA outflux from adipocytes. Furthermore, it acts as an activator of the NFkB pathway resulting in pro-inflammatory cytokine release, inhibiting insulin sensitivity of adipocytes, which links inflammation with the insulin signaling pathway [112].

In obesity, increased expression of pro-inflammatory cytokine production primarily occurs due to macrophage infiltration and polarization. Adipose tissue macrophages (ATMs) can span from pro-inflammatory M1 macrophages to anti-inflammatory M2 macrophages. With obesity, the ATMs switch from M2 to M1 phenotype [113]. Moreover, increased accumulation of FFA stress the adipocytes and secretes macrophage-related chemokines and cytokines such as TNFα and MCP1 recruiting more macrophages from circulation [114]. This establishes a vicious cycle of cytokine/chemokine production and macrophage recruitment, resulting in systemic insulin resistance and subsequent metabolic complications, including T2D (Figure 1.8).

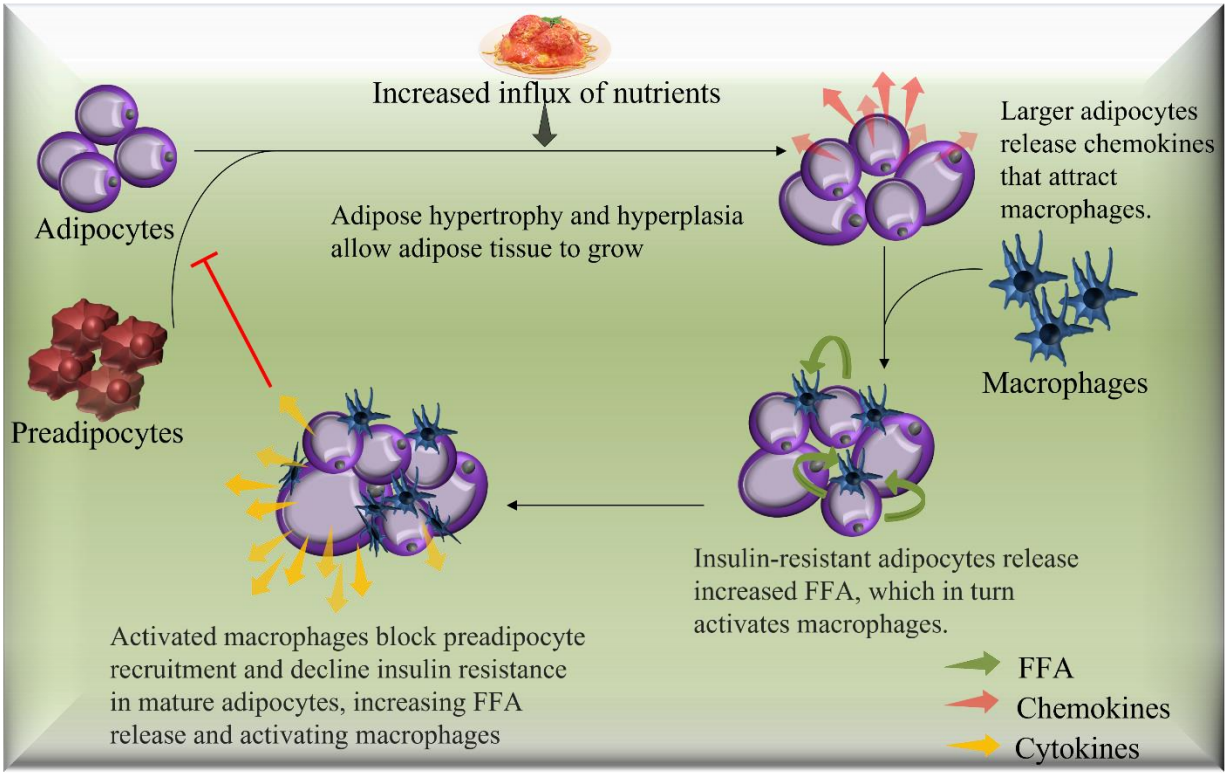

Figure 1.8: Representation of vicious cycle of adipocyte hypertrophy, macrophage recruitment, and activation. Adipocyte hypertrophy triggers the recruitment of macrophages, wherein hypertrophied adipocytes release increased levels of FFA and activate the macrophages. The activated macrophages, in turn, secrete cytokines that not only further impair adipocyte insulin sensitivity, resulting in additional FFA release, but also hinder the recruitment of pre-adipocytes, thereby promoting the enlargement of adipocytes.

Indeed, chemokines are important in recruiting macrophages to adipose tissue. Obesity is marked by the increased number of ATMs and MCP-1 protein is central to this process. Interestingly, MCP-1 expression occurs before the accumulation of ATMs from the initially activated macrophages due to FFA [115]. The macrophage accumulation is proportional to adiposity in human and rodent models. In obese individuals, ATMs can represent up to 40% of the overall cell percentage. Due to hypoxia and the increased size of fat cells, a substantial

increase in the death of adipocytes occurs in obesity. The necrotic-like dead cells are surrounded by macrophages for scavenging, resulting in crown-like structures.

Several studies have linked obesity to immune activation leading to metabolic dysfunction. Salicylate targets the upstream activator of NF-kB induction; treatment of obese subjects with salicylate abolished diet-induced obesity and improved the glycaemic control of T2D patients. Furthermore, TNF-α expression was observed only in AT in obese whereas in the liver and muscle, its expression was undetectable [116]. Genetic deficiency of CCL2 in obese mice reduced ATM levels and reversed the IR and steatosis in the liver [117]. Taken together, these studies suggest that obesity-associated inflammation initiates in adipose tissue. In the context of chronic obesity, macrophages are recruited, and the production of various pro-inflammatory cytokines/chemokines increases. Excessive synthesis of these cytokines may be released into circulation. The circulation of these cytokines, along with FFAs, can ultimately affect other tissues and organs, resulting in ectopic fat deposition, inflammation, and various metabolic disorders.

1.8.2 Adipose tissue fibrosis

Obesity may cause adipose tissue dysfunction and it cannot expand appropriately to store the surplus energy [72]. This causes ectopic fat deposition in various organs that govern metabolic balance, insulin resistance, and a higher risk of T2D. Dysfunctional WAT is characterized by increased fibrosis and hypoxia (Figure 1.9) [72].

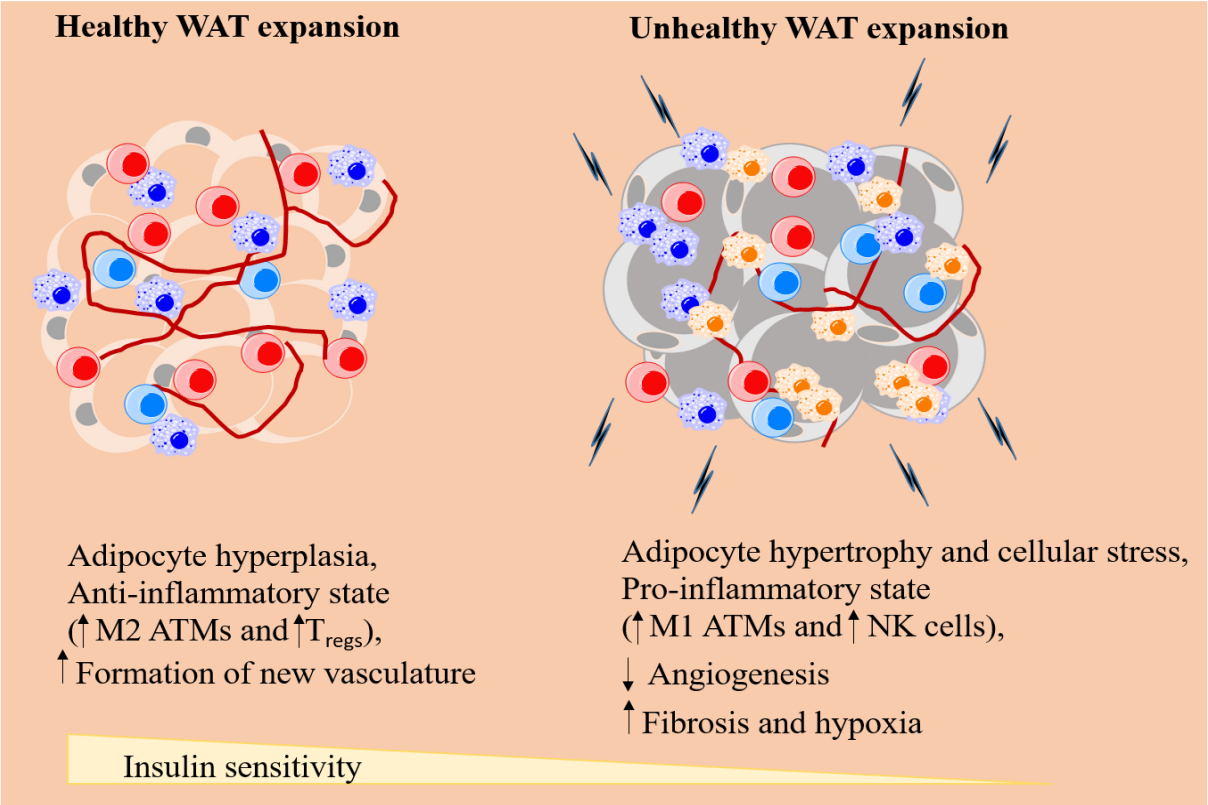

Figure 1.9: Difference between healthy and unhealthy WAT expansion. Adipose tissue expansion follows distinct patterns in both healthy and unhealthy states. In healthy WAT, the adipocytes will increase in number (hyperplasia), and the number of anti-inflammatory adipose tissue macrophages (ATMs) will be higher compared to M1 macrophages. On the other hand, in unhealthy WAT expansion, the adipocytes will increase in size.

Adipose tissue fibrosis can be defined as the increased accrual of ECM proteins, resulted due to an imbalance between excessive synthesis and impairment in the ECM degradation. It is a hallmark of adipose tissue malfunction and is linked to insulin resistance and T2D [118]. In healthy adipose tissue, ECM undergoes remodeling to adapt to normal fluctuations in adipocyte size. As a result of increased fibrosis, the rigidity of adipose tissue increases which further restricts the expandability of adipose tissue (reduced adipose tissue plasticity), resulting in ectopic lipid accumulation [119]. Among the ECM proteins, collagen and fibronectin are more prevalent in adipose tissue. With a focus on AT fibrosis, collagen VI (COL6) has

been reported for its fibrotic role [108]. Moreover, the collagen alpha-3 (VI) chain (COL6a3) (endotrophin) has been found to stimulate fibrotic collagen accumulation, inflammation, and insulin resistance [120].

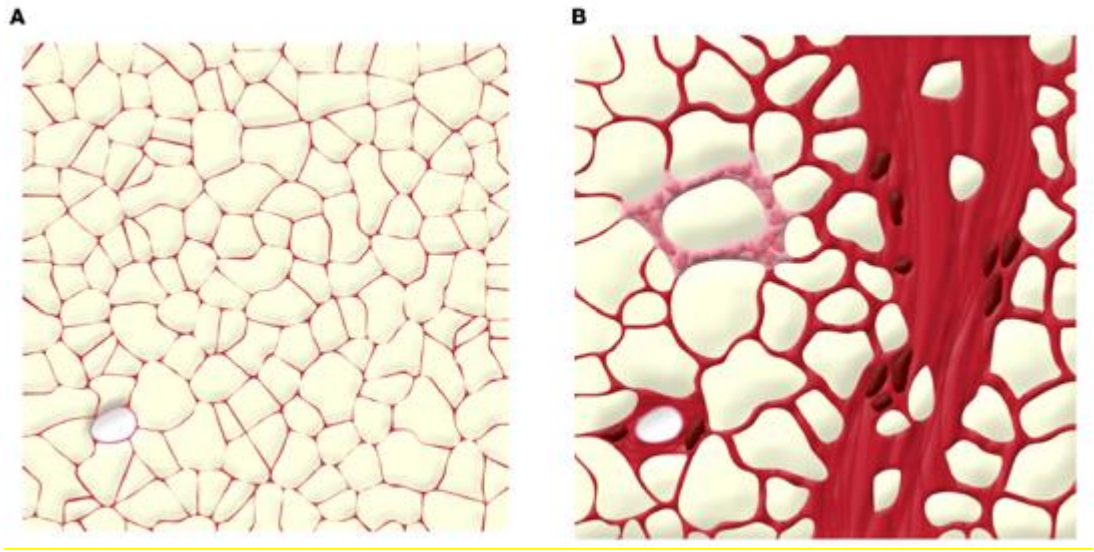

Figure 1.10: Illustration of adipose tissue fibrosis in obese subjects (picture courtesy Marcelin et. al, 2019). This picture shows the difference between healthy and fibrotic adipose tissue. In fibrotic adipose tissue, there is the accumulation of collagen fibres and increased infiltration of immune cells as compared to healthy tissue.

1.8.3 Development of fibrosis during obesity

The expansion of adipose tissue and adipocyte hypertrophy occur faster than neovascularization during the onset of obesity, thus adipocytes rapidly surpass the diffusional limit of oxygen and thus create hypoxia. The hypertrophic adipocytes produce several pro-inflammatory cytokines such as IL-6, TNF-α, TGF-β, and CCL2 (Figure 1.11). Additionally, in adipocytes higher expression of pro-fibrosis genes was observed upon the High-fat diet (HFD) feeding [121].

The hypoxic environment raises the level of hypoxia-inducible factor 1 (HIF-1) and activates HIF target genes such as collagen type I, alpha 1 (COL1A1), COL3A1, and lysyl oxidase, an

enzyme that promotes collagen cross-linking [122,123].

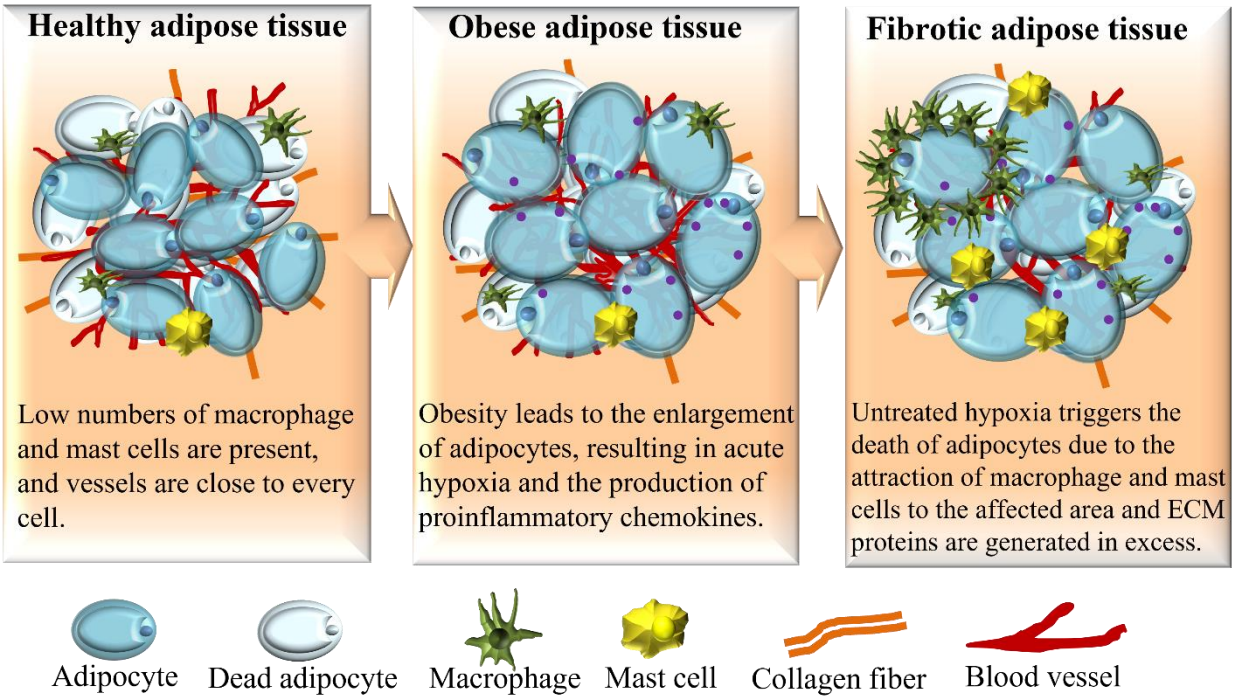

Figure 1.11: Proposed mechanism for the development of fibrosis during obesity. During obesity, the adipocytes enlarge in size, leading to an acute hypoxic environment. Additionally, there is secretion of pro-inflammatory cytokines. Persistent hypoxia leads to adipocyte necrosis and accumulation of extracellular matrix (ECM) proteins (as shown in the figure).

1.8.4 Cellular origin of ECM deposition/fibrosis in adipose tissue

Various cell types present in adipose tissue, including adipocyte progenitors, adipocytes, fibroblasts, and myofibroblasts, produce ECM proteins (Figure 1.12) [124]. In mice and humans, Marcelin *et al;* showed increased PDGFRα+ progenitor subsets with high CD9 expression enhance WAT fibrosis and are associated with metabolic decline [125]. In human preadipocytes, macrophage-secreted factors were reported to promote a profibrotic phenotype [126]. In addition, the depletion of macrophages has been shown to lessen adipose tissue fibrosis in HFD obese mouse models [127]. Jones et al, reported that in response to HFD, the adipocyte develops a

fibroblast-like transcriptional signature [121]. These adipocytes are characterized by increased expression of ECM, focal adhesion, and cytoskeletal genes, as well as inhibition of numerous adipocyte programs, particularly those related to mitochondria [121].

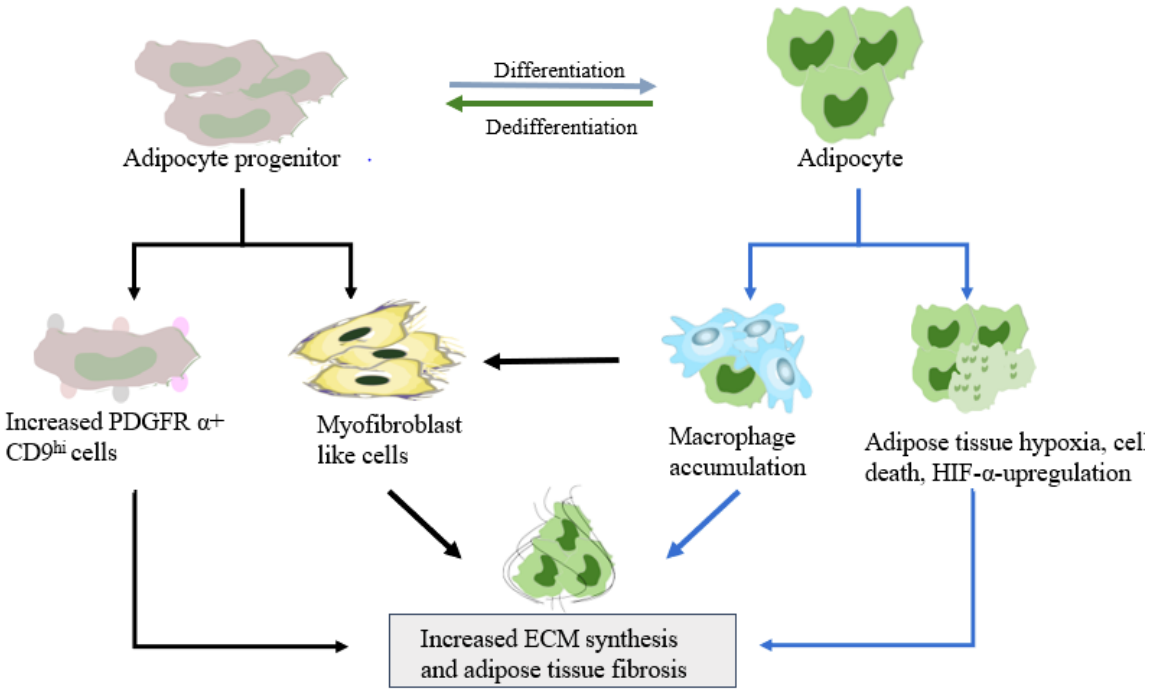

Figure 1.12: Schematic diagram showing the cellular origin of adipose tissue fibrosis. ECM proteins can be secreted by various cell types in adipose tissue including adipocytes, myofibroblast, and adipocyte progenitor cells. Recently, PDGFRα+ progenitors with CD9high expression have been reported to induce fibrosis in eWAT.

1.9 Signaling pathways involved in adipose tissue fibrosis

1.9.4 Hypoxia and Hypoxia-inducible factor (HIF)- 1α activation:

In response to hypoxia, HIF-1 is the primary regulator. HIF-1α and HIF-1β are the two subunits of HIF1 and are encoded by Hif1a and Hif1b genes respectively. The HIF-1α level is altered by the availability of oxygen [128].

Under normoxic conditions, HIF-1α is quickly degraded. Briefly, the HIF-1α is hydroxylated by prolyl hydroxylase proteins (PHD) on proline residues. The hydroxylated HIF1α is recognised by E3 ubiquitin ligase, the von Hippel-Lindau (VHL) protein, and ubiquitylated. The polyubiquitylated HIF-1α degrades in 26S proteasome. On the other hand, The O_2-dependent hydroxylation of HIF-1α subunits by PHD is suppressed and leads to its accumulation under hypoxia. HIF-1α is translocated to the nucleus along with HIF-1β and forms the heterodimer and binds to hypoxia-responsive elements (HREs), and modulates the expression of hypoxia-responsive genes (as shown in Figure 1.13).

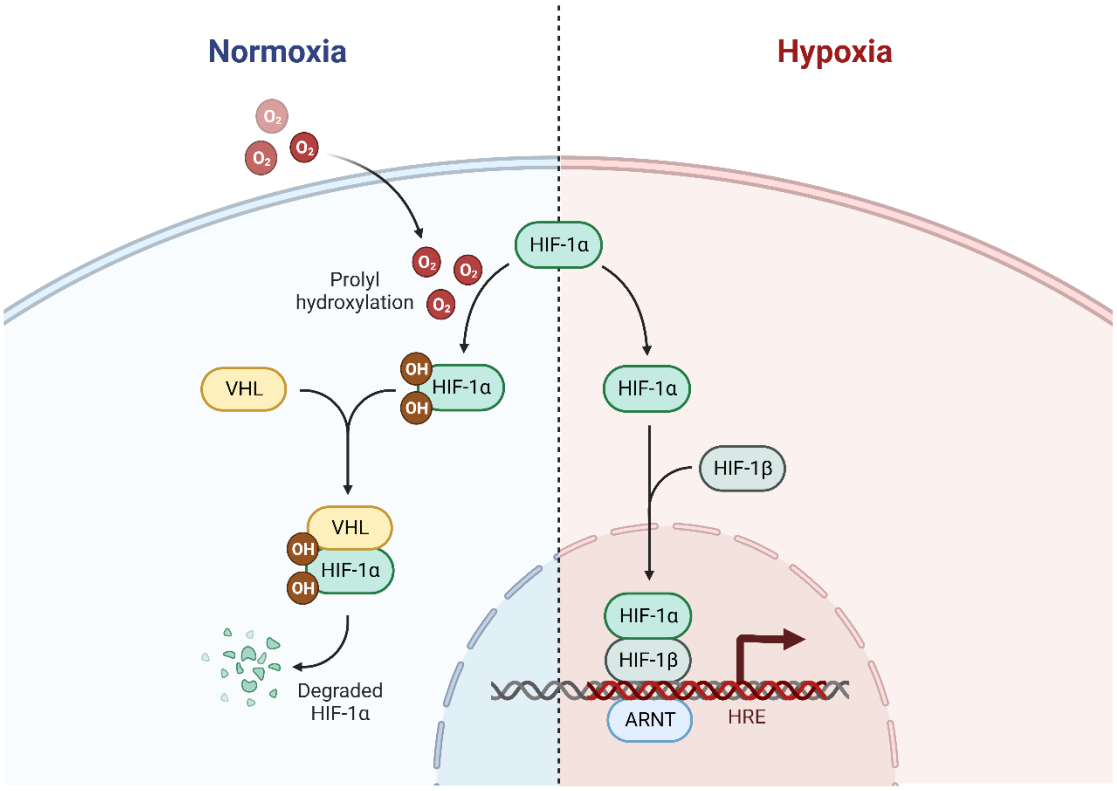

Figure 1.13: Pathway showing activation of HIF1-α under hypoxia condition. Under normal conditions, HIF-1α is hydroxylated by PHD. These hydroxylated HIF1-α molecules are ubiquitinated by VHL (a ubiquitin ligase) and undergo proteasomal degradation. Conversely, under hypoxic conditions, the hydroxylation of HIF1-α is suppressed. As a result,

HIF-1α is translocated to the nucleus and binds to HIF-1β to alter the expression of hypoxia-responsive genes.

ECM induction is triggered by hypoxia, serving as a significant initiating factor [129]. Under the hypoxic condition, the HIF-1α is expressed. Instead of promoting proangiogenic conditions in adipose tissue (AT), HIF-1α stimulates the production of extracellular matrix (ECM) components, resulting in fibrosis. [122]. HIF-1α may also induce a change in redox status, and affect the enzymes (lysyl oxidase and prolyl-4-hydroxylase) involved in collagen cross-linking and stabilization [130]. The role of HIF-1α in fibrosis is supported by evidence showing that fibrosis can be effectively prevented by either using a chemical HIF-1α inhibitor (PX-478) or by overexpressing a dominant-negative HIF-1α mutant in obese fat pads [131]. Hypoxia can upregulate the key inflammatory genes, including IL-6 and macrophage inflammation factor 1 (MIF1) through HIF-1α induction [131]. Adipose tissue oxygenation (pO2) has shown a negative association with pro-fibrotic gene expression including COL3A1, COL6A2, CTGF, LOXL2, and MMP9, and inflammatory cytokines CCL2, IL-6, TNF, CD68, and CCL5 in human subjects under obese condition (Figure 1.14) [98]. Interestingly, adipose tissue pO2 was positively associated with the expression of the BCAA catabolic gene in adipose tissue [98]. Thus, this study suggested the involvement of BCAA catabolism in AT fibrosis for the first time.

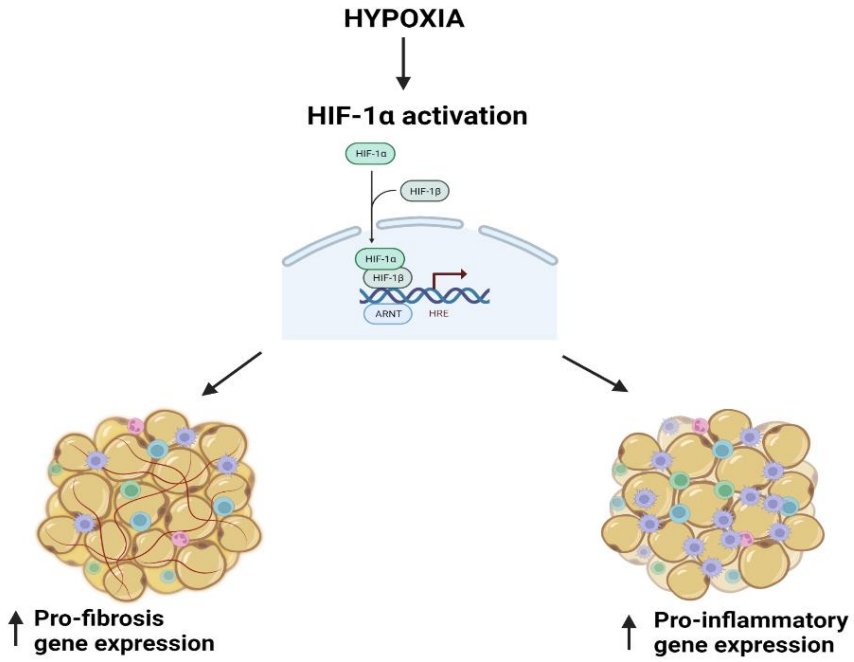

Figure 1.14: Activation of HIF1-α induces inflammation and fibrosis in adipose tissue. Under hypoxic conditions, the activation of HIF1-α leads to increased expression of both pro-fibrosis and pro-inflammatory genes in adipose tissue.

1.9.5 Transforming Growth Factor-beta (TGF)-β:

TGF-β acts as a master regulator and promoter of fibrosis in various tissues, including adipose tissue. The TGF-β superfamily comprised of above 33 members such as TGF-β1, 2, and 3, growth differentiation factors (GDFs), activins, and bone morphogenetic proteins (BMPs). They control different processes such as cell growth and differentiation, and specification of cell fat [132]. The proteins from the TGF-β family are also crucial for adipose tissue remodeling and their roles in the induction of adipose tissue fibrosis during obesity.

Myofibroblasts play a key role in the process of tissue repair and are characterised by the expression of alpha-smooth actin (SMA) (also known as ACTA2) and collagen secretion. Of note, the increased myofibroblast-mediated collagen synthesis is linked to fibrosis [133].

Multiple cell types within adipose tissue, such as adipocyte progenitors, adipocytes, fibroblasts, and myofibroblasts, contribute to the production of extracellular matrix (ECM) proteins [124]. TGF-β and activin A are reported to stimulate myofibroblast-like phenotypes in human adipose tissue progenitor cells [126,134] Additionally, TGF-β is identified as the main factor secreted from the macrophage and induces the myofibroblast-like phenotypes in progenitor cells [134].

1.9.6 PDGFRα activation:

PDGFRα+ adipocyte progenitors' cells are reported to acquire myofibroblast phenotypes in obese adipose tissue [125]. CD9 has been suggested to have a functional role, as observed in studies where CD9 knockdown using small interfering RNA (siRNA) resulted in reduced proliferation and higher expression of pro-adipogenic markers in human adipose tissue progenitor cells [135]. Moreover, in human obesity, the frequency of $CD9^{high}$ PDGFR-α+ correlated with omental WAT (oWAT) fibrosis and it's also related to the severity of IR and T2D [125].

1.10 Adipose tissue senescence

Cellular senescence is characterized by irreversible cell cycle halt, DNA damage (Figure 1.15), and the production of a senescence-associated secretory phenotype (SASP) [136]. In obesity oxidative stress, hyperglycemia, hyperinsulinemia, fatty acids, and telomere shortening are the possible inducers of cellular senescence [137]. Upregulation of P53, and P21, increased β-galactosidase activity, inflammatory factors secretion, and build-up of phosphorylated H2AX are the features observed in senescence cells.

The SASP consists of a diverse range of cytokines, chemokines, pro-inflammatory agents, and extracellular matrix remodeling factors. These SASP-related factors are upregulated at the

transcriptional level and dynamically released into the milieu, impacting a variety of processes including angiogenesis induction, tissue remodeling, and fibrosis [136]. Furthermore, SASP can transmit signals to cause senescence in peripheral cells. Among the pro-inflammatory cytokines IL-1β, IL-6, and chemokine MCP-1 are common SASP [136].

Among different tissues, WAT is more prone to senescence. Independent of chronological age, WAT cells are more prone to becoming senescent not only with aging but with obesity, and T2D[136]. Senescence in WAT is associated with adipocyte hypertrophy, dyslipidemia, and insulin resistance [136].

Different cell types in adipose tissue including progenitor cells and adipocytes are involved in senescence. The preadipocytes (or adipose progenitor cells) are prone to cellular senescence. Adipose tissue progenitor cells from obese human subjects were shown to have finite replicative potential and elevated senescence markers in comparison to adipose tissue progenitor cells from lean control [138]. Senescence in progenitor cells can affect the adipogenic potential in subcutaneous fat in hypertrophic obese human subjects [139].

Two different studies concentrated on senescence in adipocytes including an obese mouse model (induced by agouti peptide) and polymerase η knockout mice, showed DNA damage response (one of the characteristic features of senescence) can be triggered in mature adipocytes. The finding was supported by an increase in p21, p53, and inflammatory cytokines TNF-a, IL-6 [136]. Mature adipocytes showed high ROS production, increased DNA damage, and p21 and p53 levels following two weeks of HFD. Thus, DNA damage occurs in adipocytes at the early stages, even before the onset and establishment of obesity, preceding the development of adipose tissue inflammation, insulin resistance, and glucose intolerance [140].

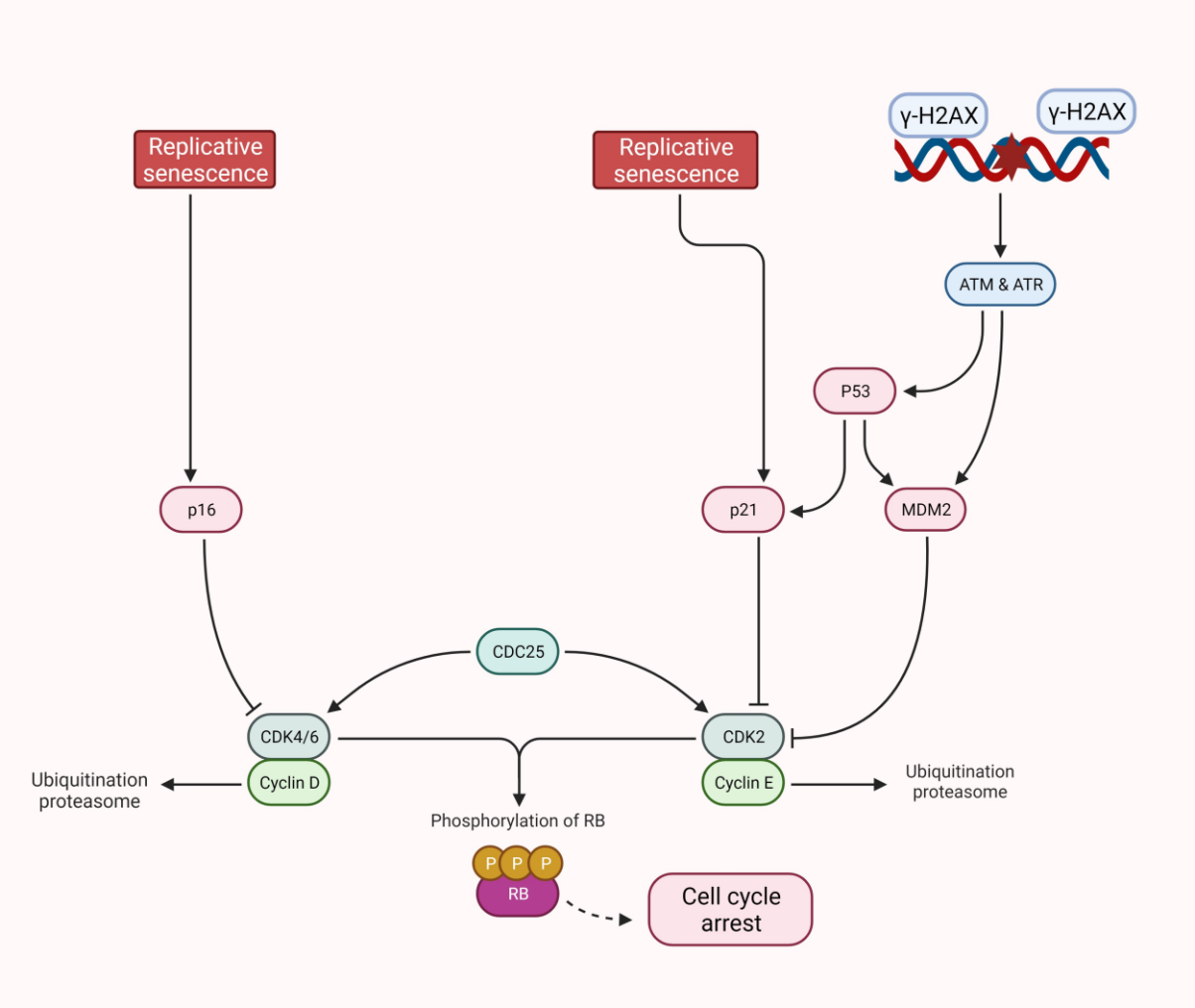

Figure 1.15: Schematic representation of cell cycle arrest during DNA damage/ or replicative senescence. Cell cycle arrest happens during senescence in response to DNA damage and other stress. It occurs via the activation of the P53/P21 or P16/phospho-retinoblastoma (Rb) pathways. The kinases ataxia-telangiectasia mutated (ATM) and ataxia telangiectasia and Rad3-related protein (ATR) are activated by the DNA damage response (DDR). This allows the activation of P53, which then activates P21 to arrest the cell cycle by inhibiting cyclin-dependent kinase 2 (CDK2) and restricting the entry from the G1 to S phase of the cell cycle. The activation of P16 directly inhibits CDK (CDK4/6), preventing the phosphorylation of Rb and blocking the transcription of genes crucial for DNA replication.

1.11 Scope of the study:

BCAAs are essential for maintaining the physiological functions in adipose tissue such as they are utilised as a substrate for adipogenesis, lipogenesis, and thermogenesis [77,81,82]. On the other hand, adipose tissue participates in the regulation of systemic BCAA levels (as adipose tissue is reported to modulate the circulatory BCAA levels) [78].

Elevated serum/tissue BCAA levels are associated with obesity/T2D, NAFLD, and aging [42,67]. Additionally, reduced expression of BCAA catabolic genes including BCAT2, BCKDHA, and PPM1K is observed in different metabolic tissues including adipose tissue in metabolic diseases. The enzyme PPM1K is essential for the activation of the rate-limiting enzyme BCKDHA in the BCAA degradation pathway, thus regulating the BCAA catabolism. The SNP of PPM1K is associated with a higher risk of developing T2D in human subjects [42,46] Additionally, in diabetic adipose tissue reduced protein expression of PPM1K is observed in mice [89]. Altogether, these findings from the literature suggest the dysregulated expression of PPM1K is present in obesity/T2D, however, there is a lack of evidence on understanding the role of PPM1K in the etiology of obesity/T2D.

This study aimed to investigate the role of PPM1K in regulating glucose, lipids, and energy metabolism in adipose tissue and the underlying mechanisms.

1.12 Hypothesis

BCAA is important for adipose tissue function including adipogenesis, lipogenesis, and thermogenesis as reported. The enzyme PPM1K regulates BCAA catabolism by activating the rate-limiting enzyme BCKDHA. Interestingly, SNPs of PPM1K are not only linked with higher serum BCAA but also associated with a higher incidence of T2D[55,56]. However, how PPM1K regulates adipose tissue functions is not known. This study hypothesizes that PPM1K plays an important role in the regulation of adipose tissue functions.

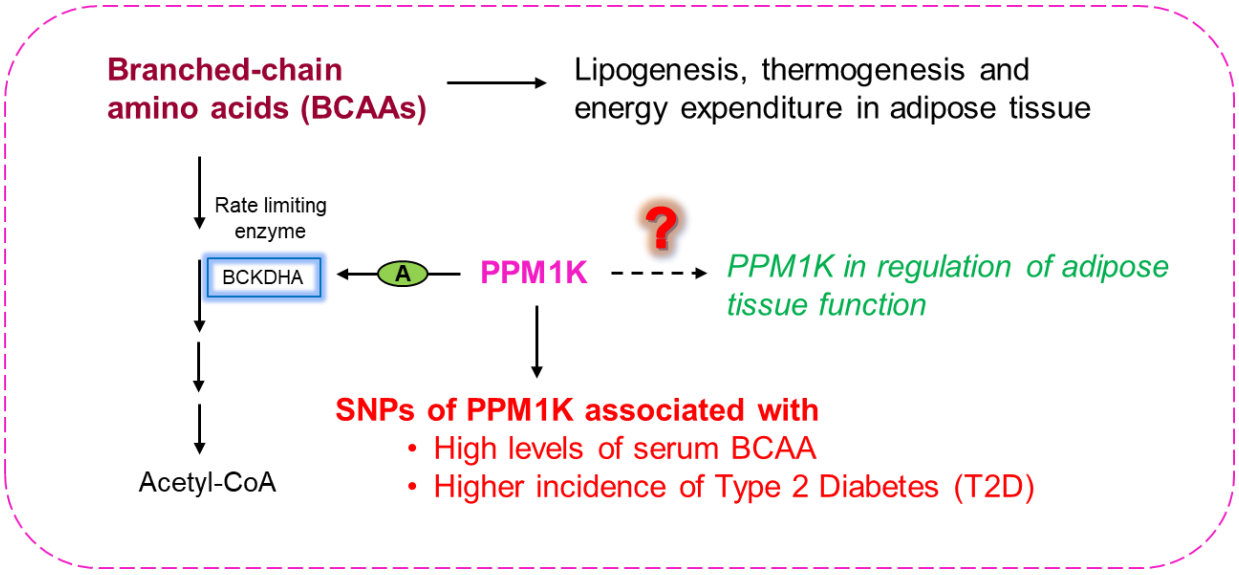

Figure 1.16: A schematic diagram showing the hypothesis utilized for the study

1.13 Objectives

1. To study the impact of PPM1K deficiency on adipose tissue functions and its underlying mechanism.
2. To investigate the role of adipocyte PPM1K in the regulation of adipose tissue functions.

Chapter 2 – Materials and Methods

2.1. Materials:

2.1.1 Chemicals and reagents

Chemical/ reagent	Name of company	Catalog no.
For mass spectrometry		
Chloroform	Sigma-Aldrich	#650498
Acetonitrile (ACN, LC/MS grade)	DUKSAN	#3040
Methanol (LC/MS grade)	DUKSAN	#3041
Formic acid	Sigma-Aldrich	#695076
Ammonium formate	Sigma-Aldrich	#09735
o-Phenylenediamine (OPD)	Sigma-Aldrich	#P9029
Hydrochloric acid (37%)	Analar Normapur	#20252.420
Ethyl acetate	Sigma-Aldrich	#270989
Sodium sulphate (Na_2SO_4)	Sigma-Aldrich	#239313
Ammonium acetate	Sigma-Aldrich	#A1542
L-Valine	Sigma-Aldrich	#I2752
L-Leucine	Sigma-Aldrich	#L8000
L-Isoleucine	Sigma-Aldrich	#V0500
Sodium α-keto isovalerate (KIV)	Sigma-Aldrich	#198994
Sodium α-keto isocaproate (KIC)	Cayman Chemical	#21052
Sodium α-keto β-methylvalerate (KMV)	Sigma-Aldrich	#K7125
L-Valine (D_8)	Cambridge Isotope Laboratories	#DLM-311-PK
KIV (D_7)	Cambridge Isotope Laboratories	#DLM-4646-PK
UPLC BEH Amide 1.7µm 2.1x100mm	Waters	#86004801
ACQUITY UPLC BEH C18 1.7µm 2.1x50mm Col	Waters	#186002350

HPLC-glass micro inserts	HK labware	#06-09-0357
HPLC-glass vials		
For Genotyping		
Direct PCR (Tail)-lysis reagent	Viagen	#102-T
2xTaq Plus MasterMix (Dye)	Cwbiotech	#CW2849L
Proteinase K	Sigma	#70663
SYBR safe DNA gel stain	Apex bio	#A8743
100 bp DNA ladder	Vazyme	#B2142CAA
For RNA isolation and qPCR		
RNAiso plus (Trizol)	TaKaRa	#9101
Absolute Ethanol	Sigma-Aldrich	#459844
Isopropyl alcohol	DUKSAN	#d2377
QuantiNova SYBR Green PCR Kit	Qiagen	#208057
For western blotting		
Acryl/Bis30% Solution (acrylamide solution)	Sangon Biotech Co., Ltd.	#B546018-0500
Ammonium Persulfate (APS)	Sigma-Aldrich	#A3678
TEMED	Thermo Fisher Scientific	#17919
PVDF membrane	SOLARBIO	#BSP0161
Protease Inhibitor Cocktail	MedChemExpress	#HY-K0010
Phosphatase Inhibitor Cocktail	Bimake	#B15002
2-Mercaptoethanol	Bio-Rad	#1610710
PageRuler™ Plus Prestained Protein Ladder	Thermofisher	#26620
Bovine serum albumin (BSA)	Sigma-Aldrich	#05470
Medical X-ray film	Fuji film	#Super HR-U30
Clarity Western ECL Substrate	Bio-Rad	#1705061
Clarity Max Western ECL Substrate	Bio-Rad	#1705062

For Histological analysis		
10% neutral buffered formalin	Epredia	#110909
Histological paraffin	Thermo Fisher Scientific	#8331
Xylene	Sigma-Aldrich	#185566
Absolute ethanol	Sigma-Aldrich	#459844
Haematoxylin	SOLARBIO	#G1121
Adhesive Glass Slide	Matsunami Glass	#210268W-SP6E
Cryomatrix	Epredia	#112070
Eosin	SOLARBIO	#G1121
DAPI	Thermo Fisher Scientific	#P36985
DPX mountant	Sigma-Aldrich	#06522
Acetic acid	VWR	#64-19-7
Picro Sirius Red Solution	Abcam	#ab246832
Oil Red O	powder Hopkin & Williams	#11950
For cell culture		
Dulbecco's Modified Eagle Medium (DMEM)	Gibco™	#12800082
Penicillin- Streptomycin (PS)	Thermo Fisher Scientific	#15140122
Fetal Bovine Serum (FBS)	Thermo Fisher Scientific	#10270106
Trypsin	Gibco™	#25200056
Opti-MEM I reduced serum medium (Opti-MEM)	Gibco™	#31985070
Lipofectamine™ RNAi MAX transfection	Invitrogen™	#13778150
Trypan Blue Stain (0.4%)	Thermofisher	#T10282
Collagenase, Type II, powder	Thermofisher	#17101015
100 µm Cell Strainer	Falcon	#352360

Dexamethasone		
3-Isobutyl-1-Methylxanthine (IBMX)	Sigma-Aldrich	#858455
Rosiglitazone		
Human Insulin	Sigma-Aldrich	#9077-M
For Seahorse analysis		
XF DMEM base medium, pH: 7.4	Agilent Technologies, Inc	#103575-100
XF RPMI medium, pH: 7.4	Agilent Technologies, Inc	#103576-100
Seahorse XF calibrant solution	Agilent Technologies, Inc	#100840-000
XFe24 sensor cartridge	Agilent Technologies, Inc	#102340-100
XF24 V7 PS tissue culture microplate	Agilent Technologies, Inc	#100777-004
Islet Capture Microplate	Agilent Technologies, Inc	#101174-100
Rotenone	Cayman Chemical	#13995
Antimycin A1	Cayman Chemical	#19433
Trifluoromethoxy carbonylcyanide phenylhydrazone (FCCP)	Cayman Chemical	#15218
2-deoxy-D-Glucose (2-DG)	Cayman Chemical	#14325
Oligomycin	Cayman Chemical	#11341
Others		
Pierce™ TMB Substrate Kit	Thermofisher, USA	#34021
Glucose	FLUKA	#49138
Tyloxapol	Sigma-Aldrich	*#T8761*
Ketamine (10%)	Alfasan International B.V.	*#0904088-05*
Xylazine (2%)	Alfasan International B.V.	*#1205117-05*

High fat high cholesterol diet (HFHC)-Mice diet	Research Diets, Inc. USA)	*# D12079Bi*

2.1.2 Biochemical Assays/Kits

Name	Name of company	Catalog no.
Pierce™ BCA Protein Assay Kit	Thermofisher	#23225
Mouse IL-1 beta/IL-1F2 DuoSet ELISA	R&D Systems	#DY401
Mouse CCL2/JE/MCP-1 DuoSet ELISA	R&D Systems	#DY479
Mouse Adiponectin ELISA kit	ImmunoDiagnostics Limited	#32010
Reverse transcription kit	Promega	#15596026
Stanbio Cholesterol LiquiColor®	Stanbio Laboratory	#1010
Stanbio ALT/GPT (Liqui-UV®)	Stanbio Laboratory	#2930
Stanbio AST/SGOT (Liqui-UV®)	Stanbio Laboratory	#2920
Stanbio triglyceride LiquiColor®	Stanbio Laboratory	#2100
NEFA assay kit	Nanjing Jiancheng Bioengineering Institute	# A042-2-1
β-hydroxybutyric acid detection	Nanjing Jiancheng Bioengineering Institute	

2.1.3 Primer sequence

Name of target	Forward primer (5'-3')	Reverse primer (5'-3')
Acta2	GCATCCACGAAACCAC CTA	CACGAGTAACAAATCA AAGC
Col1a1	CAATGGTGAGACGTGG AAAC	GGTTGGGACAGTCCAG TTCT
Col3a1	CTGTAACATGGAAACT GGGGAAA	CCATAGCTGAACTGAA AACCACC
Col4a1	CTGGCACAAAAGGGAC GAG	ACGTGGCCGAGAATTT CACC
Col6a3	GCCCATCACCACTCTAA CCT	GTTGAGTCTGCGAACG ATCC
Loxl2	ATTAACCCCAACTATGA AGTGCC	CTGTCTCCTCACTGAAG GCTC
18S	AGTCCCTGCCCTTTGTA CACA	CGATCCGAGGGCCTCA CTA
36b4	CGACCTGGAAGTCCAA CTAC	ATCTGCTGCATCTGCTT G
Adipoq	GGAGAGAAAGGAGATG CAGGT	CTTTCCTGCCAGGGGTT C
Cebpa	CAAGAACAGCAACGAG TACCG	GTCACTGGTCAACTCCA GCAC
Fabp4	ATCAGCGTAAATGGGG ATTTGG	GTCTGCGGTGATTTCAT CGAA
Pparγ	GCATGGTGCCTTCGCTG A	TGGCATCTCTGTGTCAA CCATG
Tnf-α	ACGGCATGGATCTCAA AGAC	AGATAGCAAATCGGCT GACG
IL-1β	CTGGTGTGTGACGTTCC CATTA	CCGACAGCACGAGGCT TT
Mcp1	CCACTCACCTGCTGCTA CTCA	TGGTGATCCTCTTGTAG CTCTCC
Inos	CCAAGCCCTCACCTACT TCC	CTCTGAGGGCTGACAC AAGG
F4/80	CTTTGGCTATGGGCTTC CAGTC	GCAAGGAGGACAGAGT TTATCGTG
A-fabp4	CCGCAGACGACAGGA	CTCATGCCCTTTCATAA ACT

P16	CCTGGTGATGTCCGACC TG	CCATGAGCGCATCGCA ATC
P21	GCAGATCCACAGCGAT ATCC	CAACTGCTCACTGTCCA CGG
Ucp1	ACTGCCACACCTCCAGT CATT	CTTTGCCTCACTCAGGA TTGG
Cidea	TGCTCTTCTGTATCGCC CAGT	GCCGTGTTAAGGAATC TGCTG
Dio2	CAGTGTGGTGCACGTCT CCAA TC	TGAACCAAAGTTGACC ACCAG
Ppm1k	TGTCTGCTGATGCAAGC CTCCTG	TGGGGCTGTCCCAGGCT ATTCC
Ppm1k-genotyping	CCCATCCTTAGGAGAG GTCG	CAGCAGAATTGGCTCA TCAA ATGGTGGATCCTGAGA CTGG
Ppm1k-F/F	ATTTACCTCATCCGATG GACAGAC	GTGAGTTAAGCCAAGC TCAGATTC
Adipo-cre	GGATGTGCCATGTGAG TCTG	ACGGACAGAAGCATTT TCCA
siRNA-Ppm1k	UUGUCUUCGGUACCGU ACUGU	AGUACGGUACCGAAGA CAACA
siRNA-scramble	UAGCGACUAAACACAU CAAUU	AAUUGAUGUGUUUAGU CGCUA

2.1.4 Buffers and their recipe

Buffer/ Medium	Composition
RIPA-lysis buffer	50 mM Tris HCl, 150 mM NaCl, 2 mM EDTA, 0.1% SDS, 1% NP-40 (pH: 7.4)
FACS buffer	1 mM EDTA, 25 mM HEPES, 1% FBS in 1XPBS
RBC lysis buffer	155 mM NH_4Cl, 10 mM $KHCO_3$, 0.1 M EDTA
Phosphate-buffered saline (PBS)	137 mM NaCl, 2.7 mM KCl, 1.8 mM KH_2PO_4, 10 mM Na_2HPO_4 (pH: 7.4)
Tris-buffered saline (TBS)	150 mM NaCl, 20 mM Tris (pH: 7.6)
1XPBST	1 X PBS (pH: 7.4) with 0.1 % Tween-20
1XTBST	1 X TBS (pH: 7.4) with 0.1 % Tween-20
Antigen retrieval buffer	10 mM Tris base, 1 mM EDTA, 0.05% Tween-20 (pH: 9.0)
Blocking buffer for IF	10% fetal bovine serum (FBS) and 0.1% Triton-X100 detergent in 1XPBST
Primary diluent for IF	3% BSA and 0.1% Triton-X100 detergent in 1xPBS
Transfer buffer	192 mM glycine, 25 mM Tris
Running buffer	192 mM glycine, 25 mM Tris, 0.1% SDS
5Xloading dye	0.05% Bromophenol blue, 0.25M Tris-Cl (pH: 6.8), 50% Glycerol, 10% SDS
Blocking buffer for western blotting	5 % skimmed milk in 1 X TBST
10XTAE buffer	0.4 M Tris, 0.01 M EDTA, 0.2 M Acetic acid (pH:8.0)
ELISA diluent	1% BSA in 1XPBS buffer
EISA wash buffer	1xPBST added with 0.05% Tween 20
Complete DMEM	DMEM with 10% fetal bovine serum (FBS) and 1% solution of penicillin and streptomycin (PS)
Sirius red stain	0.5 g Sirius red powder in 500 mL of saturated acetic acid

2.1.5 List of antibodies used

Antibody	**Name of company**	**Catalog no.**
HSP90	Cell Signaling Technology	#4877
P21	Abcam	#ab188224
ACTA2	Cell Signaling Technology	#19245
IL-1β	Cell Signaling Technology	#12242
Total BCKDHA	Abcam	#ab90691
P-BCKDHA	Abcam	#ab200577
Total AKT	Cell Signaling Technology	#9272
P-AKT (Ser-473)	Cell Signaling Technology	#9271
iNOS	Santa Cruz Biotechnology	#sc-651
F4/80	Thermo Fisher Scientific	#4-4801-82
PERILIPIN	Santa Cruz Biotechnology	#sc-47319
HIF-1A	BD-Bioscience	#610959
Alexa Fluor 488 Goat anti-rabbit	Thermo Fisher Scientific	#A11008
Alex Fluor 488 Rabbit anti-goat	Thermo Fisher Scientific	#A11078
Alex Fluor 594 Goat anti-rat	Thermo Fisher Scientific	#A11007
Flow cytometry antibody		
Anti-CD11b (BV605)	BD Biosciences (Horizon)	#563015
Anti-CD45 (APC-Cy7)	BD Bioscience (Pharminogen)	#557833
Anti-CD206 (PerCP/Cy5.5)	Bio legend	#141716
Anti- F4/90 (PE)	Bio legend	#123116
Anti-CD11C (FITC)	Bio legend	

2.1.6 Equipment and software

Equipment	**Name of the company**
Agilent 6460 Liquid Chromatography – Electrospray Ionisation Triple Quadrupole Mass Spectrometer	Agilent Technologies, Inc
Refrigerated CentriVap Centrifugal Concentrator and CentriVap Cold Traps	Labconco
NanoDrop 2000 Spectrophotometer Thermo Fisher Scientific	Thermo Fisher Scientific
Varioskan LUX Multimode Microplate Reader	Thermo Fisher Scientific
96 Microplate Reader	Bio-Rad Laboratories
Real-Time PCR System	Applied Biosystems
Viia7 Real-time PCR	Applied Biosystems
Excelsior AS Tissue Processor	Thermo Fisher Scientific
Paraffin Embedding Station	Thermolyne™
Leica RM2235 (Manual microtome)	Leica Biosystems
Nikon Eclipse Ni-U Fluorescent Microscope	Nikon Instruments Inc.
Nikon Polarizing Microscope	Nikon Instruments Inc.
Countess II FL Automatic Cell Counter	Invitrogen™
Agilent Seahorse XFe24 Extracellular Flux Analyser	Agilent Technologies
BD FACSAria™ III Cell Sorter	BD Biosciences
Accu-Check Performa Glucose Meter	Roche
Promethion metabolic cage system	Stable Systems international
Bruker minispec LF90II Body Composition Analyzer (The Hong Kong University)	Bruker
Software	
GraphPad Prism 8.0.1	GraphPad
ImageJ 1.50	NIH
IBM SPSS Statistics	IBM
FlowJo 7.6.2	FlowJo, LCC

2.2. Methodology:

2.2.1. Animal studies

PPM1K global Knockout mice were kind sharing from Dr. Yinbing Wang from the University of California at Los Angeles and mice colonies were further expanded at Centralized Animal Facilities (CAF) of The Hong Kong Polytechnic University.

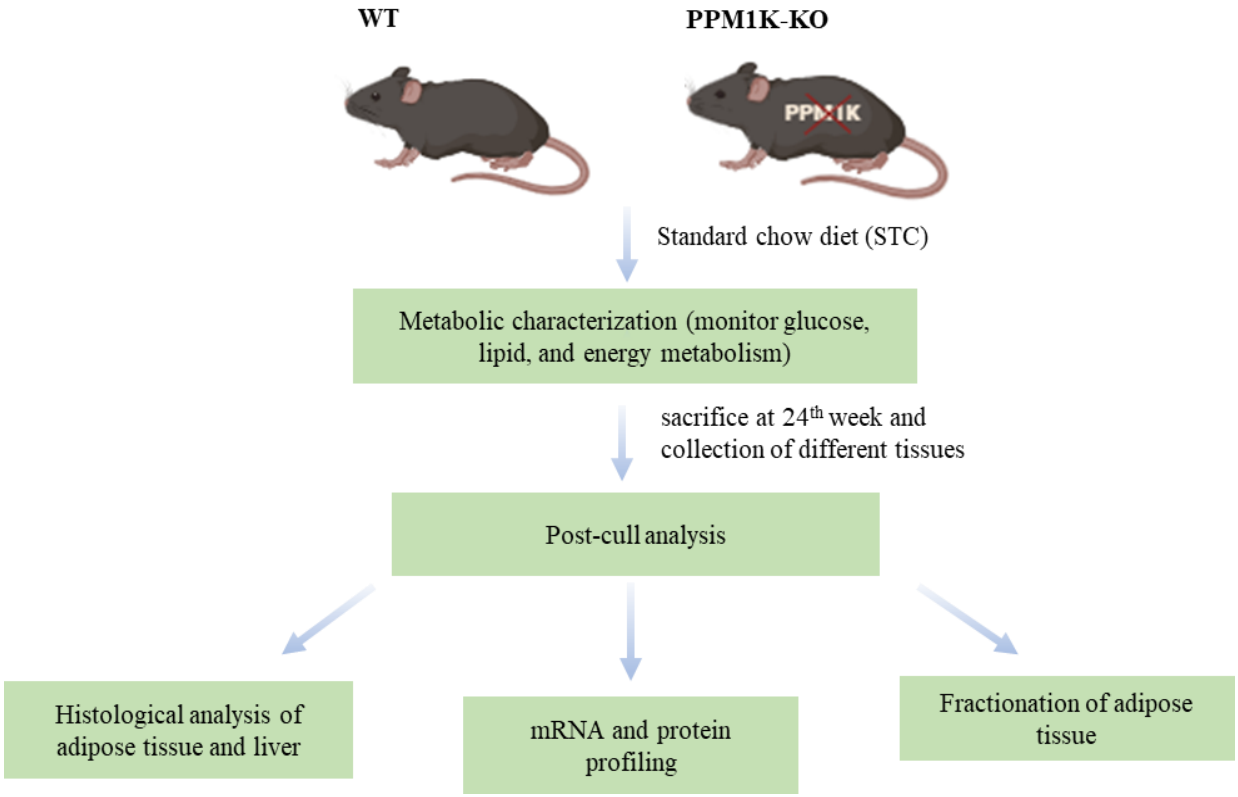

Figure 2.1: Study design for PPM1K global KO mouse model.

Additionally, adipocyte-specific PPM1K knockout (A-KO) and wild-type (WT) mice were created. Adipo-PPM1K KO mice were created by the deletion of exon three in the PPM1K gene using the Cre/LoxP system on C57/BL6 background. The PPM1K flox mice were bought from Nanjing Biomedical Research Institute (NBRI), China. The LoxP site was inserted between exons two and four (flox/flox mice). These flox/flox mice were crossed with mice containing adiponectin-Cre transgene and resulted in approximately 50% of the offspring

containing heterozygous LoxP site and Cre transgene. The mice containing heterozygous LoxP site and Cre transgene were crossed with the flox/flox mice. This mating led to the generation of offspring with flox/flox and Cre transgene (hemizygous for Cre transgene), flox/flox without Cre transgene, and heterozygous floxed mice with or without Cre. The flox/flox mice with Cre transgene were grouped as KO while the flox/flox mice without Cre transgene were regarded as WT control. The littermates were allowed to be weaned at 21-25 days of age and the genotyping was confirmed by detection of adiponectin-Cre and flox gene using PCR in ear biopsy samples collected at four weeks. The mice were grouped based on genotype and sex. The mice were fed a standard chow diet (STC) and high-fat high cholesterol (HFHC) diet based on the aim of the study (Figure 2.1).

All animals were kept in CAF, PolyU in rooms with temperature and humidity conditions ((22±1°C and 60±10%) along with a 12-hour light-dark cycle. Unless specified otherwise, mice had *ad libitum* access to both food and water. All the experiments were conducted by the procedure approved by the Department of Health HKSAR Government (Ordinance Cap. 340) and the Animal Subjects Ethics Sub-Committee (ASESC) of the Hong Kong Polytechnic University.

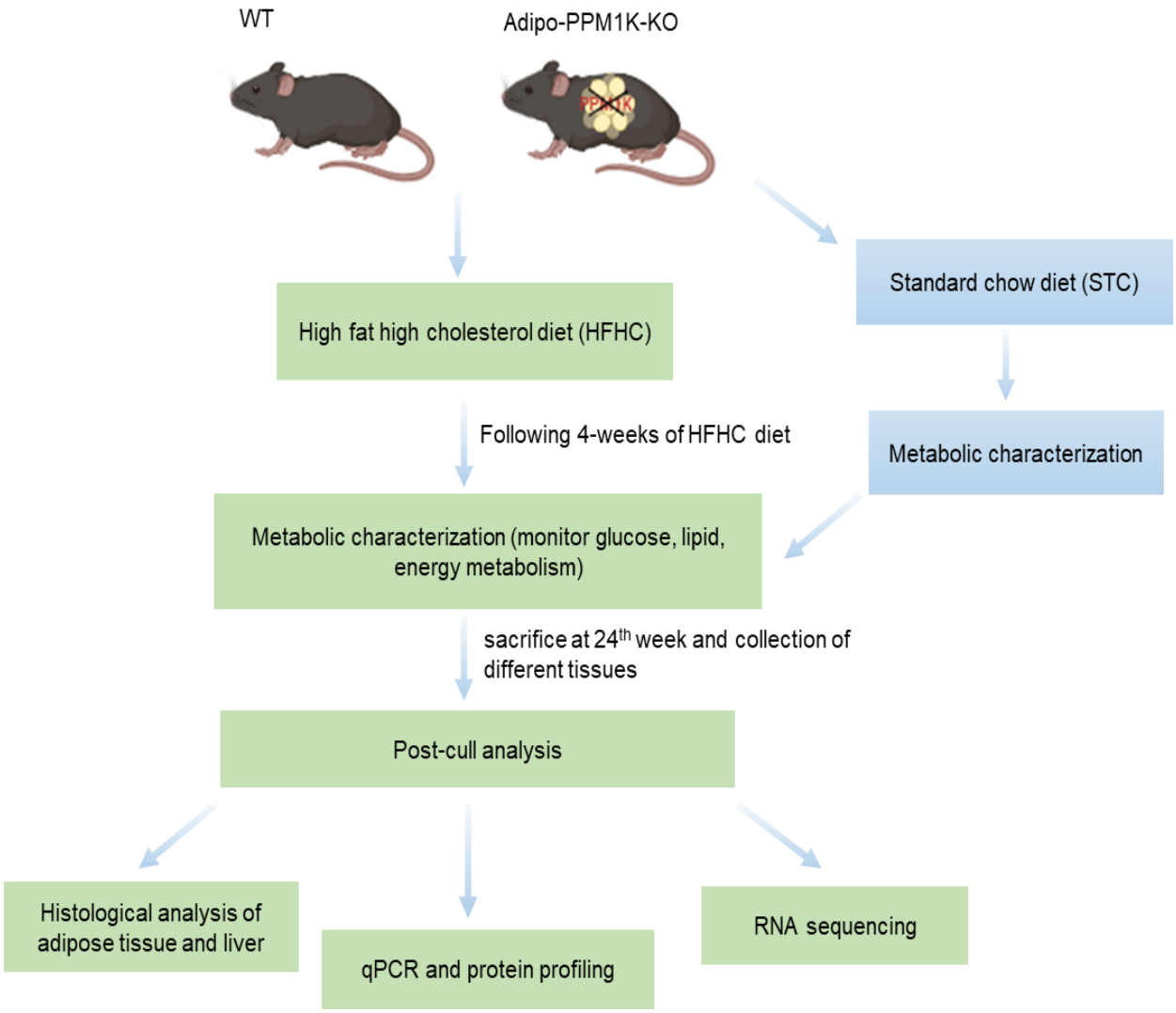

Figure 2.2: Study design for adipocyte-specific PPM1K knockout mouse model.

2.2.2 Genotyping of PPM1K global KO and adipo-PPM1K mice

Ear biopsy samples were collected in 4th week and digested with the Direct PCR lysis reagent (Tail). For each sample, 100 µl of lysis buffer was added supplemented with 0.5 mg/ml proteinase K. These samples were incubated in the water bath at 55˚C overnight, and proteinase K was further inactivated by placing them at 85˚C for an hour. The samples were cooled down and stored for genotyping.

For the genotyping, 0.8 µl of DNA template was added to each reaction, as given below:

Table 2.1. PCR reaction set up for genotyping

Name of Reagent	**Volume**	**Final concentration**
2xTaq MasterMix (dye)	10 µl	1x
Forward primer (10 µM)	0.5 µl	0.25 µM
Reverse primer (10 µM)	0.5 µl	0.25 µM
Ear lysate (DNA)	0.8 µl	-
Nuclease free-H_2O	Made up to 20 µl	-

Table 2.2. PCR reaction setup for genotyping

Steps	**Temperature**	**Time**
Initial denaturation	95˚C	5 minutes
Denaturation	95˚C	35 cycles
Annealing	60˚C	
Extension	72˚C	
Final extension	72˚C	10 minutes

For the genotyping of adipo-PPM1K mice, both the PPM1K-floxP site and adiponectin Cre were detected. The PCR product was analyzed using DNA electrophoresis a 2% agarose gel containing SYBR™ Safe DNA Gel Stain to visualize the DNA. The DNA bands were visualized using Gel Doc XR+ (Bio-Rad).

2.2.3. Dietary treatment and metabolic characterization

The PPM1K global KO was maintained on STC throughout the experimental duration. For adipo-PPM1K mice, the mice were shifted to a high-fat high cholesterol diet (HFHC) (17 kcal% protein, 43 kcal% carbohydrates, and 40 kcal% fat, Catalog# D12079Bi, Research Diets, Inc. USA) at 10-11 weeks of age to induce obesity and its associated hepatic steatosis.

Parallelly, the mice continued to feed with an STC diet as a control (lean). The weekly body weight and food intake were measured throughout the entire duration of the experiment. Several experiments were performed for the metabolic characterization of the mice model including glucose tolerance test (GTT), insulin tolerance test (ITT), triglyceride (TG) clearance test, very-low-density lipoprotein (VLDL) secretion assay, branched-chain amino acid (BCAA) tolerance test, short-term cold challenge experiment, metabolic cage experiment, and body composition.

2.2.3.1 GTT and ITT

To perform the GTT, the mice were fasted for 16 hours (6 pm-10 am) by placing them into clean cages. After 16h of fasting, the mice were injected with D-glucose intraperitoneally (2g/kg or 1g/kg body weight based on the dietary treatment) and blood glucose was measured via the tail every 15 minutes using the glucose meter (ACCU-Check) until 120 minutes.

For ITT, mice were placed in a cleaned cage for fasting for 6 hours. The body weight and glucose level were checked and accordingly, the dosage of purified recombinant insulin was injected intraperitoneally. Further, the glucose levels were measured every 20 minutes, until 120 minutes.

2.2.3.2 TG-clearance test

For the TG-clearance test, the mice were fasted for 16 hours (6 pm-10 am) by placing them into clean cages. The mice were weighed and orally gavaged with 10 μL g−1 body weight of olive oil. The blood samples were drawn every hour from the tail until 5 hours. The serum was collected from collected blood samples by centrifuging them at 4200rpm at 4˚C. The collected serum samples were used for the TG measurement (Stanbio Triglycerides LiquiColor Test, Catalog # 2100).

2.2.3.3 VLDL-secretion assay

For the TG-clearance test, the mice were fasted for 16 hours (6 pm-10 am) by placing them into clean cages. The mice were weighed and accordingly injected intravenously with tyloxapol at 500 mg kg−1 body weight. The blood samples were drawn every hour from the tail until 5 hours. The serum was collected from collected blood samples by centrifuging them at 4200rpm at 4˚C. The collected serum samples were used for the TG measurement (Stanbio Triglycerides LiquiColor Test, Catalog # 2100).

2.2.3.4 BCAA clearance test

Mice were fasted for 6 hours by placing them into clean cages. Following 6 hours of fasting, mice were weighed and basal serum samples were collected. The mice were orally gavaged with a mixture of BCAA (Val: Leu: Ile = 1: 1.5: 0.8) at 100mg/kg body weight. The blood samples were collected at 20, 60, and 120 minutes and the serum BCAA and BCKA were measured using mass spectrometry method.

2.3.3.5 Free fatty acid and ketone body measurement

The serum levels of free fatty acid (nonesterified Free fatty acid) and ketone bodies (β-hydroxybutyrate) were quantified using commercial kits from Nanjing Jiancheng Bioengineering Institute.

2.2.3.6 Short-term cold challenge experiment

The core body temperature of mice was measured at room temperature (RT) using the thermometer and mice were placed in a cold room at 4˚C temperature for five hours and every hour the body temperature was recorded.

2.2.3.7 Metabolic cage experiment

Promethion metabolic cage setup was utilized to study the changes in metabolic parameters including oxygen consumption, production of CO_2, energy expense, food and water uptake, and activity (movement along the different axis-XYZ). The respiratory quotient can also be calculated using the oxygen and CO_2 data.

To perform this experiment, mice were placed in the metabolic cage (single occupancy for each cage). Initially, mice were allowed to acclimatize to the environment of the cage (for 12 hours approximately). The experimental program was set up as follows (in order):

Firstly, 12 hours for acclimatization at 30˚C temperature, two days at 30˚C, two days at 24˚C, one day at 16˚C, one day at 4˚C, and kept for a few hours at RT in the metabolic cage. In the metabolic cage program, the light and dark cycle was set up for 12-12 hours and the data was recorded for different parameters.

2.2.3.8 Body composition analysis

The body composition of mice including lean mass, fat mass, total body fat, and fluid content was measured *in-vivo* with the use of Bruker minispec LF90II Body Composition Analyzer and data was collected. It utilizes the time domain-nuclear magnetic resonance (NMR) to access the mentioned parameters *in-vivo*.

2.2.3 Animal sacrifice and collection of tissue samples

At the endpoint of the dietary treatment regime, mice were culled using the overdose of anaesthesia (ketamine and xylazine). The cardiac puncture was performed using a 25G needle to collect the blood samples. The blood samples were kept at RT for 3-4 hours for clotting and the serum was separated by centrifugation at 4000rpm for 15-20 minutes. The pellet was

discarded and the supernatant was centrifuged again to maximize the recovery of serum samples. The serum samples were kept at -80˚C until further use.

Following blood collection, different tissue samples were harvested, weighed, and snap-frozen in liquid nitrogen before putting them in -80˚C freezer storage. All tissue samples were kept at -80˚C. A small piece of tissue was put into a cassette (for tissue processing) and placed in 10% neutral formalin for fixation for 24 hours and further proceeded with Excelsior™ AS Tissue Processor.

2.2.4 Measurement of pro-inflammatory cytokines, insulin, and adiponectin levels

The serum insulin and adiponectin levels were quantified using ImmunoDiagnostics ELISA kits and assays were performed as per the instructions given in the kit manual.

The measurement of pro-inflammatory cytokines including interleukin 1 β (IL1-β) and chemoattractant protein-1 (MCP-1) in serum samples was performed using DuoSet ELISA kits (R&D systems). The assay was performed as per the given instructions in the kit. The dilution of serum samples was performed in FFA-free bovine serum albumin (BSA).

2.2.5 SVF and mature adipocytes isolation from adipose tissue and culture

The sWAT was collected from mice for the isolation of SVF. Briefly, the collected sWAT was washed with sterile phosphate buffer saline (PBS) and minced with the help of sterile scissors. The minced tissue was then subjected to enzymatic digestion using a 2mg/ml solution of collagenase II (dissolved in PBS and filtered with a 0.22µm filter). The minced tissue was transferred to a tube containing collagenase II solution and placed in a 37˚C water bath (with parafilm) under shaking conditions for 40-45 minutes. The enzymatic digestion was aborted by adding 2 times the volume of PBS to the volume of the tube containing the digested tissue. The solution was then passed through the 100µm sterile filter and centrifuged at 500g for 5

minutes. After centrifugation, the tube contains the upper layer consisting of mature adipocytes and a pellet containing the SVF part. Based on the aim of the experiment, the mature adipocyte and SVF fraction were collected. For the culturing of SVF cells, the pellet was resuspended in complete DMEM media containing 10% Fetal bovine serum (FBS) and 1% antibiotics (Pen strep). The resuspended cells were placed in a 10cm cell culture dish and cells were allowed to adhere to the dish surface. The media was changed after 12-18 hours after culturing the cells. The cells were allowed to reach 80-90% confluency before they were cultured for further experiments.

2.2.6 Differentiation of SVF into mature adipocytes

The SVF cells were isolated from sWAT (as described earlier) and allowed to reach the confluence. The SVF cells were trypsinized, and collected for centrifugation. The cells were counted using an automated cell counter (Invitrogen countess 3) and cells were seeded at the density of 80-90x10^3 per well in a six-well plate. Once the cells reached 100% confluency, they were maintained in complete media for 48-60 hours in a cell incubator. Following that cells were supplemented with the differentiation cocktail containing dexamethasone (0.25µM), 3-Isobutyl-1-Methylxanthine (IBMX) (0.5Mm), recombinant insulin (10µg/ml), and rosiglitazone (100nM). The media was replenished when it turned yellow. The differentiation cocktail was replaced with the maintenance media containing 1µg/ml insulin after 4-5 days. The cells were observed under the microscope to check the maturation of SVF into mature adipocytes (observe the lipid droplets). The maintenance media was replenished every 2-3 days (once it turned yellow) until day 10. The cells were observed under the microscope before being collected for further experiments.

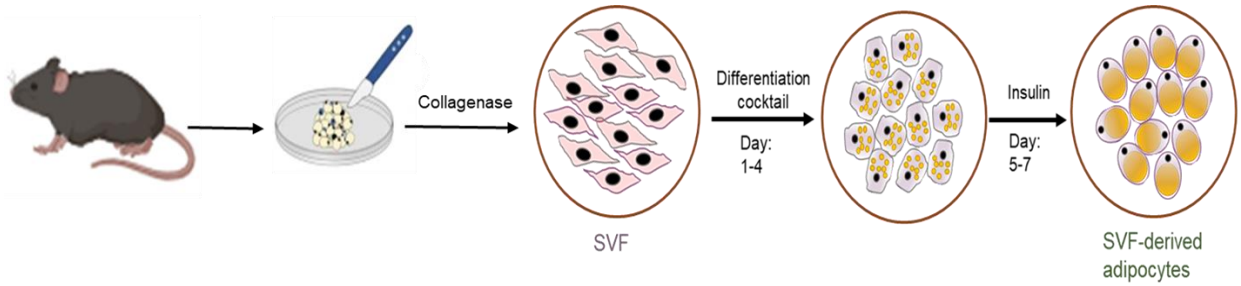

Figure 2.3: Schematic diagram showing differentiation of SVF into mature adipocytes.

2.2.7 Flow cytometry analysis of SVF fraction

Firstly, the SVF was isolated from adipose tissue as mentioned previously (in section 2.2.5). The SVF cell pellet was washed twice with sterile PBS containing 1% FBS to get rid of the digestion solution (centrifuged at 500g for 5 minutes, 4°C). The RBC lysis was done by adding 500µL of 1XRBC lysis buffer to the cell pellet and incubating for 5 minutes at RT. To stop the reaction, 500µL of 1XHBSS buffer was added and centrifuged at 500g for 5 minutes, 4°C, and the cell pellet was suspended with FACS buffer (prepared freshly and filters).

For antibody staining, the antibody cocktail was diluted in FACS buffer (1:200 dilution). For unstained and single antibody stained control (for compensation) was also prepared. The diluted antibody was added to cells and incubated in the dark for 25-30 minutes. The cells were then washed twice by adding 700-800 µL of FACS buffer and centrifuged at 500g for 5 minutes, 4°C to collect the cell pellet. The collected cell pellet was resuspended with 200-300 µL of FACS depending upon the cell density. The FACS was performed using BD FACSAria III Cell Sorter and data was collected, and analyzed with FlowJo 7.0 software.

2.2.8 Tissue processing and histological analysis

Following 24-36 hours, the tissue sample was retrieved from 10% neutral formalin and placed for processing in Excelsior™ AS Tissue Processor. The following program is used for the processing:

	Chemical	Time for processing
1.	Alcohol	30 minutes
2.	Alcohol	75 minutes
3.	Alcohol	75 minutes
4.	Alcohol	60 minutes
5.	Alcohol	60 minutes
6.	Alcohol	60 minutes
7.	Xylene	60 minutes
8.	Xylene	60 minutes
9.	Xylene	120 minutes
10.	Wax	60 minutes
11.	Wax	60 minutes
12.	Wax	180 minutes

After completing the process, the tissues were removed and placed in freshly melted paraffin wax at 60°C. The machine for tissue embedding was switched on 12 hours before the embedding. Subsequently, the tissue samples were embedded in melted paraffin wax at 60°C and stored at RT until further use.

For the sectioning, the tissue samples were placed at 4°C a day before. On the day of sectioning the tissue samples were soaked in iced water for a minimum of 1-2 hours before the sectioning. The tissue samples were sectioned using Leica RM2235 Microtome at 5µm thickness and placed onto the slides. The sectioned slides were allowed to dry at 50°C overnight to remove any air bubbles and the slides were further stored at RT.

2.2.8.1 H&E staining

The sectioned tissue was deparaffinized and rehydrated before performing any staining protocol as follows:

Xylene (10 minutes X 2), 100% ethanol (5 minutes X 2), 95% ethanol (3 minutes), 70% alcohol (3 minutes), and then placed in distilled water for one minute. The slides were subjected to Harris Haematoxylin stain for 5-10 minutes (based on the type of tissue) to stain the nuclei. The excess stain was removed by washing the slides under tap water for 30-60 seconds, followed by differentiation in acid alcohol for a brief moment (by dipping inside and taking it out), and then they were placed in Scott's tap water for 10 seconds. Following, the slides were placed in eosin stain (for cytoplasm staining) for 3-5 minutes and quickly dehydrated in two washes of 75% ethanol. They were then cleaned in Xylene for 10 minutes (2 times), mounted with DPX mountant, and allowed to dry. The images were captured at 10X and 20X magnification under the light microscope. (for BAT, the pictures were taken at 40X magnification). For each slide, 4-5 pictures were taken representing the entire slide. For analysis, ImageJ was used to quantify the number of immune cell infiltration (including the counting of crown-like structure), size, and distribution of adipocytes, in the case of BAT, lipid content and number of nuclei were counted.

2.2.8.2 Sirius red staining

Following deparaffinization and rehydration (as described above), the slides were subjected to Sirius red stain (to stain the collagen fibres) for 60 minutes in the dark. Following, the slides were quickly washed twice by dipping them into 0.5% acetic acid solution. The slides were tapped on tissue paper to get rid of excess acetic acid, placed in 100% ethanol solution (3 minutes x2), and cleaned in xylene solution (10 minutes x2). The slides were mounted with DPX mountant and allowed to dry. The images were captured at 10X and 20X magnification under the light microscope. The % area of fibrosis was quantified using ImageJ software.

2.2.8.3 Immunofluorescence (IF) staining

Following deparaffinization and rehydration (as described above), the slides were subjected to an antigen retrieval step to unmask the antigen binding sites. Briefly, the sectioned tissue slides were placed in pre-boiled antigen retrieval buffer (Tris-EDTA) buffer and allowed to boil for 20 minutes (covered). The slides were cooled down under the running tap water. The samples were subjected to blocking (to avoid the non-specific binding) by adding a blocking buffer containing 10% FBS and 0.1% triton X-100 (in PBS) for 40 minutes. Then, the samples were incubated overnight with the primary antibody (1:100) diluted in antibody dilution buffer (3% BSA and 0.1% triton X-100 in PBS) at 4°C. Following the primary antibody incubation, the samples were washed thrice with 1XPBST (5 minutes each, 2 minutes shaking condition, and 3 minutes stand still). After the washing step, the fluorescent-labeled secondary antibody was added to samples (1:1000 diluted in antibody buffer) and incubated for 60 minutes (protected from light). Following incubation, the samples were washed thrice with 1XPBST (5 minutes each, 2 minutes shaking condition, and 3 minutes stand still) to wash out the unbound antibody and avoid light. The slides were finally mounted with DAPI and stored in

the dark at 4°C (the images on the same day of staining, storing the slides for a long time will fade out the signal). The pictures were taken using a Nikon Eclipse Ni-U microscope at different wavelengths based on the secondary antibody colour (DAPI: 405nm, FITC: 498nm, and TRITC: 550nm).

2.2.8.4 Oil Red O (ORO) staining

ORO staining is used to stain the neutral fat (lipid droplets). For staining of lipid droplets in liver sections, the OCT-fixed tissue sections were sectioned using cryo-sectioning. The sectioned slides were stored at -20°C until further use.

To begin, slides were removed from the -20^{o}C refrigerator and placed at room temperature for 30 minutes to defrost. The slides were then rinsed for 10 seconds in a 10X PBS solution before being fixed in 10% neutral buffered formalin for 1 minute and washed in tap water for 20 seconds to remove the 10% neutral buffered formalin. Slides were submerged in 60% isopropanol for 5 minutes to prevent water carryover, which disrupts staining with oil-soluble ORO dye. The slides were then stained for 10 minutes in the dark in freshly prepared ORO staining solution (aluminium foil was used to wrap the staining dish). Following the staining step, the slides were washed twice with 75% isopropanol to remove excess stain. The slides were then counterstained with Hematoxylin stain (as described in the H&E staining section). Finally, the slides were cleaned with tap water for 20 seconds before being immersed in water for microscopic examination. The pictures were taken immediately after the staining was performed.

For Oil red staining to measure the lipid accumulation in differentiated mature adipocytes from the SVF the following protocol was used. Briefly, once the cell reached the maximum differentiation capacity, the culture media was removed carefully and washed twice with

1XPBS gently. After washing with PBS, cells were fixed with 10% (V/V) formalin for 60 minutes at RT. The fixed cells were then washed twice with 1XPBS and incubated at RT for 5 minutes with 60% isopropanol. The oil red stock solution (0.5% solution in isopropanol) was prepared and placed in the water bath at 56°C for one hour. The working solution was prepared by adding three units of stock oil red solution to two units of water, mixing properly, and filtering through a 0.22µm filter. The cells were incubated with an oil-red working solution for 20 minutes in the dark. The staining solution was discarded, and the cells were washed with water three times to remove the excess stain. The cells were further counter-stained with Hematoxylin for one minute and washed with water three times. Further, cells were covered with water (to avoid drying) and images were captured at 20X resolution using a light microscope. The quantification of lipid droplets was performed using the ImageJ software.

2.2.9 Total RNA isolation

For isolation of RNA from the whole tissue, a small amount of tissue (~20mg for liver and ~60-70 mg for adipose tissue) was placed in a homogenization tube, and 1 ml TRIzol reagent was added to it. The tubes were subjected to homogenization using Precellys 24 tissue homogenizer (Bertin Instruments). After homogenization, the tubes were placed on ice for 15 minutes and centrifuged at 4˚C, 15000rpm for 15 minutes. The supernatant was collected in a separate tube and again subjected to centrifugation at 12000 g for 5 minutes at 4˚C. After centrifugation, the upper oil layer was removed to avoid any interference with RNA isolation. For the RNA isolation using cell samples, 1ml TRIzol reagent was used for each 6-well (containing ~1 x 10^6 cells). For 1 ml of TRIzol reagent, 200ul of chloroform was added and was shaken vigorously (using hand shaking or vortex). The samples were allowed to be left

still at RT for 5-10 minutes and subjected to centrifugation at 4˚C, 12000 g for 15 minutes. Following centrifugation, the upper aqueous layer was collected in a separate Eppendorf tube (avoid mixing with other layers), and 500 µl of isopropanol was added to the tube and gently mixed. The samples were incubated for 10 minutes at RT and centrifuged at 4˚C, 12000 g for 15 minutes to precipitate the RNA. After centrifugation, a barely visible RNA pellet was observed at the side bottom of the tube. The RNA pellet was washed using 1ml of 75% ethanol (by flicking the tube) and centrifuged at 7500g for 15 minutes, 4˚C. The RNA pellet was air-dried (until it became translucent) and resuspended in nuclease-free water. The quantification of RNA was done using NanoDrop™ 2000 Spectrophotometer (Thermo Scientific).

2.2.10 Reverse transcription (RT-PCR)

Following RNA quantification, 1 µg of RNA was utilized to synthesize the cDNA using the RT-PCR kit ((Go Script™ Reverse Transcription Mix, Random Primers (Promega)).

The following reaction setup was used for a 10 µl reaction volume:

Name of Components	**Volume**
GoScript™ reaction buffer, random primer (5X)	2 µl
GoScript™ enzyme mix	1 µl
Total RNA	1 µg
Nuclease-free water	Top up to 10 µl
Final volume	10 µl

The reaction volume was mixed up and proceeded for PCR reaction set-up for reverse transcription as follows:

Steps	**Temperature**	**Time**
Annealing	25˚C	5 minutes

Extension	42˚C	60 minutes
Inactivation	70˚C	15 minutes
Hold	4˚C	∞

The cDNA samples were stored at -20˚C or -80˚C until further use.

2.2.11 Real-time quantitative PCR (qPCR)

The ViiA 7 Real-Time PCR System (Applied Biosystems) was utilized to perform the real-time Quantitative PCR. The different sets of qPCR primers specific to particular genes were used (the sequence of primers was listed in the table). For reaction, the cDNA was diluted 20-40X based on the abundance of the target gene and QuantiNova SYBR® was used. The primer was also diluted with nuclease-free water to 10uM. For each reaction, the components are mentioned below:

Name of Components	**Volume**
QuantiNova SYBR® (2x)	5 µl
Primer mix (forward and Reverse)	0.5 µl
ROX (reference dye)	0.05 µl
Diluted cDNA	4.5 µl
Final volume	10 µl

All reactions are formed in duplicate or triplicate to avoid the pipetting error.

The quantification of the relative abundance of the target gene was done using the delta-delta Ct ($2^{-\Delta\Delta Ct}$) method and normalization with the housekeeping genes. The specificity of the primer sequence was ensured by checking the melting temperature (Tm) and DNA electrophoresis analysis of the qPCR product.

2.2.12 Immunoblotting

For the isolation of proteins from the whole tissue, a small amount of tissue (~20mg for liver/BAT and ~60-70 mg for adipose tissue) was placed homogenization tube. The RIPA lysis buffer with added protease inhibitor and phosphatase inhibitor cocktail was added to samples (the volume of RIPA buffer was decided based on tissue amount and type) and homogenized using Precellys 24 tissue homogenizer (Bertin Instruments). After homogenization, the tubes were placed on ice for 15 minutes and centrifuged at 4˚C, 15000rpm for 15 minutes.

For the isolation of proteins from the cultured cells, the cells were washed twice with PBS and scrapped in RIPA lysis buffer, and collected in Eppendorf tubes. The cells were incubated on ice for 30 minutes and subjected to centrifugation at 4˚C, 15000rpm for 15 minutes.

The protein amount in samples was quantified using the BCA method of protein quantification with Pierce™ BCA Protein Assay Kit. The protein samples were prepared for SDS-PAGE by denaturing them at 95˚C using a heat block. They were mixed with a loading dye containing 2-mercaptoethanol and incubated for 5 minutes. An equal amount of protein samples was loaded to each well of SDS-PAGE (Mini Trans-Blot® Cell) and the gel was run at 80V until crossing the stacking gel and eventually, the voltage was changed to 100-120V (constant voltage). The proteins were transferred to the PVDF membrane using the transfer buffer at 100V for 1-2 hours based on the size of the target protein. Following the transfer, the membrane was blocked with 10% skimmed milk fat for 1-1.5 hours under shaking conditions at RT. After blocking, the membrane was incubated overnight with diluted antibody (in 5% BSA in TBST) at 4˚C. Following incubation, the membrane was washed thrice (5 minutes each) with 1XTBST to remove the unbound antibodies and incubated with secondary antibody

(diluted 1:5000, 5% skimmed milk in 1XTBST) for 1-1.5 hours at RT. The membrane was washed three times (10 minutes each) with 1XTBST and placed in 1XTBST buffer. The membrane was developed using enhanced chemiluminescence reagents and X-ray films to visualize the protein bands. The quantification analysis (densitometry) of protein bands was done by using ImageJ software.

2.2.13 Mass spectrometry (MS)

2.2.13.1 Preparation of Calibration curve

The stock concentration of pure chemicals including valine, leucine, isoleucine (BCAAs), KIV, KMV, KIC (BCKAs), C3 and C5 acylcarnitine, and D7-KIV and D_8-valine (internal standard) was prepared in water at 100mM concentration and stored in -80˚C. For the preparation of the calibration curve, the serial dilution of these chemicals was performed in water. The methanol (100%) was used for the dilution of internal standard for serum samples and in methanol: water (4:1: v: v) for cell samples and tissue samples.

2.2.13.2 Processing of serum samples for Liquid chromatography/MS/MS

The cold methanol (100%) containing internal standard (3 μM of D8-valine and D7-KIV) was added to serum samples. For 10ul of serum samples, 100ul of absolute methanol was added and vortexed at high speed for 50-60 seconds. The samples were subjected to centrifugation at 4°C, 10,000 rpm for 15 minutes. The supernatant was collected in a separate tube for analysis. For BCAA measurement, 20μL of supernatant was transferred to an HPLC vial containing an insert. The remaining supernatant (50μL) was stored in a separate Eppendorf tube and proceeded for the BCKA derivatisation protocol (the supernatant can be freeze-dried using CentriVap Centrifugal Concentrator and stored at -80˚C until further processing).

2.2.13.3 Processing of tissue samples for LC/MS/MS

For the adipose tissue sample processing, an equal amount of tissue sample was placed in a homogenization tube along with beads. The cold methanol containing 3μM internal standard (MeOH: H2O, 4 parts:1 part) was added to the homogenization tube containing tissue. These samples were subjected to homogenization using Precellys 24 tissue homogenizer (Bertin Instruments). After homogenization, the tubes were placed on ice for 15 minutes and centrifuged at 4˚C, 15000rpm for 15 minutes and the supernatant was collected in a separate tube. Further, for BCAA measurement, 20μL of supernatant was transferred to an HPLC vial containing an insert. The remaining supernatant was stored in a separate Eppendorf tube and proceeded for the BCKA derivatisation protocol (the supernatant can be freeze-dried using CentriVap Centrifugal Concentrator and stored in -80˚C until further processing).

2.2.13.4 BCKA derivatization procedure

The methanol-extracted serum and tissue samples were reconstituted with 40μL methanol and subjected to derivatization. For derivatization, 12.5 mM OPD solution was freshly prepared in 2M HCL, and 500μL of OPD solution was added to each sample, mixed well, and placed in a heat block for 20 minutes. After 20 minutes, the samples were placed on ice for 10 minutes to cool down and short-spun to collect the samples. The equal volume of the derivatised sample was placed in a new Eppendorf tube carrying 80mg of Na_2SO_4 powder and vortexed till Na_2SO_4 was fully dissolved. Further, 500μL of ethyl acetate was added and mixed by brief vortex for 50-60 seconds and centrifuged at 500g for 5 minutes at RT. The upper extracted layer of ethyl acetate was collected in a new Eppendorf tube carrying 80mg of Na_2SO_4 powder and the remaining lower layer was extracted again with 500μL of ethyl acetate. The upper layer was collected following centrifugation and mixed with the first upper layer, and

subjected to centrifugation. After centrifugation, 700µL of supernatant was collected in a new Eppendorf tube and subjected to freeze drying using CentriVap Centrifugal Concentrator (freeze-dried samples can be stored at -80˚C until further processing). The freeze-dried samples were reconstituted using 200mM of ammonium acetate (40µL) and vortexed to mix, and subjected to centrifugation at 4˚C, 10000rpm for 15 minutes. Following centrifugation, 20µL of supernatant was transferred to an HPLC vial containing an insert for measurement of BCKA.

2.2.13.5 LC/MS/MS sample run and analysis

The LC/MS/MS analysis was performed by utilising Agilent 6460 Liquid chromatography system and Electrospray Ionization Triple Quadrupole Mass Spectrometer (ULS, PolyU). For BCAA and acylcarnitine measurement, 2µL of sample volume was injected to ACQUITY UPLC BEH Amide 1.7µm 2.1x100mm column for separation, and 0.3ml/min flow rate of aqueous–organic mobile phase was set. Before the sample run, the column was equilibrated using mobile phase A and B buffer 50-50%). The composition of mobile phase A was ACN: water (10: 90, v: v), 0.1% formic acid, and 5 mM ammonium formate, and phase B consisted of ACN: water (90: 10, v: v), 0.1% formic acid, and 5 mM ammonium formate and both phases were prepared freshly before the run. For BCKA, ACQUITY UPLC BEH C18 1.7µm 2.1x50mm Column was used and the composition of the mobile phase comprised of 0.1% formic acid in water and 0.1% formic acid in ACN.

The MS/MS data were obtained by multiple reaction monitoring (MRM) (in positive ion mode). For the mass spectrometer setting, the voltage was set to 3.5 kV and the source temperature was kept at 300°C. The LC/MS/MS data was normalised with internal standard and protein concentration.

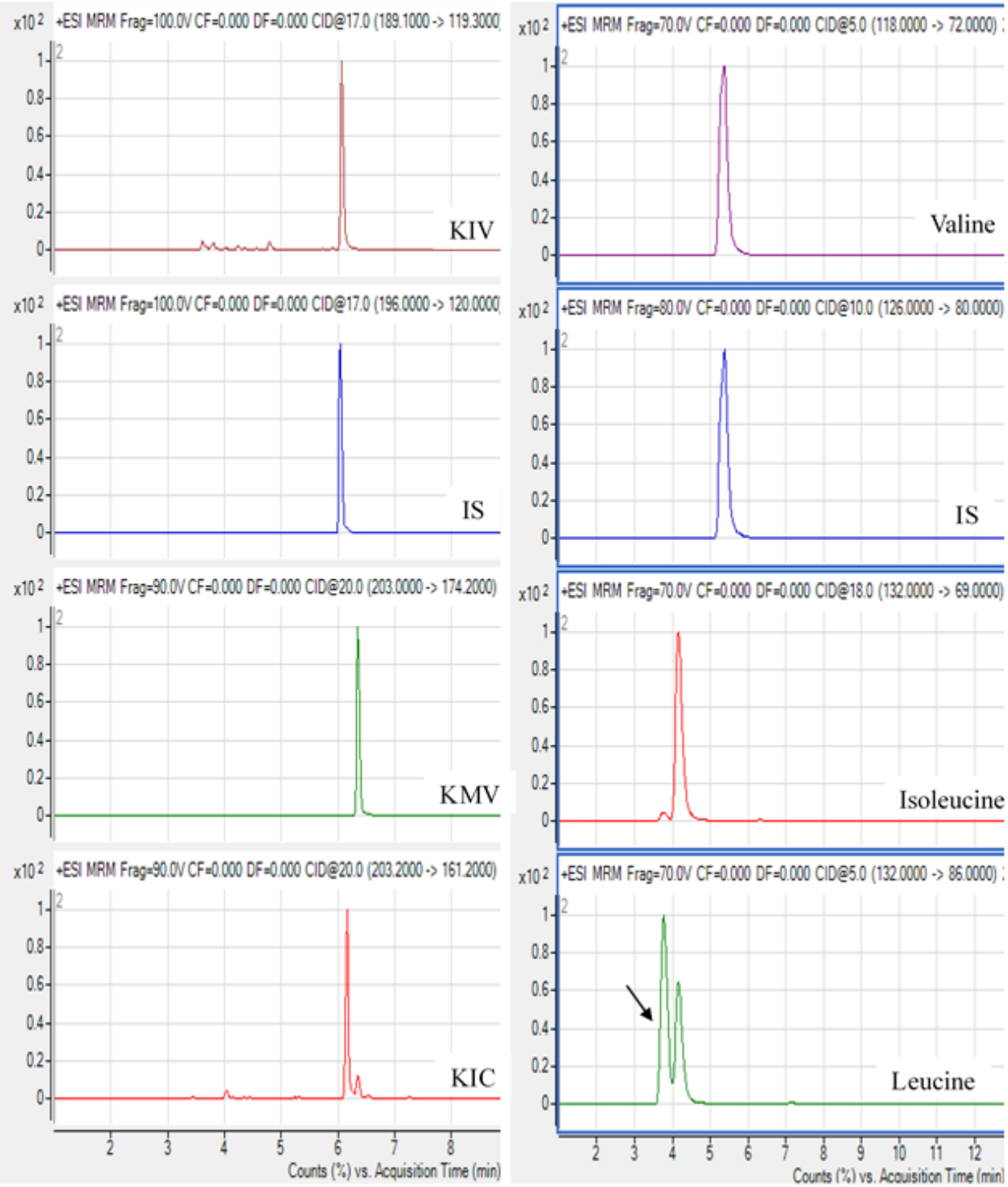

Figure 2.4: BCAAs and BCKAs detection by LC-MS/MS. Representative chromatogram showing detection of BCAAs and BCKAs.

HPLC-gradient for mobile phase

Amide column			C18 column		
Time (minutes)	A (%)	B (%)	Time (minutes)	A (%)	B (%)
0.00	2	98	0.00	98	2
4.00	2	98	2.00	98	2
10.00	30	70	5.00	60	40
12.00	50	50	6.00	40	60
14.00	50	50	9.00	40	60
17.00	2	98	11.00	98	2
19.00	2	98	13.00	98	2

2.2.14 Seahorse analysis for OCR and ECAR measurement

The seahorse experiment was performed as per the instruction given (from the Agilent). Briefly, the cells were seeded (30x10^6 or depending upon the cell type) in each well a day before the experiment (no cells in the blank). For the tissue samples, the islet capture plate was used, and a small piece of tissue (~2-3mg) was placed and fixed in the islet capture plate. The sensor cartridge was put for hydration by placing 1ml calibrant in each well in the non-CO2 incubator overnight at 37˚C and the seahorse analyser and software were connected for overnight warming. On day 2, the XF media was prepared by adding glucose, glutamine, and pyruvate to it and the pH was adjusted to 7.4. Following, the cells were washed twice with XF-media and added 500ul of fresh media, and placed the cell culture plate to in a non-CO2 incubator meanwhile the drugs (including oligomycin, FCCP, and antimycin A/Rotenone) for the treatment were prepared in XF-media. The 10x final concentration of each drug was added to the respective port (A, B, C, and D) of the sensor cartridge and it was placed in the seahorse analysis machine for calibration for 30 minutes and the program for the reaction run was also set up. Following calibration, the cells plate or islet capture plate was placed in a seahorse

analyser and allowed the reaction to run. At the end of the reaction, the data was collected and analyzed using the seahorse analysis software. For the normalization of data, the protein amount in each sample was quantified using the BCA method.

2.2.15 β-Galactosidase staining

The β-Galactosidase staining to access the senescence in adipose tissue was performed using the kit assay (Senescence β-Galactosidase Staining Kit #9860) as per kit instructions. Briefly, the fresh tissue collected during the cull of mice was washed with 1XPBS and fixed in 1xfixative solution overnight at RT. The staining solution was prepared as mentioned in the kit by adding different components. After overnight incubation, the fixative was replaced with the staining solution and the plate was sealed with a cover and placed at 37˚C incubator. The tissue samples were checked every two hours to see the colour. Once the colour was developed the reaction was stopped by placing the tissue in a sterile PBS buffer and the images were captured. For long-term storage, the tissue samples were stored in glycerol solution at 4˚C. The quantification was done using the ImageJ software.

2.2.16 siRNA transfection

The siRNA-mediated transfection was performed using Lipofectamine® 3000 Transfection (Thermo Fisher). Briefly, 80-100×10^4 SVF cells were seeded into each well of a six-well plate and cultured until they reached 70-80% confluency. The media was replaced with fresh media two hours before the transfection. The transfection, the siRNA oligo (75 pmol), and lipofectamine 3000 reagents (5μL) were separately diluted in 125μL of Opti-MEM media and mixed with gentle pipetting. The mixture of diluted lipofectamine and siRNA (transfection media) was incubated for 30 minutes at RT and added gently (dropwise) to cultured cells. The cell culture plate was swirled to evenly mix up the transfection media. The transfection media

was replaced with the fresh media after 7-8 hours of transfection and allowed to grow for 48 hours and cells were collected for further experiment.

2.2.17 RNA sequencing

RNA-seq (library preparation and sequencing run) was performed by BGI Health (HK). RNA was extracted using the RNeasy mini kit (Qiagen) following the manufacturer's instructions. Total RNA was quantified with NanoDrop (Thermo Fisher) and quality control was performed using an Agilent Bioanalyzer system (Agilent Technologies). Ribosomal RNA was depleted before library preparation, for which the DNBseq sequencing platform was used. Reads were aligned to a mouse reference genome GRCm38 using the STAR read aligner (STAR v2.7.10b). Differential gene expression analysis was performed using the DESeq2 package (v1.36.0) of Bioconductor in R. Gene set enrichment analysis (GSEA) was performed using Cluster Profiler package (v4.4.4) of Bioconductor in R.

2.2.18 Statistical analysis

GraphPad Prism 8.0 or SPSS was utilised for the data analysis and figures were created with GraphPad Prism 8.0.

Before the statistical analysis, the normality distribution of data was checked using the Anderson-Darling (A2*), D'Agostino-Pearson omnibus (K2), Shapiro-Wilk (W), and Kolmogorov-Smirnov (distance) test and Levene's test to check the equal variance. For the normally distributed data, a two-tailed independent t-test was used to compare two groups and one-way ANOVA with Bonferroni correction for the comparison among three or more groups. For the data that did not pass the normality test, the Mann–Whitney U test was used for comparison between the two groups, and the Kruskal-Wallis test with Dunn's multiple tests.

All data were represented as means ±SEM (unless specified) and a p-value <0.05 was treated as statistically significant

Chapter 3: Global genetic deletion of BCAA catabolic gene PPM1K causes adipose tissue dysfunction in a mouse model.

3.1 Introduction:

Adipose tissue serves as an energy reservoir to store excess energy. Normal BCAA levels are important for maintaining adipose tissue functions. BCAAs are utilised as a substrate for adipogenesis, lipogenesis, and thermogenesis in adipose tissue [77,81,84]. Both *in vitro* and *ex vivo* evidence showed that adipose tissue can metabolise a large amount of BCAAs [78,79 80]. The importance of BCAAs during the differentiation of pre-adipocytes is revealed by the higher consumption of BCAA in the differentiation process [81]. The acyl Co-A produced by BCAA catabolism can be used to synthesize monomethyl branched-chain fatty acids (mmBCFA) and utilized as a precursor for lipogenesis [77]. Both in humans and mice, BAT is reported to consume BCAA for thermogenesis and increases systemic BCAA clearance upon cold exposure [84]. These evidences suggest that an intact BCAA catabolic machinery is important for maintaining adipose tissue functions.

On the other hand, a positive association between increased plasma BCAA levels and obesity/T2D has been reported [42,49,50]. The protein PPM1K activates the rate-limiting enzyme BCKDH by dephosphorylating it and thus regulates the BCAA catabolism. Of note, PPM1K rs1440581 allele C was reported to be linked with increased serum Valine, total BCAAs, and cardiovascular disease (CVD) risk [55]. However, the role of defective BCAA catabolism in promoting adipose tissue dysfunction still needs to be explored.

Adipose tissue dysfunction is one of the primary factors contributing to the etiology of T2D. Unresolved inflammation, improper ECM remodeling (fibrosis), and insufficient angiogenic potential are the three major factors in the pathophysiology of dysfunctional adipose tissue in obesity or T2D [97].

The main objective of this chapter is to study the role of the BCAA catabolic gene PPM1K in the regulation of adipose tissue function and to delineate the underlying mechanism.

3.2 Results

3.2.1. PP1MK showed differential expression in sWAT in obese human subjects.

Elevated plasma BCAA levels are positively associated with a higher risk of developing obesity/T2D in different rodent models and human subjects [51–53]. Interestingly, the SNP of PPM1K is linked with higher serum BCAA and risk of obesity/T2D and NAFLD [55 56]. Based on these findings from the literature, two publicly human RNA sequencing datasets (GSE152991 and GSE159924) were utilised to check the expression of *PPM1K* under healthy and obese conditions. As expected the expression of *PPM1K* was reduced under obese conditions in both databases (Figure 3.1A, B). Although different studies have also shown reduced PPM1K expression in adipose tissue of HFD and streptozotocin (STZ)-induced T2D mouse models (91), however, the role of PPM1K in regulating adipose tissue functions remains elusive

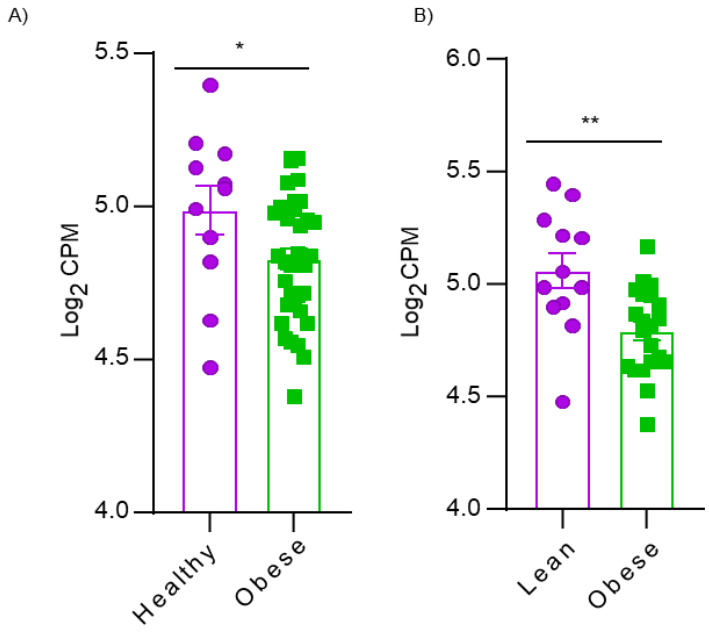

Figure 3.1: *PP1MK* showed differential expression in sWAT in obese human subjects. *PPM1K* expression in metabolically healthy and obese subjects in the human datasets

(GSE152991). B) *PPM1K* expression in lean and obese human datasets (GSE159924). Data are represented as mean ± SEM. *p < 0.05 and **p < 0.01.

3.2.2. PP1MK Global knockout (KO) mice displayed defects in glucose, lipids, and energy metabolism.

The RNA sequencing analysis using different human datasets showed differential expression of PPM1K. The obese subjects showed attenuated expression of PPM1K in sWAT as compared to healthy subjects. To further explore the role of PPM1K, the global KO mice were utilised, and these mice were fed on STC diet for six months. Different metabolic parameters were checked such as glucose tolerance, insulin sensitivity, triglyceride (TG) clearance, TG levels under different nutritional status, and oxygen consumption at different time points.

The metabolic characterization of PPM1K global KO mice showed defects in glucose, lipids, and energy metabolism. The KO mice showed a higher glucose intolerance and lower insulin sensitivity as compared to wild-type (WT) control as revealed by the glucose tolerance test (GTT) and insulin tolerance test (ITT) (Figure 3.2A, B). Further, the alteration in lipid metabolism was evaluated by checking the FFA and TG levels under feeding, fasting, and re-feeding conditions. The clearance of TG from the bloodstream was also checked by olive oil (gavage) as an external source of lipids. The levels of FFA and TG were increased in KO mice in comparison to WT control (Figure 3.2C, D). In addition, KO mice showed lower TG clearance as shown by higher levels of circulatory TG in KO mice (Figure 3.2E). The secretion of hepatic TG-VLDL was assessed by injecting the mice with tyloxapol via the tail vein. Tyloxapol is a lipase inhibitor that inhibits the catabolism of TG-VLDL in peripheral tissues. The circulatory TG levels were elevated significantly upon tyloxapol injection in KO mice (Figure 3.2F) suggesting the role of PPM1K in regulation of TG-VLDL secretion. The

metabolic cage analysis showed a reduction in oxygen consumption (VO2) suggesting a defect in energy expenditure in KO mice (Figure 3.2G). Thus, overall these data suggest that the absence of PPM1K affects glucose, insulin, lipid metabolism, and oxygen consumption.

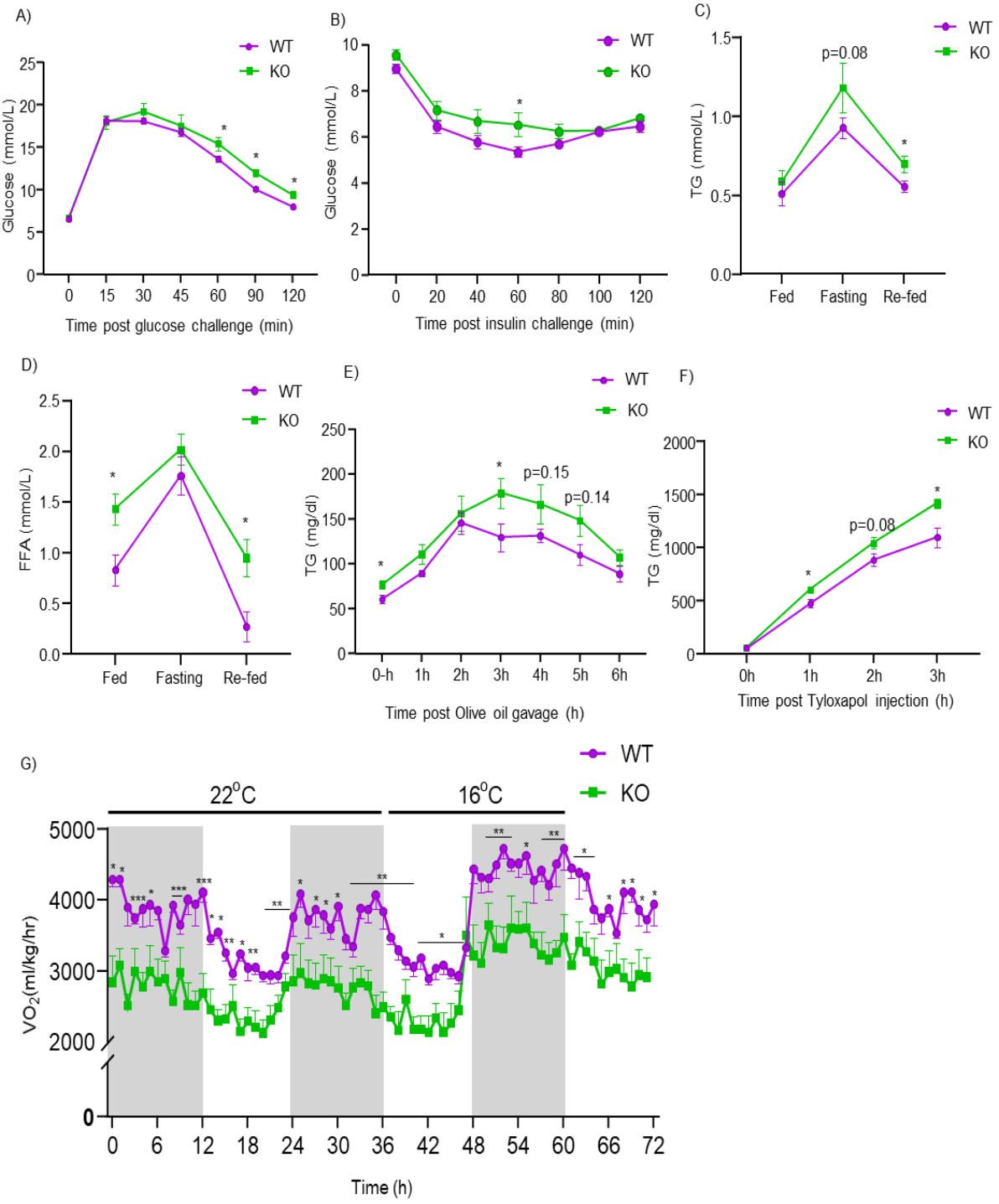

Figure 3.2: Genetic deletion of PPM1K causes defects in glucose, lipid, and energy metabolism. A) Intraperitoneal glucose tolerance test (2 g/kg BW) in 16-week-old mice PPM1K WT and KO mice. B) Insulin tolerance test (0.5IU insulin/kg BW) in 6-h fasted mice at 18 weeks. C) Serum TG levels during feeding, fasting (16h), and re-feeding state. D) Serum-FFA levels during feeding, fasting (16h), and re-feeding state. E) Serum TG levels during triglyceride clearance test using olive oil oral gavage in 16h fasted mice F) Serum TG levels after tyloxapol injection in the 16 h fasted mice. G) O_2 consumption (VO_2) measured in the Promethion metabolic cage. All data are represented as mean ± SEM. *$p < 0.05$ and **$p < 0.01$ (n=5-6).

3.2.3. Changes in tissue weight and serum biomarkers in PPM1K global KO mice.

Apart from changes in glucose, lipids, and energy metabolism, PPM1K KO mice were heavier than the WT mice. The increase in body weight may be due to higher fat mass and reduced lean mass (i.e. increase in adiposity) in KO mice. A post-cull weight measurement of different tissues also showed a higher adipose tissue weight (including eWAT, sWAT, and perirenal) in KO mice in comparison to WT (Table 3.1, &2).

Apart from body/tissue weight, changes were observed in different serum markers such as increased pro-inflammatory cytokines MCP1 and liver function marker ALT levels (Table 3.3). In further studies, histological analyses were performed to evaluate the role of PPM1K in inducing inflammation and liver function impairment. As expected, the serum BCAAs levels were significantly higher in KO mice as compared to WT. Hence, PPM1K deletion negatively affects different parameters including body/tissue weight and serum markers such as MCP1 ALT, and serum BCAA levels.

Table 3.1: Body and tissue weight (% of body weight)

	Mouse genotype		
Tissue weights	WT	KO	*P*
Body weight (g)	30.15±3.52	36.07±3.12	**
sWAT/ BW (%)	1.34±0.36	2.13±0.72	*
eWAT/BW (%)	3.24±0.97	5.56±1.41	**
Peri renal fat/BW (%)	0.84±0.24	1.27±0.28	**
BAT/BW (%)	0.40±0.07	0.35±0.07	NS
Liver/BW (%)	4.17±0.09	3.89±0.14	**

Kidneys/BW (%)	1.54±0.08	1.50±0.10	NS
Spleen/BW (%)	0.27±0.04	0.24±0.01	NS
Pancreas/BW (%)	0.89±0.25	0.85±0.20	NS
Muscle/BW (%)	0.045±0.00	0.036±0.00	*
Lean mass/BW (%)	66.72±3.42	57.95±2.89	**
Fat mass/BW (%)	13.57±2.08	18.13±3.97	*

* All data are represented as mean ± SD. *p < 0.05 and **p < 0.01.

Table 3.2: Body and tissue weight (actual values in grams)

	Mouse genotype		
Tissue weights	WT	KO	*P*
Body weight (g)	30.15±3.52	36.07±3.12	**
sWAT (g)	0.41±0.14	0.78±0.33	*
eWAT(g)	1.00±0.40	2.02±0.58	**
Peri renal fat (g)	0.26±0.10	0.46±0.11	**
BAT (g)	0.12±0.03	0.12±0.03	NS
Liver (g)	1.25±0.14	1.40±0.13	NS
Kidneys (g)	0.46±0.05	0.54±0.04	*
Spleen (g)	0.08±0.01	0.08±0.00	NS
Pancreas (g)	0.89±0.7	0.85±0.61	NS
Muscle (g)	0.013±0.00	0.013±0.00	NS

Lean mass (g)	19.88±1.60	21.16±0.73	NS
Fat mass (g)	4.10±1.00	6.70±1.85	**

* All data are represented as mean ± SD. *p < 0.05 and **p < 0.01 (n=5-6).

Table 3.3: Serum markers

	Mouse genotype		
Characteristics	WT	KO	P
Glucose (mmol/L)	8.77±0.69	8.81±1.28	NS
Adiponectin (ug/mL)	32.92±6.08	33.25±3.39	NS
MCP1 (pg/mL)	12.72±5.28	20.95±8.63	0.09
ALT (U/L)	20.87±3.11	26.47±6.16	0.07
AST (U/L)	41.96±4.53	40.45±10.42	NS
HDL-C (mmol/L)	1.91±0.36	1.86±0.51	NS
LDL-C (mmol/L)	0.16±0.15	0.13±0.09	NS
Isoleucine (μM)	47.15±12.12	71.68±9.16	*
Leucine (μM)	246.03±34.18	479.75±62.36	**
Valine (μM)	140.65±13.47	190.11±13.17	**

* All data are represented as mean ± SD. *p < 0.05 and **p < 0.01.

3.2.4. PPM1K global KO mice showed higher levels of BCAA and BCKA in adipose tissue.

PPM1K expression regulates the BCAA catabolism by activating the BCKDH complex. Genetic deletion of PPM1K led to higher serum levels of BCAA (as shown in Table 3.2). Additionally, the BCAA and BCKA levels were also increased significantly in adipose tissue (eWAT) of KO mice. Thus, the accumulation of BCAAs and BCKAs in both serum and adipose tissues indicates the defective BCAA catabolism in KO mice.

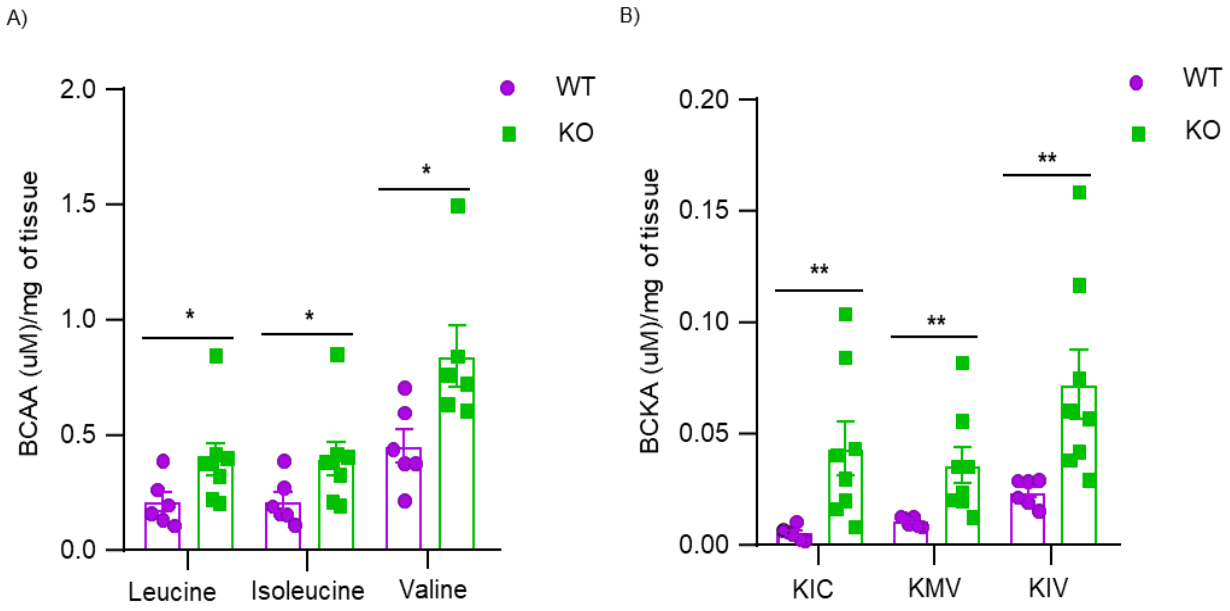

Figure 3.3: PPM1K global KO mice showed higher levels of BCAA and BCKA in adipose tissue. A) BCAAs, and B) BCKAs in adipose tissue of PPM1K WT and KO mice**.** All data are represented as mean ± SEM. *$p < 0.05$ and **$p < 0.01$.

3.2.5. Genetic deletion of PPM1K induces fibrosis in WAT, not in BAT and liver tissue.

The metabolic characterization data showed defects in glucose, lipids, and energy metabolism in KO mice. Of note, adipose tissue is important for maintaining several key regulatory functions including whole-body energy metabolism, insulin sensitivity and glucose homeostasis, and lipid metabolism. So, the next step was to assess the histological alteration in adipose tissue.

In healthy adipose tissue, ECM can be remodeled to accommodate normal fluctuations in adipocyte size. As a result of increased fibrosis, the rigidity of adipose tissue increases which further restricts the expandability of adipose tissue (reduced adipose tissue plasticity), resulting in ectopic lipid accumulation [119].

The Sirius red staining was performed to check the deposition of collagen fibres (fibrosis) in adipose tissues. Interestingly, increased fibrosis (more deposition of collagen fibres) is observed in WAT (both eWAT and sWAT) (Figure 3.4A) however the BAT did not follow the same trend in KO mice (Figure 3.4D). To further corroborate these findings, the expression of pro-fibrotic genes including *Acta2*, *Col1a1*, *Col3a1*, *Col4a1*, and *Col6a3* was checked in adipose tissue. Consistently with histological analysis data, the expression of pro-fibrotic genes increased in KO samples in WAT (Figure 3.4B, C). This data suggests that the global deletion of PPM1K causes fibrosis in WAT.

The next step was to examine if the fibrosis event was limited to WAT, so Picrosirius red staining was performed in the liver samples. Interestingly, no significant difference was observed in terms of fibrosis between WT and KO liver samples (Figure 3.4D).

Thus, these findings suggest that PPM1K deletion causes fibrosis in WAT but not in BAT and the liver.

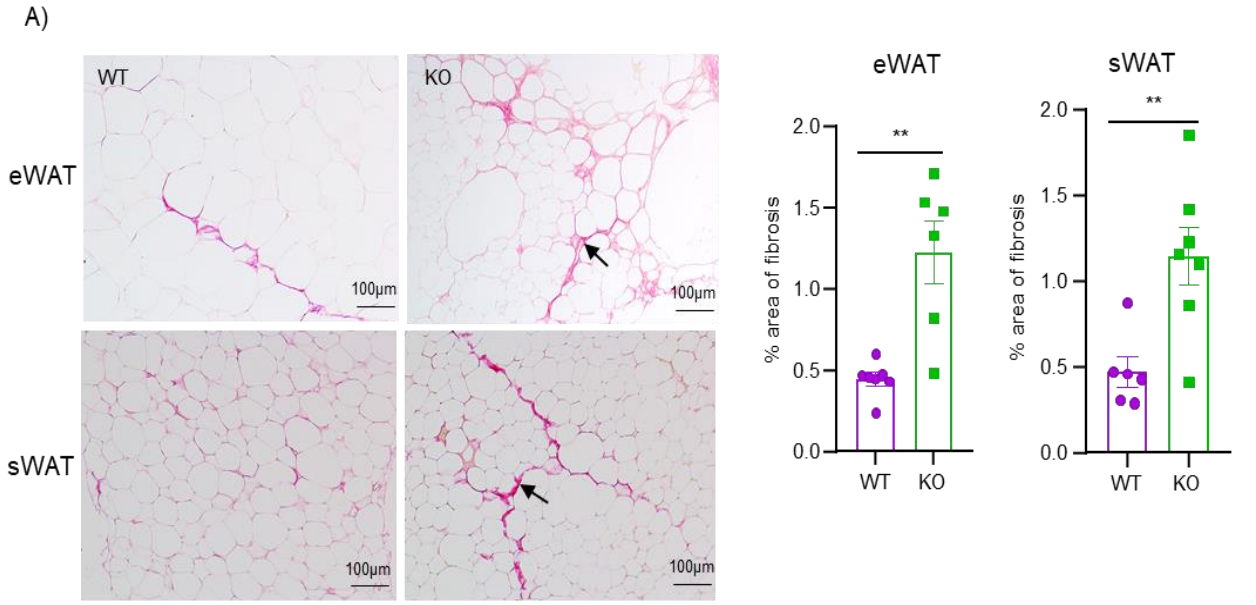
A)
WT
KO
eWAT
sWAT
100μm
eWAT
sWAT
% area of fibrosis
**
WT
KO

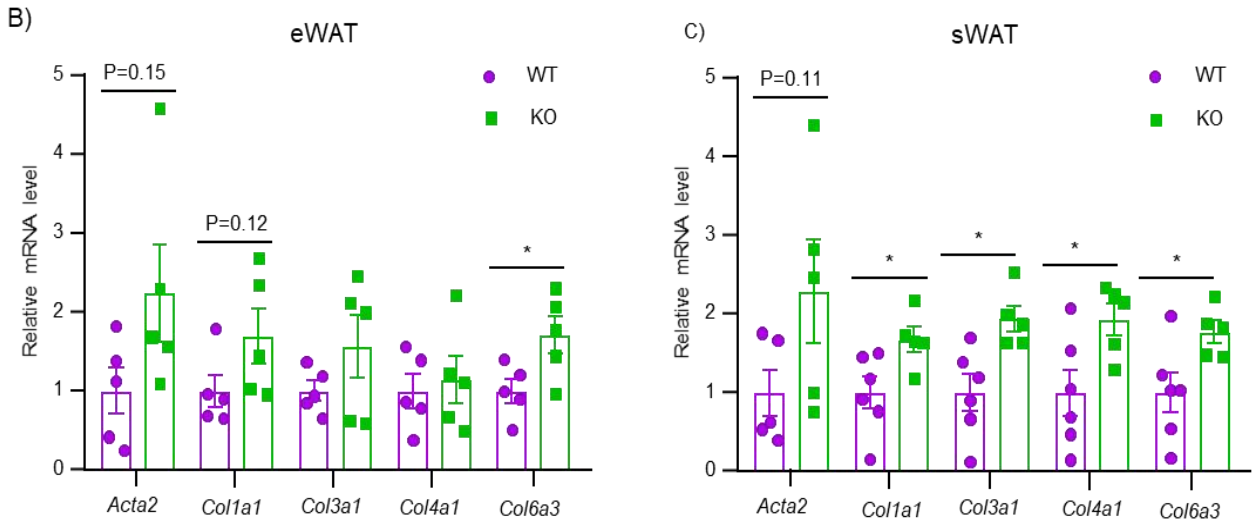
B)
eWAT
C)
sWAT
Relative mRNA level
P=0.15
P=0.12
P=0.11
*
WT
KO
Acta2
Col1a1
Col3a1
Col4a1
Col6a3

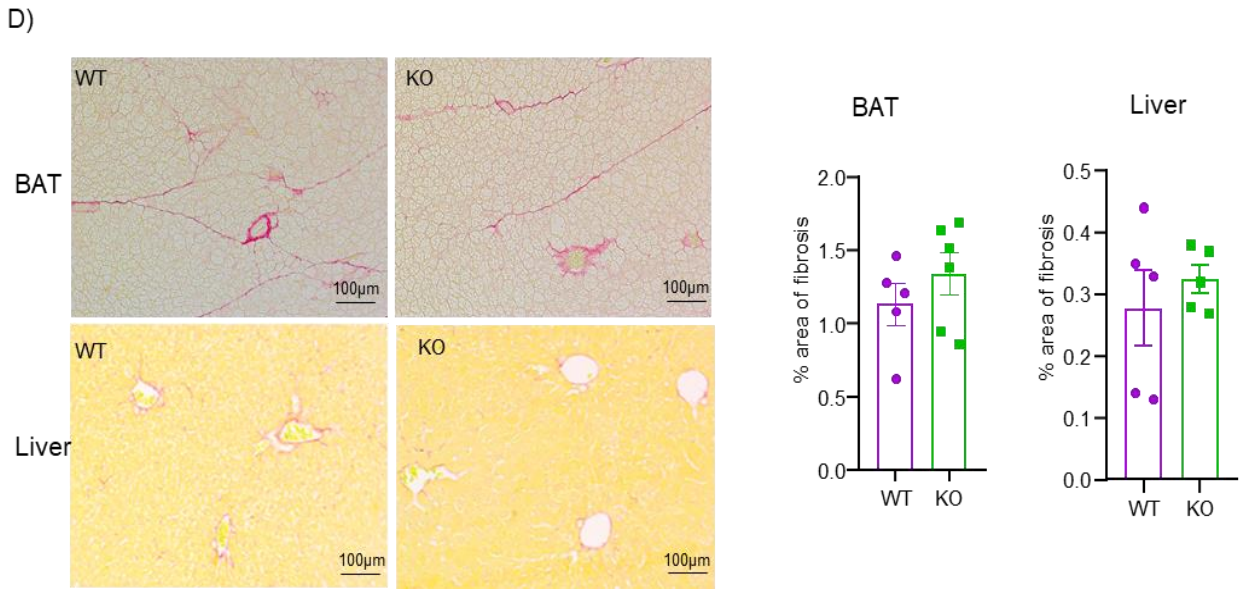

Figure 3.4: Genetic deletion of PPM1K induces fibrosis in WAT, not in BAT and liver tissue. A) Representative images and quantification data of picrosirius red staining in eWAT and sWAT from PPM1K-WT and KO mice; scale bar, 100um. mRNA expression of fibrosis markers in B) eWAT and C) sWAT of PPM1K-WT and KO mice (n=5-6). D) Representative images and quantification data of picrosirius red staining in BAT and liver of PPM1K-WT and KO mice (n=5-6) (as labelled in the figure). Data are represented as mean ± SEM. *p < 0.05 and **p < 0.01.

3.2.6. PPM1K absence leads to loss of cold tolerance and BAT whitening.

Although picrosirius red staining did not show any changes in BAT in terms of fibrosis, the other aspects of BAT functions were evaluated such as short-term cold challenge, lipid content, and cellularity of BAT. The short-term cold challenge experiments at 4^{o} C showed less tolerance to cold temperatures in KO as compared to WT mice (Figure 3.5A) since they could not maintain the core body temperature under cold conditions. Further, the histological analysis (H&E staining) data showed more lipid content and less cellularity in KO mice (Figure 3.5B, C). This data suggests the role of PPM1K in regulating thermogenesis and whitening in BAT. However, more experimental evidence such as UCP1 staining, and expression profile of thermogenic genes is further needed to evaluate it.

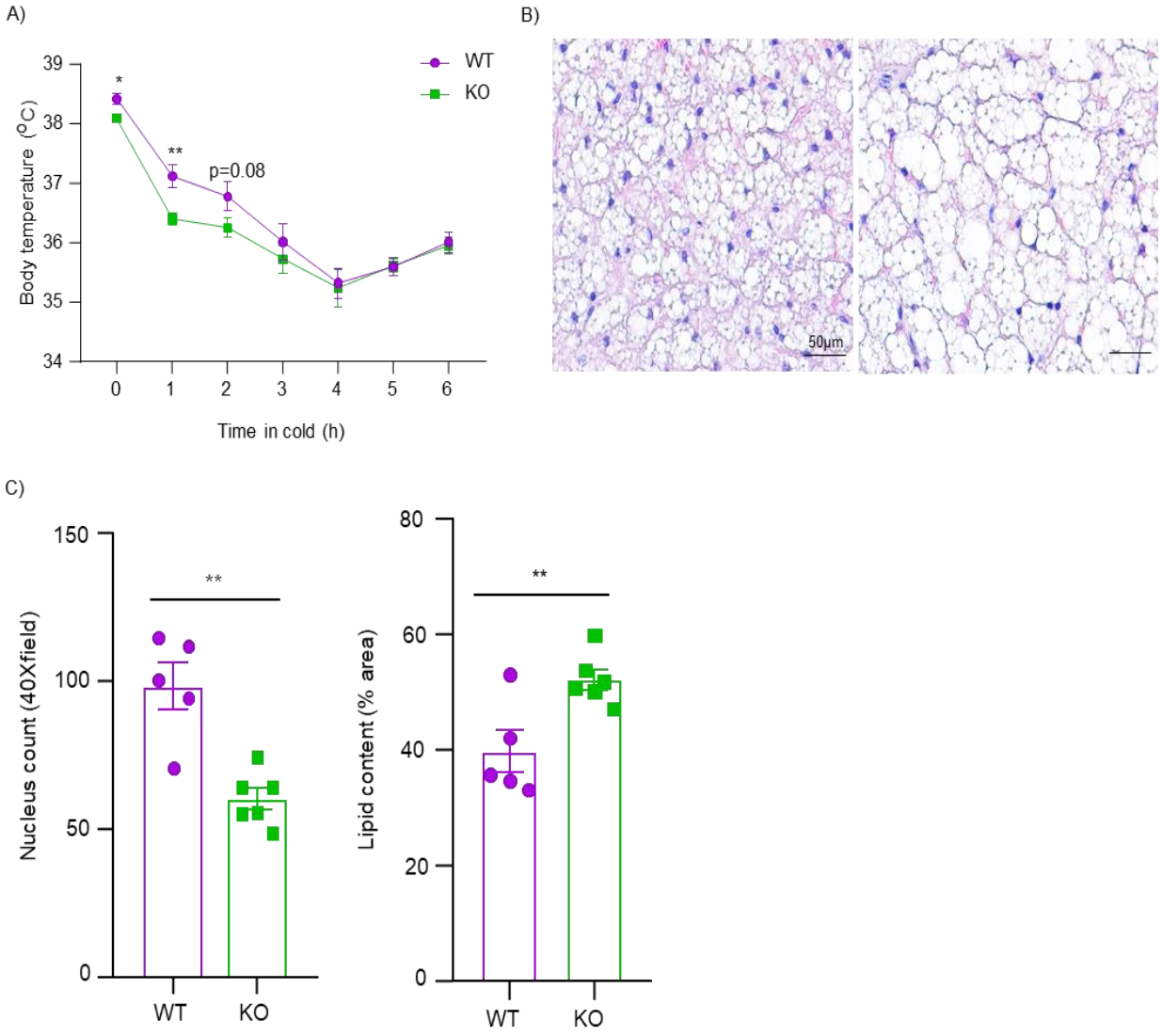

Figure 3.5: PPM1K absence led to loss of cold tolerance and brown adipose tissue whitening. A) Measurement of the cold body temperature response to short-term (6 hours) cold challenge at 4 °C, B) representative images, and C) quantification data of Hematoxylin and eosin (H&E) staining in BAT from PPM1K-WT and KO mice and quantitative analysis of cellularity and lipid content; scale bar, 100um (n=5-6). Data are represented as mean ± SEM. *p < 0.05 and **p < 0.01.

3.2.7. PPM1K showed a negative association with the expression of pro-fibrotic genes in sWAT in human databases.

The histological and mRNA expression profile data showed increased adipose tissue fibrosis in KO samples as compared to the WT control. The next step was to check if there was any association between *PPM1K* and pro-fibrosis genes in human adipose tissue samples. Different human datasets were analysed to check the correlation between *PPM1K* and the expression of pro-fibrotic genes in WAT. The human RNA sequencing data (GSE152991) consisting of metabolically healthy lean (MHL), metabolically healthy obese (MHO), and metabolically unhealthy obese (MHU) showed a negative correlation between *PPM1K* and pro-fibrotic genes (*COL3A1*, *LOXL1*, and *LOXL2*) in sWAT (Figure 3.6A). In addition, another human RNA sequencing database (GSE159924) comprised of lean and obese subjects also showed a negative correlation between PPM1K and pro-fibrosis genes (*COL13A1*, *COL5A1*, *CCN2*, *LOXL1*, and *LOXL2*) in sWAT (Figure 3.6B). These data further corroborated the findings of increased adipose tissue fibrosis in PPM1K-KO mice and its relevance in human samples too. Thus, PPM1K plays an important role in the pathophysiology of adipose tissue fibrosis.

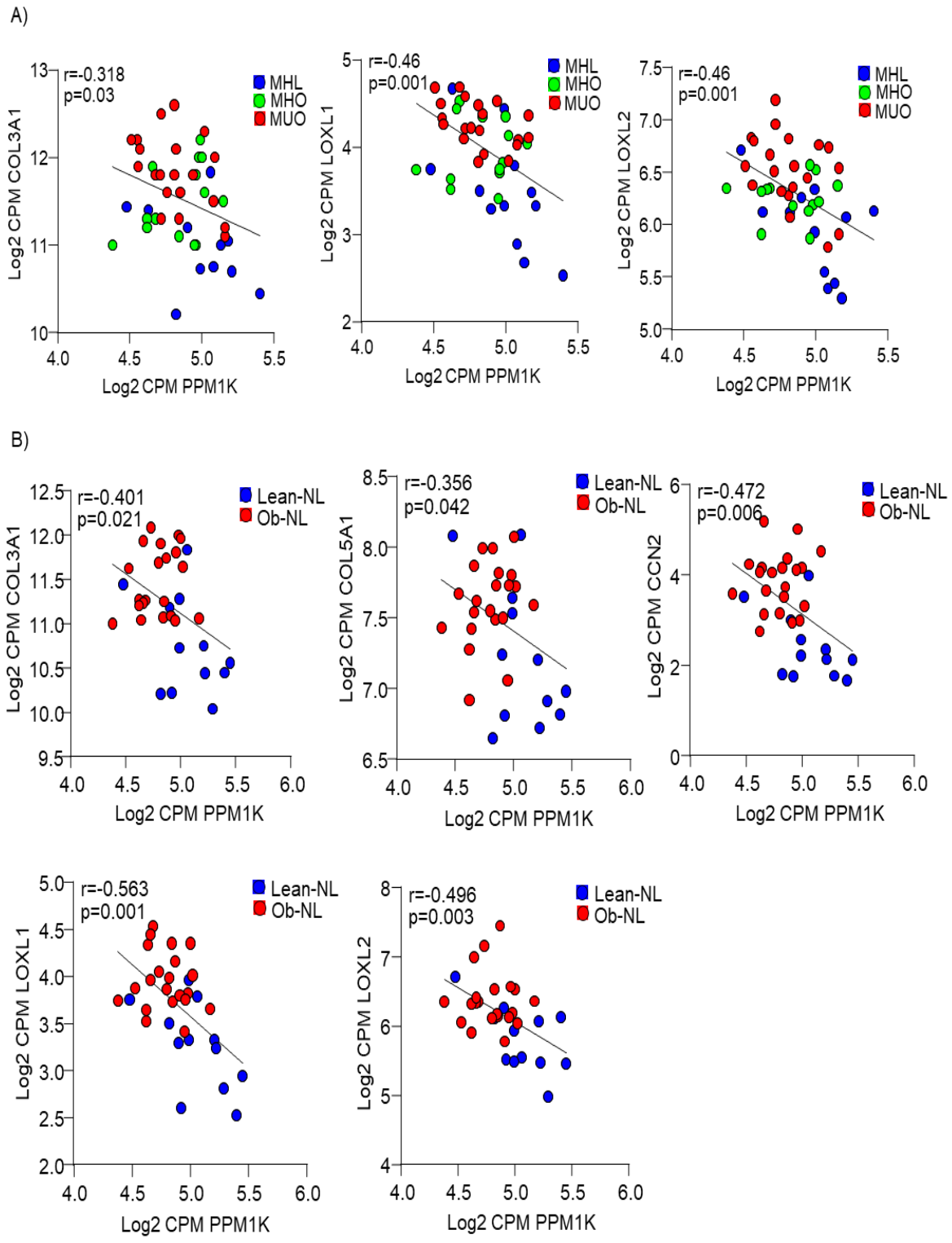

Figure 3.6: BCAA catabolic gene PPM1K showed a negative association with pro-fibrotic genes in sWAT in different human databases. A) Correlation analysis of PPM1K

with pro-fibrotic genes in sWAT of metabolically healthy lean (MHL), metabolically healthy obese (MHO), and metabolically unhealthy obese (MUO) in the human database (GEO GSE152991). B) Correlation analysis of PPM1K with pro-fibrotic genes in sWAT of lean-normal liver (lean-NL), and obese-normal liver (ob-NL) using human database (GEO GSE159924). The SPSS software is used for the correlation analysis. *$p < 0.05$ and **$p < 0.01$.

3.2.8. PPM1K KO showed increased fibrosis and attenuated adipogenesis in SVF but no changes in mature adipocyte fraction.

Both histological and qPCR analyses showed a higher degree of fibrosis in WAT. In addition, the human datasets analyses showed a negative correlation between PPM1K and pro-fibrotic gene expression in sWAT. For both analyses, including mice tissue samples and human datasets, the whole adipose tissue is used.

Upon enzymatic digestion, adipose tissue yields two fractions including SVF (containing different cell types) and mature adipocyte fraction. Both fractions were collected from the sWAT of PPM1K WT and KO mice and were checked for the fibrotic gene expression profile (such as *Acta2*, *Col1a1*, *Col3a1*, *Col4a1*, and *Col6a3*). Since BCAA catabolism is reported to play a role in adipogenesis, the expression of adipogenic genes including *Adipoq*, *Cebpa*, *Fabp4*, and *Ppary* were also checked. Interestingly, SVF from KO mice showed increased fibrosis and attenuated adipogenesis (Figure 3.7A) whereas adipocyte fraction did not show any significant changes in the expression of fibrosis and adipogenesis markers (Figure 3.7B). Further, the immunofluorescence staining (IF) and western blotting of ACTA2 protein was performed on SVF to support the findings of qPCR data. In line with qPCR, both IF and western blotting data showed elevated expression of ACAT2 in SVF (Figure 3.7D).

Therefore, these data suggest that the global absence of PPM1K led to increased fibrosis and impaired adipogenesis in SVF but did not affect the mature adipocytes.

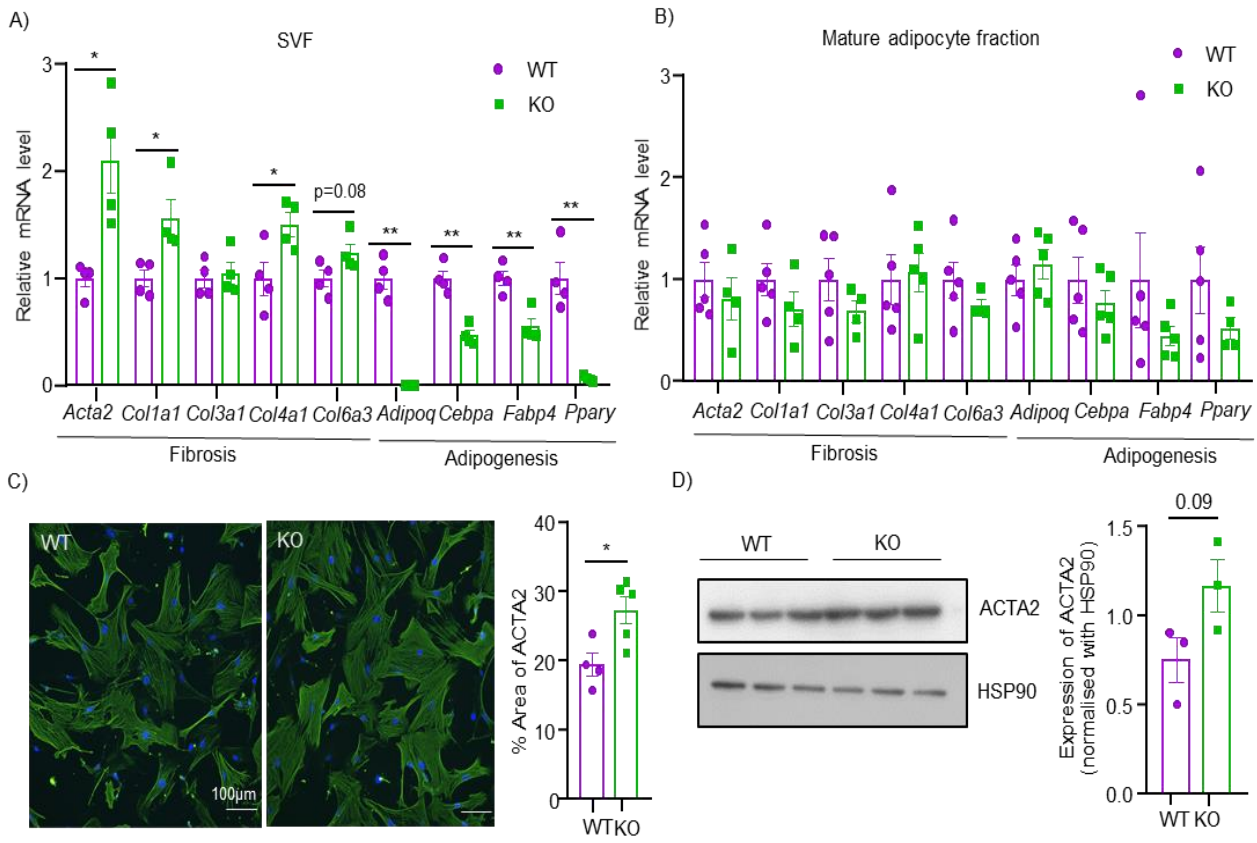

Figure 3.7: PPM1K KO showed increased fibrosis and attenuated adipogenesis in SVF but no changes in mature adipocyte fraction. A) mRNA expression of fibrosis and adipogenesis markers in SVF and B) in mature adipocyte fraction from sWAT of PPM1K-WT and KO mice. C) Representative immunofluorescence image of ACTA2 in SVF and D) Immunoblotting of ACTA2 in SVF from sWAT of PPM1K WT and KO. All data are presented as mean ± SEM. *p < 0.05 and **p < 0.01.

3.2.9. Absence of PPM1K in SVF leads to fibrosis and impaired adipogenesis *ex-vivo*.

Following adipose tissue digestion, only SVF showed increased fibrosis and impaired adipogenesis, but no changes were observed in the mature adipocyte fraction both in terms of fibrosis and adipogenesis. To further check the adipogenic and fibrogenic potential of SVF *ex-vivo*, the SVF was differentiated into mature adipocytes and observed at different time points during the differentiation process. The cells were collected on the 6-7th day following the addition of the differentiation cocktail and ORO staining (for lipid droplets) and qPCR for fibrotic and adipogenesis markers were performed. The ORO staining data showed the formation of more lipid droplets (more differentiation capacity) in mature adipocytes derived from the WT-SVF as compared to the KO-SVF (Figure 3.8A). Additionally, the qPCR data showed increased fibrosis (such as expression of *Col1a1*, *Col4a1*, and *Col6a3*) and adipogenesis markers *Adipoq* and *Cebpa* in mature adipocytes derived from KO-SVF samples as compared to WT-SVF (Figure 3.8B).

To further support the findings, the absence of PPM1K in SVF causes fibrosis and impairs adipogenesis, SVF was isolated from C57/B6 WT mice and cultured. The siRNA-mediated transfection was performed to knock down the *Ppm1k* gene in SVF. The transfection efficiency was demonstrated by the greater than 60% reduction in mRNA expression of *Ppm1k* in the siPpm1k group in comparison with scramble control (Figure 3.8C). The qPCR data showed upregulation of pro-fibrotic genes *Acta2* and *Col4a1* and downregulation of adipogenic genes including *Adipoq*, *Cebpa*, *Fabp4*, and *Ppary* upon *Ppm1k* knockdown in SVF (Figure 3.8D).

These data suggest the absence of PPM1K in SVF induces fibrosis and attenuates the differentiation capability of SVF into mature adipocytes.

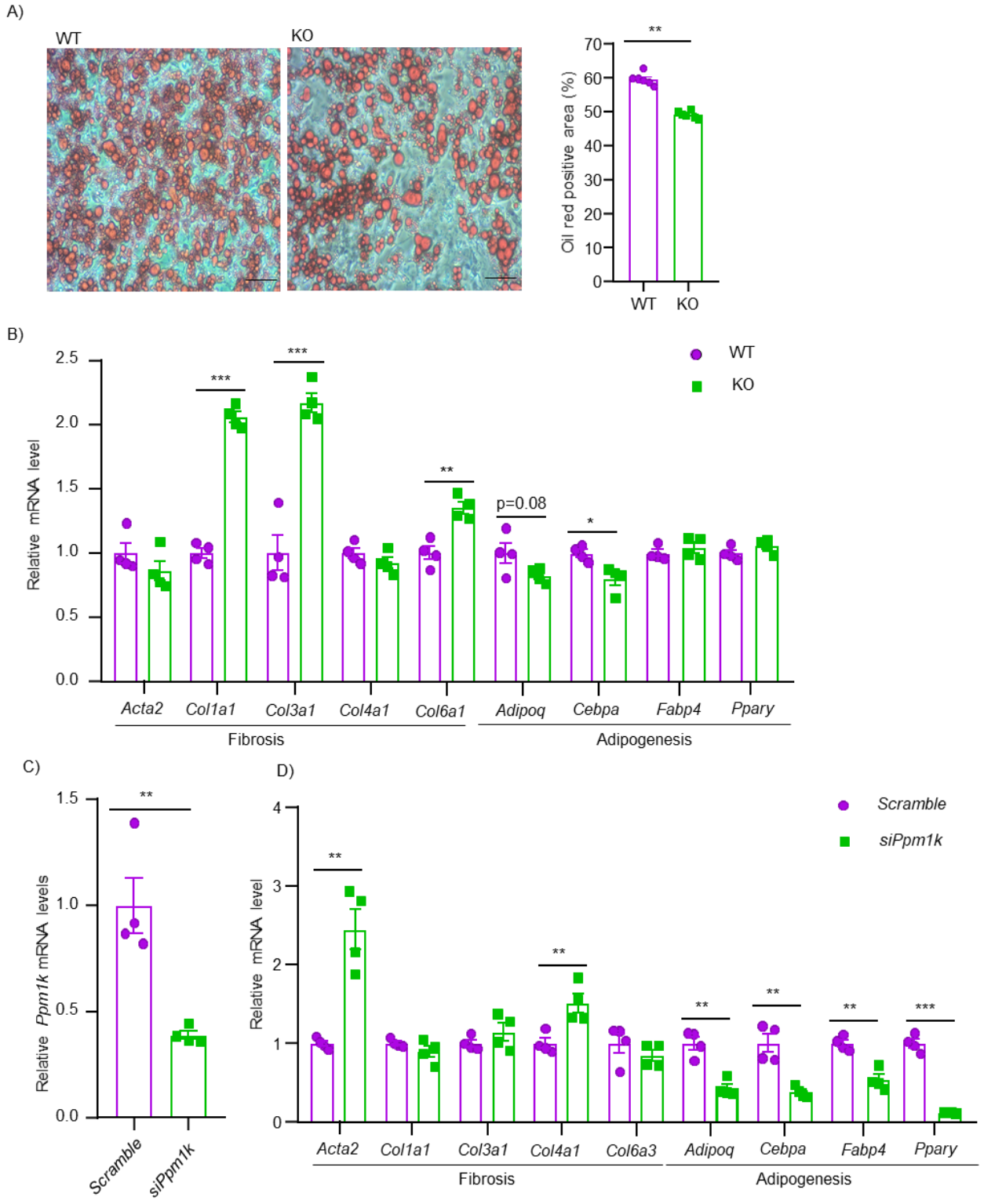

Figure 3.8: Absence of PPM1K in SVF leads to fibrosis and impaired adipogenesis *ex-vivo.* A) Representative Oil Red O staining of lipid droplets in mature adipocytes derived from

PPM1K WT and KO SVF (6-8 weeks old). B) mRNA expression of fibrosis and adipogenesis markers in mature adipocytes derived from SVF isolated from sWAT of PPM1K-WT and KO mice. C) SVF were isolated, cultured, and transfected with siRNA against *Ppm1k* and respect control. Transfection efficiency as depicted by mRNA level of *Ppm1k* in the scramble and *siPpm1k* transfected SVF. D) mRNA expression of fibrosis and adipogenesis markers in SVF transfected with scramble and *Ppm1k* siRNA. All data are presented as mean ± SEM. *$p < 0.05$ and **$p < 0.01$.

3.2.10. Deficiency of PPM1K causes inflammation in WAT.

Fibrosis and inflammation are the characteristic features of adipose tissue dysfunction and are linked to insulin resistance and T2D [118]. Adipose tissue inflammation and fibrosis are interlinked, although the sequence of these events is not well understood.

Firstly, the infiltration of immune cells in WAT was evaluated using H&E staining. The data showed more infiltration of immune-like cells and crown-like structure (CLS) in KO samples as compared to WT (Figure 3.9A). The IF co-staining using F4/80 (macrophage marker) and iNOS (M1 macrophage marker) was performed to see if the infiltrated immune cells are inflammatory M1 macrophage. In line with H&E staining data, the KO showed more macrophage infiltration i.e. M1 macrophages (Figure 3.9B, D). The mRNA expression profile of pro-inflammatory cytokines did not show significant changes (Figure 3.9F, G) (except the *Mcp1* and *F4/80* in sWAT). The flow cytometry analysis was also used to check the percentage of M1 and M2 macrophages in adipose tissue. In eWAT, a higher percentage of M1 macrophages and a low percentage of M2 macrophages were observed in KO as compared to WT (Figure 3.9H). However, in sWAT no significant difference is observed in M1 and M2 macrophage populations in flow cytometry analysis (Figure 3.9I).

These findings suggest that a deficiency of PPM1K leads to adipose tissue inflammation.

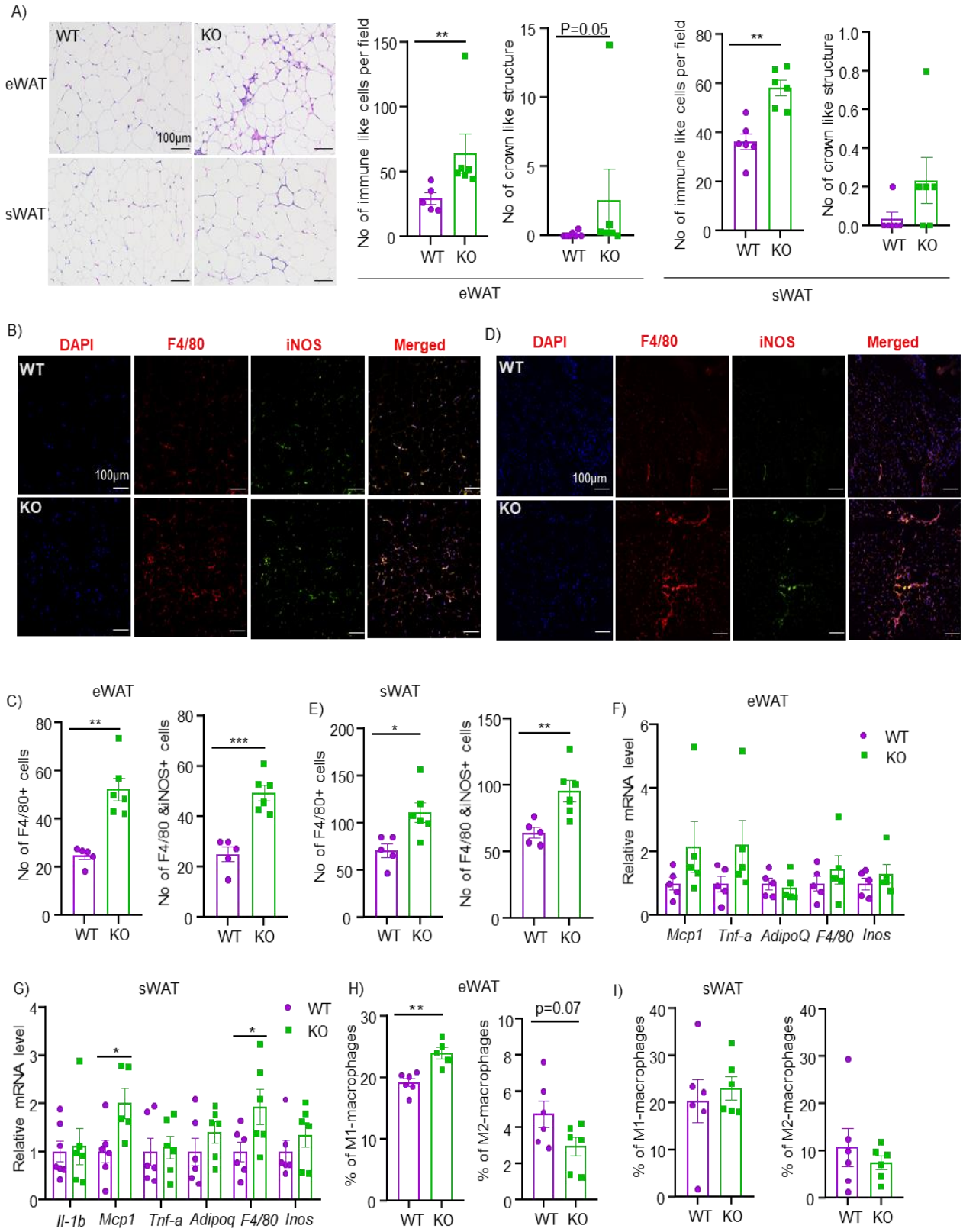
A)
WT
KO
eWAT
sWAT
100μm
No of immune like cells per field
No of crown like structure
**
P=0.05
WT KO
eWAT
sWAT
B)
DAPI
F4/80
iNOS
Merged
D)
C)
No of F4/80+ cells
No of F4/80 &iNOS+ cells
***
E)
F)
Relative mRNA level
Mcp1
Tnf-a
AdipoQ
F4/80
Inos
G)
Il-1b
Adipoq
H)
% of M1-macrophages
% of M2-macrophages
p=0.07
I)

Figure 3.9: Deficiency of PPM1K causes inflammation in WAT. A) Representative images and quantification data (immune cells and crown-like structure) of H&E staining in eWAT and sWAT from PPM1K-WT and KO mice; scale bar, 100um. Representative images and quantification data of immunofluorescence staining of F4/80 and iNOS in B, C) eWAT and D, E) sWAT from PPM1K-WT and KO mice; scale bar, 100um. mRNA expression of different cytokines in F) eWAT and G) sWAT of PPM1K-WT and KO mice (n=5-6). M1 and M2 macrophage quantification using flow cytometry analysis in SVF of H) eWAT and I) sWAT of PPM1K-WT and KO mice (n=5-7). All data are represented as mean ± SEM. *$p < 0.05$ and **$p < 0.01$.

3.2.11. Adipose tissue fibrosis and inflammation caused by PPM1K deficiency are likely to mediate through activation of HIF-1A.

The PPM1K deletion caused fibrosis and inflammation in WAT. As per the literature, hypoxia is a major initiating factor for ECM induction and also upregulates the expression of inflammatory genes including IL-6 and macrophage inflammation factor 1 (MIF1) via HIF1 α induction [129] [131]. Apart from inducing the synthesis of ECM components, HIF-1 α may also induce a change in redox status, and affect the enzymes (lysyl oxidase and prolyl-4-hydroxylase) involved in collagen cross-linking and stabilization [130]. The fibrotic response is recused by the use of HIF1α inhibitor (PX-478) in fat depots of obese mice [131]. In addition, in a recent study hypoxia is positively associated with the expression of both pro-fibrotic and inflammatory genes in obese human subjects [98]. Based on this evidence from the literature, the involvement of HIF1α in the induction of WAT fibrosis and inflammation was investigated in PPM1K-KO mice.

Both whole tissue and SVF showed increased expression of *Hif1α a*nd its associated genes in PPM1K KO mice, suggesting the HIF1α induction (Figure 3.10A, B). Further, IF data showed a higher number of HIF1α positive cells in KO mice. The number of HIF1α and fibrosis marker ACTA2 co-stained cells was also higher in KO samples as compared to WT (Figure 3.10C). The macrophage marker F4/80 and HIF1α co-stained cells were also higher in KO samples (Figure 3.10D). These findings suggest that possibly the induction of HIF1α is causing increased fibrosis and inflammation in WAT although further experimental evidence is needed to prove it.

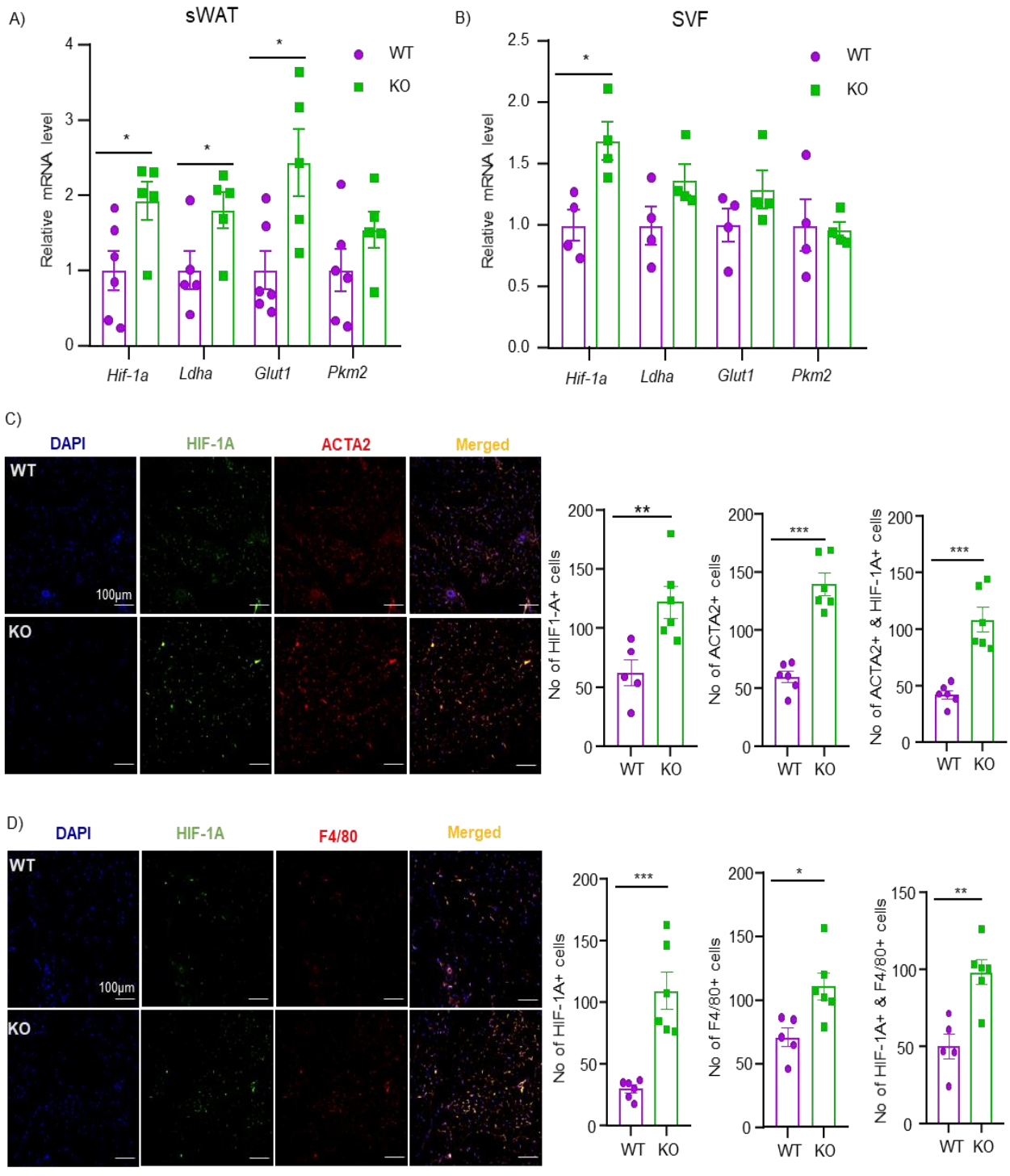

Figure 3.10: Adipose tissue fibrosis and inflammation caused by PPM1K deficiency are likely to mediate through activation of HIF-1A. A) mRNA expression of Hif-1a and related genes in sWAT (n=5-6) and B) SVF from PPM1K-WT and KO mice (n=4). C) Representative images and quantification data of immunofluorescence staining of HIF-1A and ACTA2, and

D) HIF-1A and F4/80 in sWAT from PPM1K-WT and KO mice; scale bar, 100um (n=5-7). All data are represented as mean ± SEM. *$p < 0.05$ and **$p < 0.01$.

3.3 Conclusion:

In this chapter, it was shown that the presence of PPM1K is important for maintaining metabolic health and adipose tissue functions. The genetic deletion of PPM1K led to defects in glucose, lipids, and energy metabolism. In addition, PPM1K deficiency caused defective BCAA catabolism as revealed by higher serum and adipose tissue levels of BCAAs and BCKAs. The absence of PPM1K affected the adipose tissue biology such as increased fibrosis and inflammation, attenuated adipogenesis in WAT, and whitening of BAT but no changes in liver fibrosis. Further, the *PPM1K* also showed a negative association with the pro-fibrotic genes in obese human subjects. Notably, the phenomena of increased fibrosis and reduced adipogenesis were observed only in SVF but not in mature adipocyte fraction in PPM1K KO mice. Coming to the mechanistic insight, the PPM1K deletion causes an increase in HIF1α in both adipose tissue and SVF. The activation of HIF1α is one of the major pathways known for inducing adipose tissue fibrosis. The increased expression of HIF1α in PPM1K KO mice is associated with an increase in the expression of pro-fibrosis and macrophage marker (F4/80) in adipose tissue as shown by the increase in the number of co-stained cells. It is speculated that adipose tissue fibrosis and inflammation induced by PPM1K deficiency are most likely caused by the activation of HIF1α.

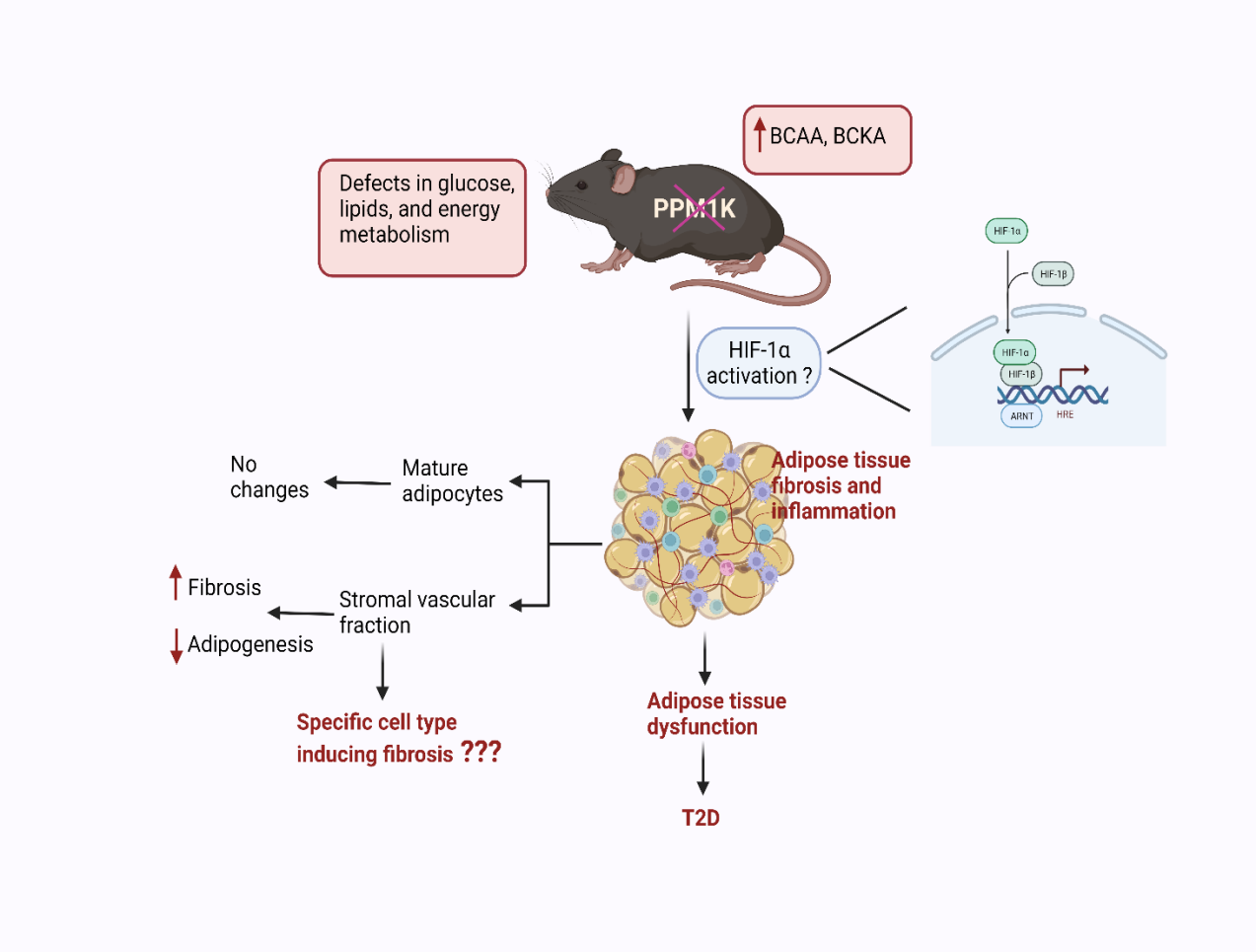

Figure 3.11: Summary diagram showing global deletion of PPM1K induces adipose tissue dysfunction.

Chapter 4: Adipocyte-specific deletion of PPM1K causes defects in glucose, lipid, and energy metabolism and circulatory BCKA levels.

4.1 Introduction:

In the last chapter, it was shown that global knockout of PPM1K causes adipose tissue dysfunctions including increased fibrosis and more infiltration of immune cells. In the global PPM1K-KO model, the PPM1K is absent in all tissues. So, it's difficult to pinpoint in which tissue the absence of PPM1K is inducing adipose tissue dysfunction in KO mice. This is one of the drawbacks of using global KO mice.

To address this issue, the adipocyte-specific PPM1K-KO (A-KO) mouse model was generated using the Cre-Lox system to study the role of adipocyte PPM1K. The tissue-specific KO mouse model is important for addressing the role of a particular gene in specific tissue. This chapter involves the generation and experimental validation of the adipocyte-specific PPM1K-KO, followed by the phenotypic and metabolic characterization under HFHC-feeding conditions.

4.2 Results

4.2.1. Successful generation of adipocyte-specific PPM1K-KO (A-KO) mouse model

To study the relevance of adipocyte PPM1K in regulating metabolic pathways, adipocyte-specific PPM1K knockout (A-KO) and wild-type (WT) mice were generated. In brief, A-KO mice were created by the deletion of exon three in the PPM1K gene using the Cre/LoxP system on C57/BL6 background. The PPM1K flox mice were bought from Nanjing Biomedical Research Institute (NBRI), China. The LoxP site was inserted between exons two and four (flox/flox mice) (Figure 4.1).

The successful generation of A-KO mice was validated using different methods. For the initial genotyping, the presence of flox/flox site and adipo-Cre was detected using the specific primers in ear biopsy samples. After the cull, the mRNA expression levels of *Ppm1k* were examined in different fat depots including eWAT, sWAT, and BAT. The expression of *Ppm1k* was reduced significantly in A-KO as compared to WT in all fat depots (Figure 4.1B). The mature adipocytes derived from SVF also showed reduced expression of *Ppm1k* in A-KO as compared to WT (Figure 4.1C). PPM1K is important for regulating the BCAA catabolism and its deletion leads to accumulation of downstream metabolites. So, levels of BCAAs and BCKAs in different fat depots were checked using mass spectrometry. As expected, the levels of BCAAs and BCKAs were observed higher in A-KO samples (Figure 4.1D, E)

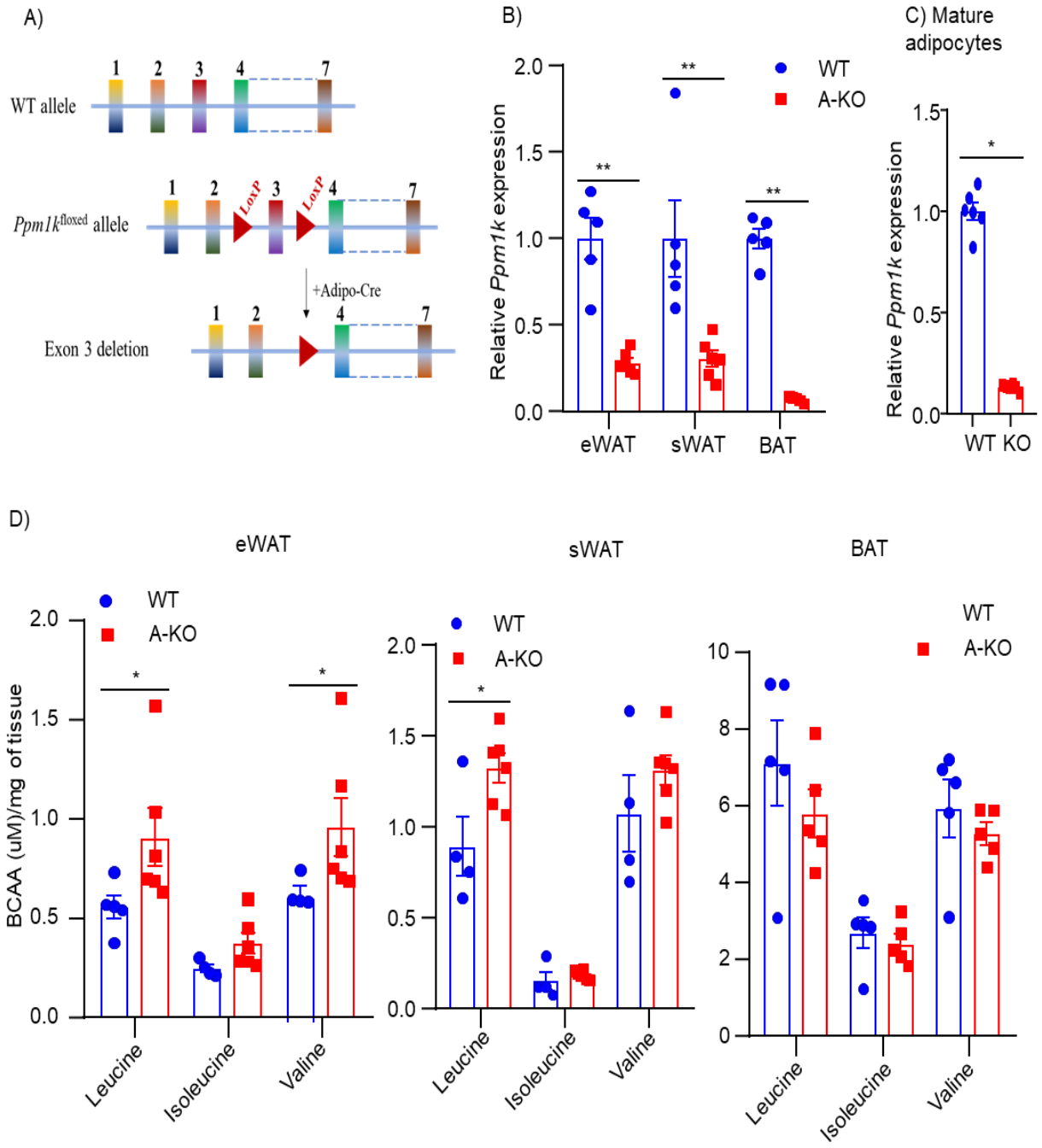
A)
WT allele
1 2 3 4 7
Ppm1k floxed allele
LoxP
LoxP
+Adipo-Cre
Exon 3 deletion
B)
WT
A-KO
Relative Ppm1k expression
eWAT
sWAT
BAT
C) Mature adipocytes
WT KO
D)
eWAT
sWAT
BAT
BCAA (uM)/mg of tissue
Leucine
Isoleucine
Valine

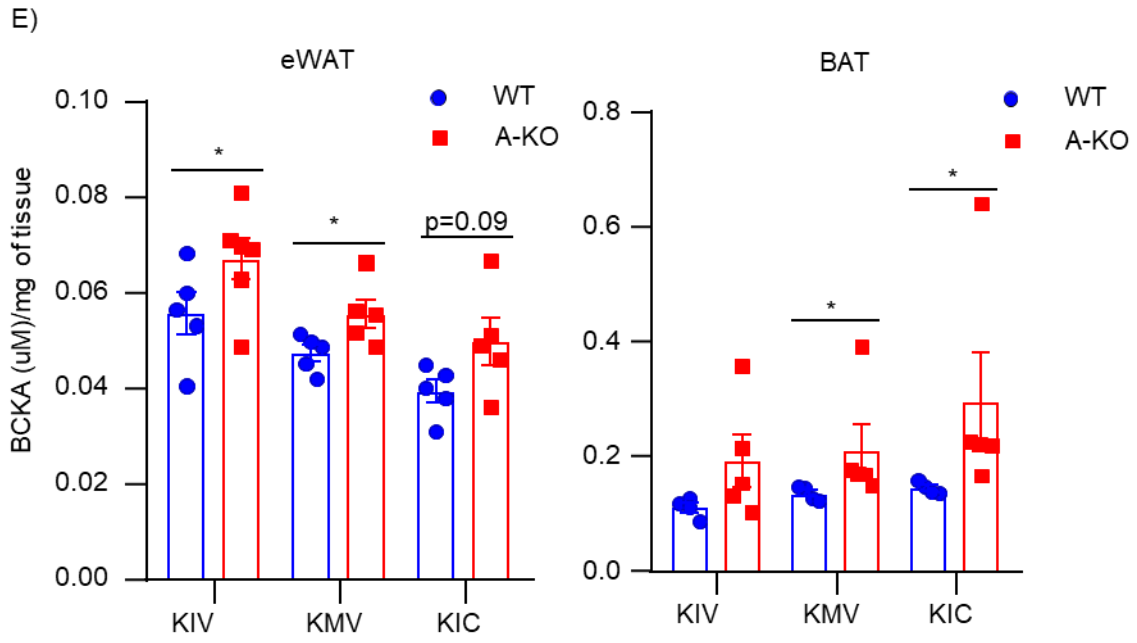

Figure 4.1: Successful generation of adipocyte-specific PPM1K-KO mice model. A) mRNA expression of *Ppm1k* in eWAT, sWAT, and BAT in WT and A-KO mice (n=5-6, 6 months old). B) *Ppm1k* expression in mature adipocytes derived from SVF from WT and A-KO mice (age: 2-3 months old). C) BCAAs levels in adipose tissue (eWAT, sWAT, and BAT) and D) BCKAs levels in adipose tissue (eWAT, and BAT) of WT and A-KO mice (n=5-6, 6 months old)**.** All data are presented as mean ± SEM. *p < 0.05 and **p < 0.01.

4.2.2. Adipocyte-specific deletion of PPM1K induces glucose intolerance, insulin resistance, and impairment in lipid metabolism.

The WT and A-KO were placed on HFHC (at 8-9 weeks) to investigate the role of adipocyte-PPM1K in pathophysiological settings such as obesity and NAFLD. Both WT and A-KO mice showed an increase in weight following the HFHC diet but the gain in body weight was significantly higher in A-KO mice (Figure 4.2A) (and also higher fat mass, data is not shown here). The A-KO showed higher glucose intolerance as observed in GTT (Figure 4.2B) and low insulin sensitivity in ITT (Figure 4.2D) as compared to the WT control. Thus, adipocyte deletion of PPM1K led to the development of insulin resistance.

Further, the effect of adipocyte PPM1K deficiency on lipid metabolism was evaluated. As compared to WT, A-KO mice showed low clearance of circulating TG following olive oil oral gavage (Figure 4.2F). In addition, the levels of free fatty acids (Figure 4.2H), β-hydroxybutyrate Figure 4.2I), and TG serum levels (Figure 4.2J) were also elevated in A-KO mice under fasting and re-feeding state compared to WT. Altogether, these data demonstrate that deletion of adipocyte PPM1K induces glucose intolerance and impaired lipid metabolism including delayed TG-clearance.

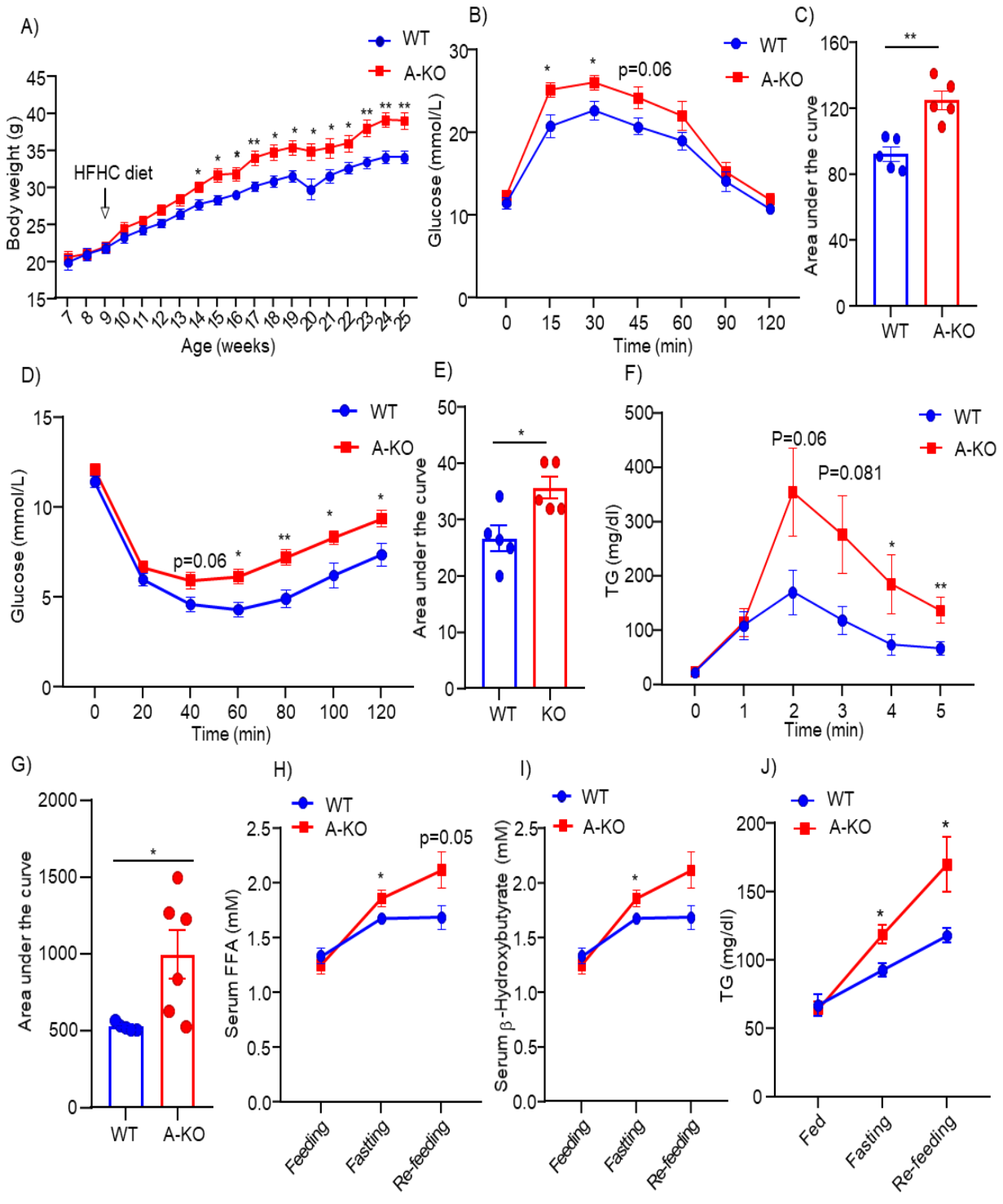

Figure 4.2: Adipocyte-specific deletion of PPM1K induces glucose intolerance, insulin resistance, and impairment in lipid metabolism. The mice were fed on the HFHC diet for 18-19 weeks and sacrificed at the age of 27-28 weeks. A) Body weight measurement after

weaning and following HFHC-diet intervention. B) Intraperitoneal glucose tolerance test (2 g/kg BW) post 12-weeks HFHC feeding in WT and A-KO mice. C) GTT-area under the curve (AUC). D) Insulin tolerance test (0.75IU insulin/kg BW) in 6-h fasted mice post 10-weeks HFHC-feeding. E) ITT-AUC. F) Serum TG levels during triglyceride clearance test using olive oil oral gavage in 16h fasted mice post 8-weeks HFHC-feeding. G) AUG-TG clearance test. H) Serum-free fatty acid, I) β-hydroxybutyrate, and J) TG levels during feeding, fasting (16h), and re-feeding state post 14^{th} week of HFHC feeding (n=5-6). All data are represented as mean ± SEM. *$p < 0.05$ and **$p < 0.01$.

4.2.3. Adipocyte-specific PPM1K-KO has defective energy metabolism.

The imbalance between energy intake and energy expense is observed during obesity and its associated dysfunctions. The effect of adipocyte PPM1K deletion was evaluated on energy metabolism by checking the oxygen consumption, carbon dioxide production, and energy expense after 10 weeks of HFHC feeding. The oxygen consumption was lower in A-KO mice under different temperatures (including 32^0C, 22^0C, 16^0C, and 4^0C) conditions as compared to WT (Figure 4.3A). The same trend was observed for carbon dioxide production (Figure 4.3B). The changes in oxygen consumption and carbon dioxide production were more prominent at 22^0C, 16^0C, and 4^0C as compared to 32^0C. The energy expense was also lower in A-KO mice as compared to WT (Figure 4.3C).

Collectively, these data suggest that deletion of adipocyte PPM1K impairs energy expenditure in mice. Thus, adipocyte PPM1K is important for maintaining energy homeostasis.

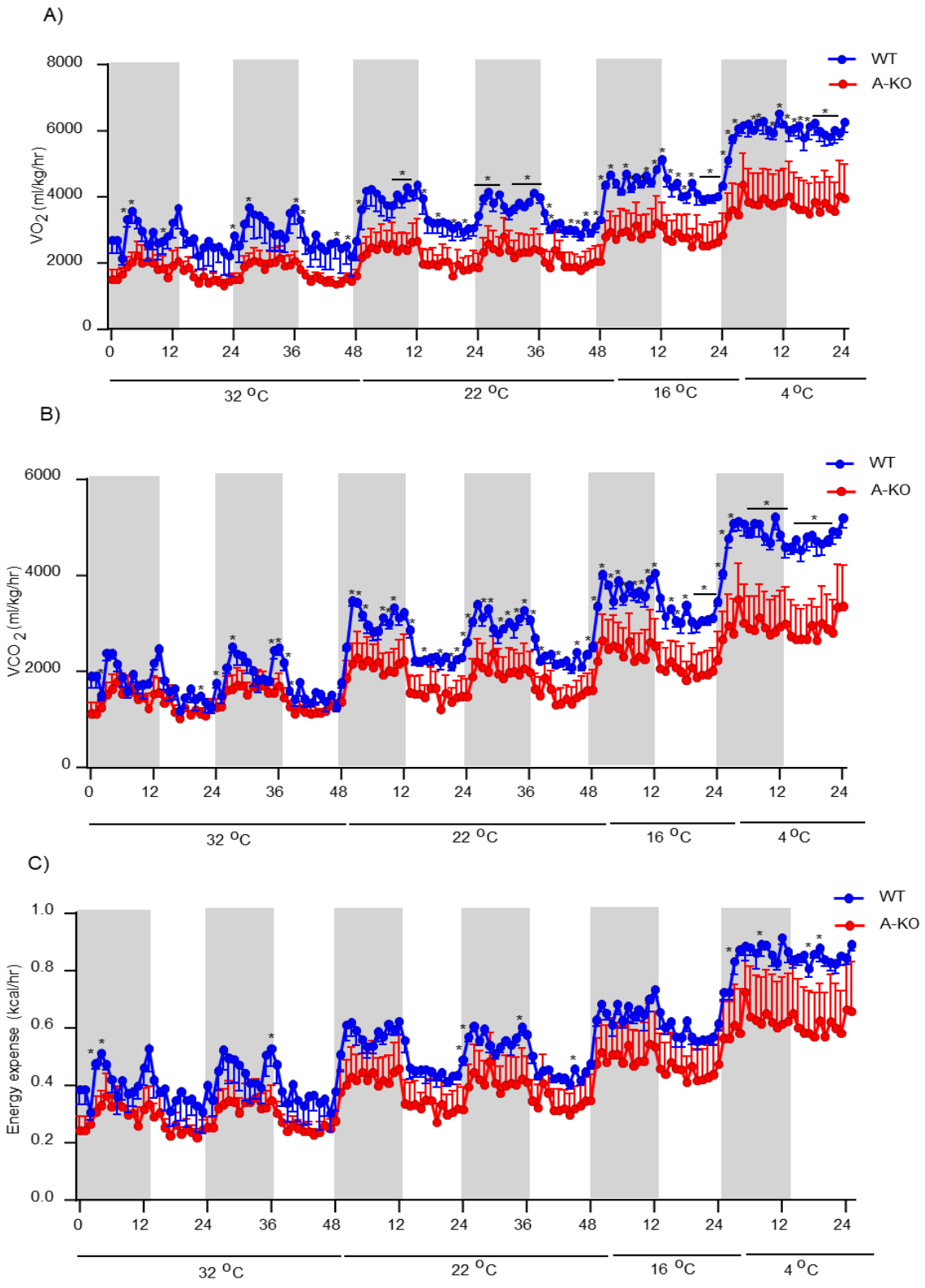

Figure 4.3: Adipocyte-specific PPM1K-KO has defective energy metabolism. The mice were placed in a metabolic cage following 10 weeks of HFHC feeding (age: 19 weeks). A)

The oxygen consumption of HFHC-fed mice, B) carbon dioxide production, and C) Energy expense in 12 h dark-light cycle at different temperatures in WT and A-KO mice (n=5-6). All data are presented as mean ± SEM. *$p < 0.05$ and **$p < 0.01$.

4.2.4. Deficiency of PPM1K in adipocytes alters the circulatory BCKA levels.

A previous study reported that adipose tissue can modulate the circulating BCAA levels as fat transplantation from WT mice to BCAT2 KO mice rescued the plasma BCAA levels [78]. The data from global PPM1K KO mice showed an increase in serum and adipose tissue BCAAs/BCKAs levels. In A-KO mice, a BCAA tolerance test was performed (as described in the methods section) post 6-7 weeks of post-HFHC feeding to investigate the role of adipocyte PPM1K in modulating circulatory BCAA levels. Interestingly, A-KO showed higher circulatory BCKAs levels as compared to WT (Figure 4.4B) suggesting the involvement of adipocyte PPM1K in modulating the BCKAs levels. In addition, the serum BCKAs levels (post-cull) were also higher in A-KO mice as compared to WT.

These findings suggest that adipocyte PPM1K can modulate the circulatory BCKA levels.

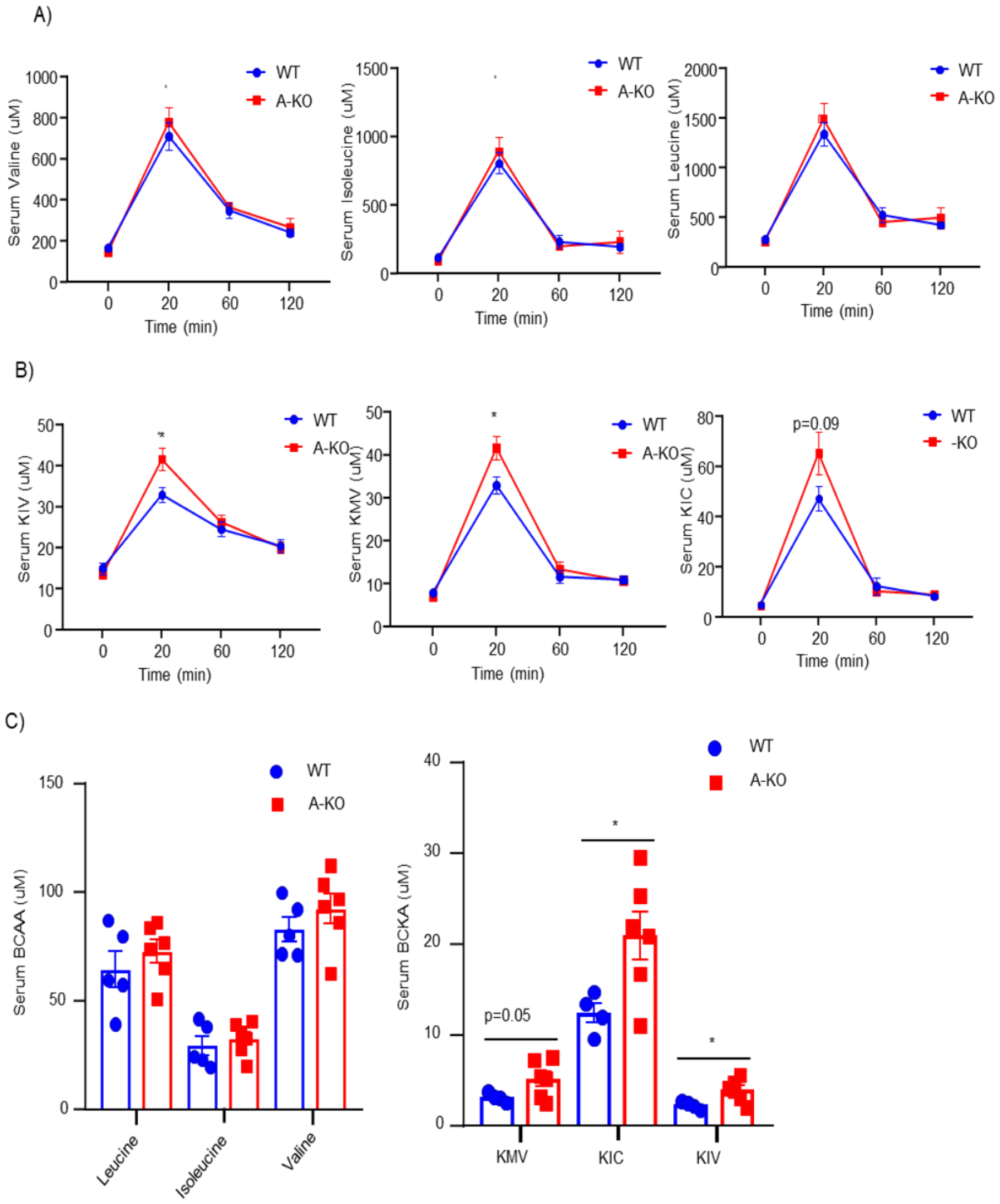

Figure 4.4: Deficiency of PPM1K in adipocytes alters the circulatory BCKA levels. BCAA tolerance test was performed in WT and A-KO mice post 10 weeks of HFHC-diet feeding. A) Serum BCAAs and B) BCKAs at different times following BCAA oral gavage.

C) Post-cull serum BCAAs and BCKAs levels (n=5-6). All data are presented as mean ± SEM. *p < 0.05 and **p < 0.01.

4.3 Conclusion:

In this chapter, firstly the successful generation and validation of the A-KO model was shown as indicated by the significant reduction of *Ppm1k* expression and increased BCAAs/BCKAs levels in different fat depots.

The deficiency of adipocyte PPM1K led to glucose intolerance, insulin resistance, and defects in lipid metabolism. In addition, the lack of adipocyte PPM1K led to less energy expenditure as revealed by the data from metabolic cage experiments. Interestingly, the adipocyte PPM1K also played an important role in maintaining circulatory BCKA levels.

Altogether, these data suggested the important role of adipocyte PPM1K in the regulation of glucose, lipids, energy metabolism, and circulatory BCAAs levels.

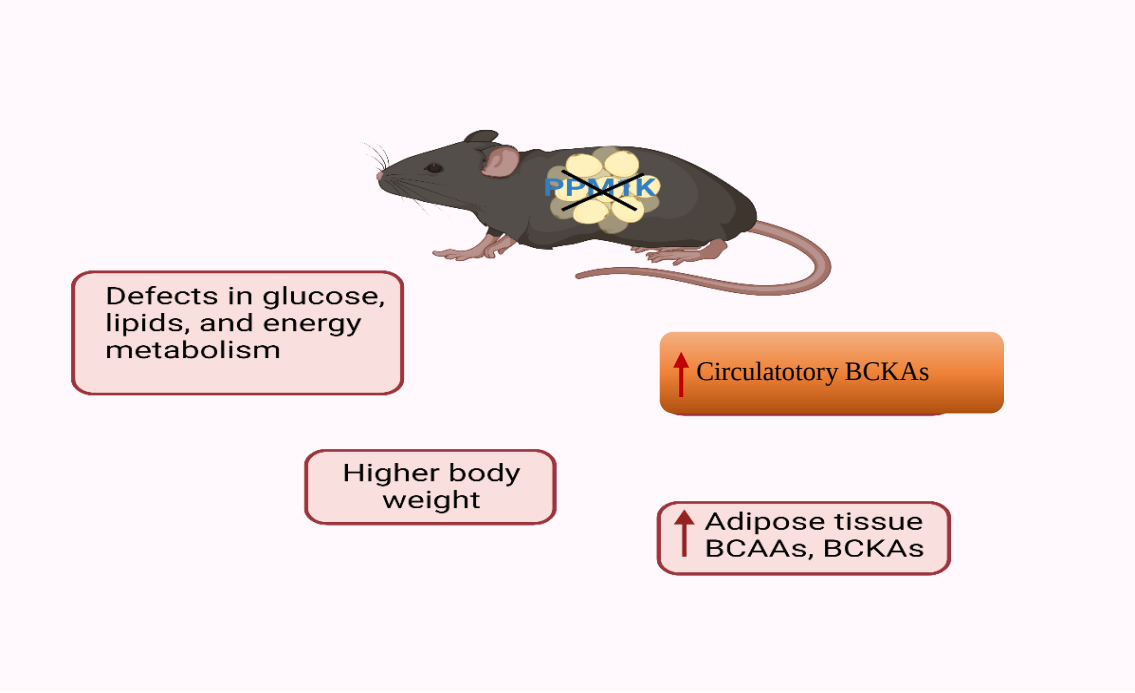

Figure 4.5: Summary figure showing adipocyte-specific deletion of PPM1K causes defects in glucose, lipid, and energy metabolism and circulatory BCKA levels.

Chapter 5: Adipocyte PPM1K deficiency induces adipose tissue dysfunction (fibrosis, inflammation, senescence) and liver steatosis.

5.1 Introduction:

In the previous chapter, the successful generation and validation of the A-KO model were shown. The metabolic characterization data showed glucose intolerance, insulin resistance, and defects in energy and lipid metabolism in A-KO mice compared to WT control. In conclusion, these data suggested that adipocyte PPM1K deletion exacerbates the obesity-induced alterations in circulatory BCKAs, glucose, lipids, and energy metabolism.

Since adipose tissue is important for maintaining glucose and energy homeostasis and whole-body energy metabolism, the next step was to evaluate the effects of adipocyte PPM1K deletion in the biology of adipose tissue. Adipose tissue fibrosis, inflammation, and senescence are pathological features of adipose tissue dysfunction. Dysfunction of adipose tissue can put the metabolism stress on other tissues such as muscle and liver. This chapter aimed to investigate the adipose tissue dysfunction caused by adipocyte PPM1K deficiency in HFHC-diet mice. In addition, the RNA sequencing gave a snapshot of the changes happening at the mRNA levels and revealed the role of adipocyte PPM1K in different processes. It also gave a clue about the possible molecular mechanism responsible for inducing adipose tissue dysfunctions and metabolic alterations in A-KO mice.

5.2 Results:

5.2.1. Adipocyte PPM1K deletion causes fibrosis in adipose tissue (both WAT and BAT)

In the last chapter, it was shown that deletion of adipocytes PPM1K induces glucose intolerance, and defects in lipid and energy metabolism. In addition, the defective BCAA metabolism was demonstrated as evidenced by the increase in BCAAs/BCKAs in fat depots. Adipose tissue is crucial for the maintenance of glucose and energy homeostasis and whole-body energy metabolism.

In the next step, the histological analysis was performed to see if deletion of adipocyte PPM1K causes alteration in adipose tissue. Picrosirius red staining was performed in different fat depots to see the abnormal deposition of collagen fibers as the phenomena of fibrosis were observed in PPM1K global KO mice. A significant increase in fibrosis was observed in three different fat depots including eWAT, sWAT, and BAT (Figure 5.1A) of A-KO mice as compared to WT mice. Further, an upregulated expression of pro-fibrosis genes including *Col1a1*, and *Col6a1* was observed in eWAT A-KO mice (Figure 5.1B). In sWAT, the expression of pro-fibrosis genes *Acta2*, *Col1a1*, *Col3a1*, *Col4a1*, and *Col6a3* was significantly upregulated in A-KO in comparison to WT (Figure 5.1C). Thus, qPCR data further supported the finding of picrosirius red staining. Interestingly, the changes in fibrosis both in picrosirius red staining and qPCR analysis are more evident in sWAT as compared to eWAT.

These data altogether indicated the adipocyte deletion of PPM1K causes adipose tissue fibrosis in mice.

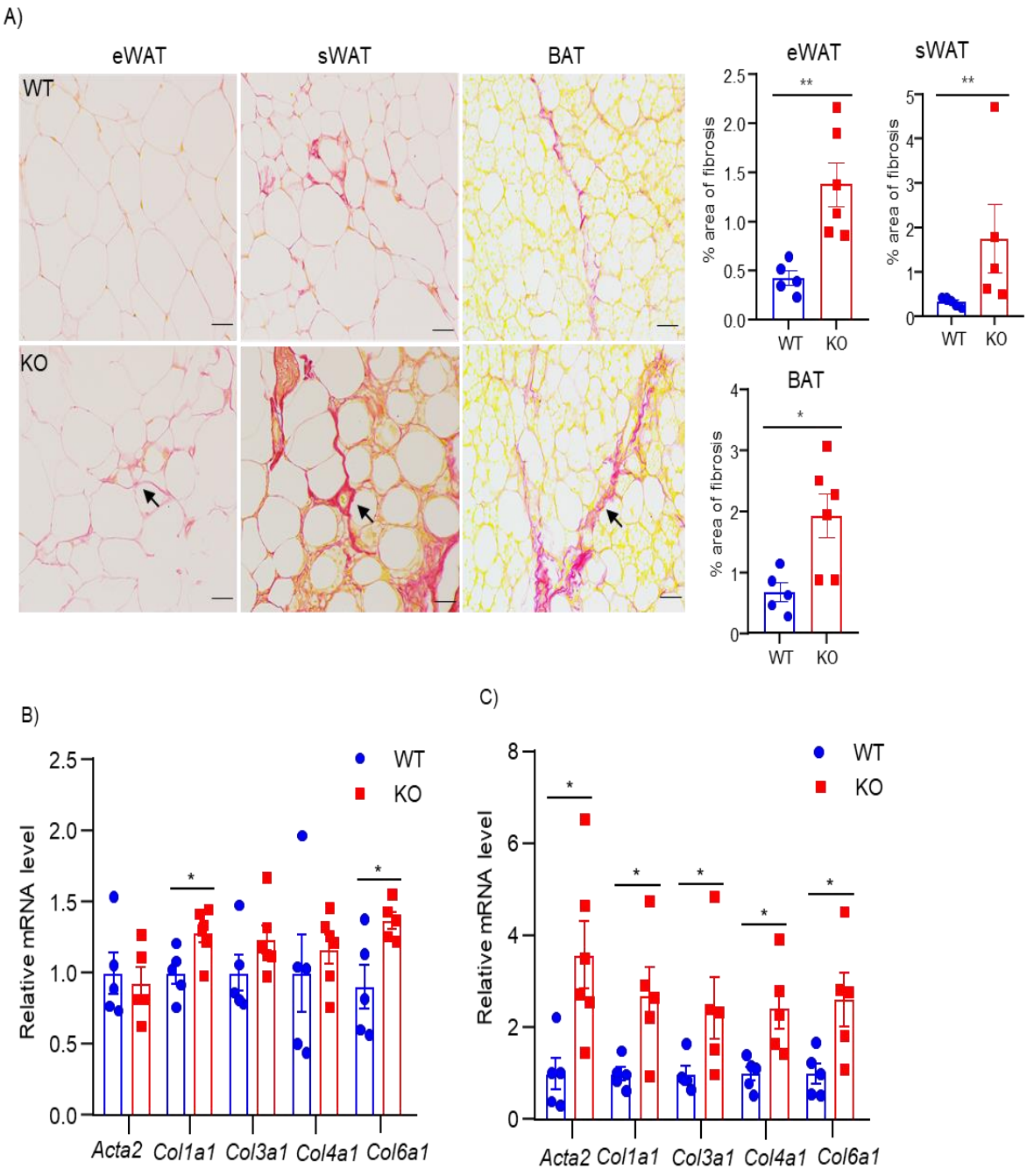

Figure 5.1: Adipocyte PPM1K deletion causes fibrosis in adipose tissue (both WAT and BAT). A) Representative images and quantification data of picrosirius red staining in eWAT sWAT, and BAT from Adipo-PPM1K-WT and KO (A-KO) mice; scale bar, 100um. B) mRNA expression of fibrosis markers in eWAT and C) sWAT of Adipo-PPM1K-WT and KO (A-KO) mice (n=5-6). All data are presented as mean ± SEM. *p < 0.05 and **p < 0.01.

5.2.2. Loss of adipocyte PPM1K induces senescence in WAT.

A previous study reported a higher abundance of senescent cells in the sWAT of obese human subjects, thus indicating the correlation between WAT senescence and obesity [141]. In A-KO mice, higher levels of circulatory pro-inflammatory cytokines including IL-1β and MCP1 were observed and these cytokines are considered common SASPs. Recently, elevated circulatory BCAA levels have been observed in aged mice, and expression of BCAA catabolic genes *Bckdha, Bckdhb, Pcca, and Pccb* and protein is reduced in aging adipose tissue [67]. These findings speculated us to investigate the role of adipocyte PPM1K in adipose tissue senescence. To evaluate the senescence in adipose tissue of A-KO mice, the senescence markers including β-galactosidase activity and expression of *P16* and *P21* were monitored. A-KO mice showed higher β-galactosidase activity (as evidenced by higher colour intensity) in both sWAT and eWAT as compared to WT (Figure 5.2A). In addition, the mRNA expression of P*16* and *P21* (Figure 5.2 B, C) and protein levels of P21 (Figure 5.2D) were significantly upregulated in adipose tissue in A-KO samples. Thus, indicating the role of adipocyte PPM1K in adipose tissue senescence.

A study has shown that DNA damage occurred in adipocytes at the outset of obesity before the development of adipose tissue inflammation, insulin resistance, and glucose intolerance [140]. In A-KO glucose intolerance and insulin resistance were observed. Next, the adipocyte senescence was monitored using the perilipin (adipocyte marker) and P21 immunofluorescence co-staining in sWAT. The data showed increased senescence in adipocytes in A-KO as indicated by the higher number of perilipin & P21+ cells compared to the WT control.

Collectively, these data suggest deletion of adipocyte PPM1K induces cellular senescence in adipose tissue.

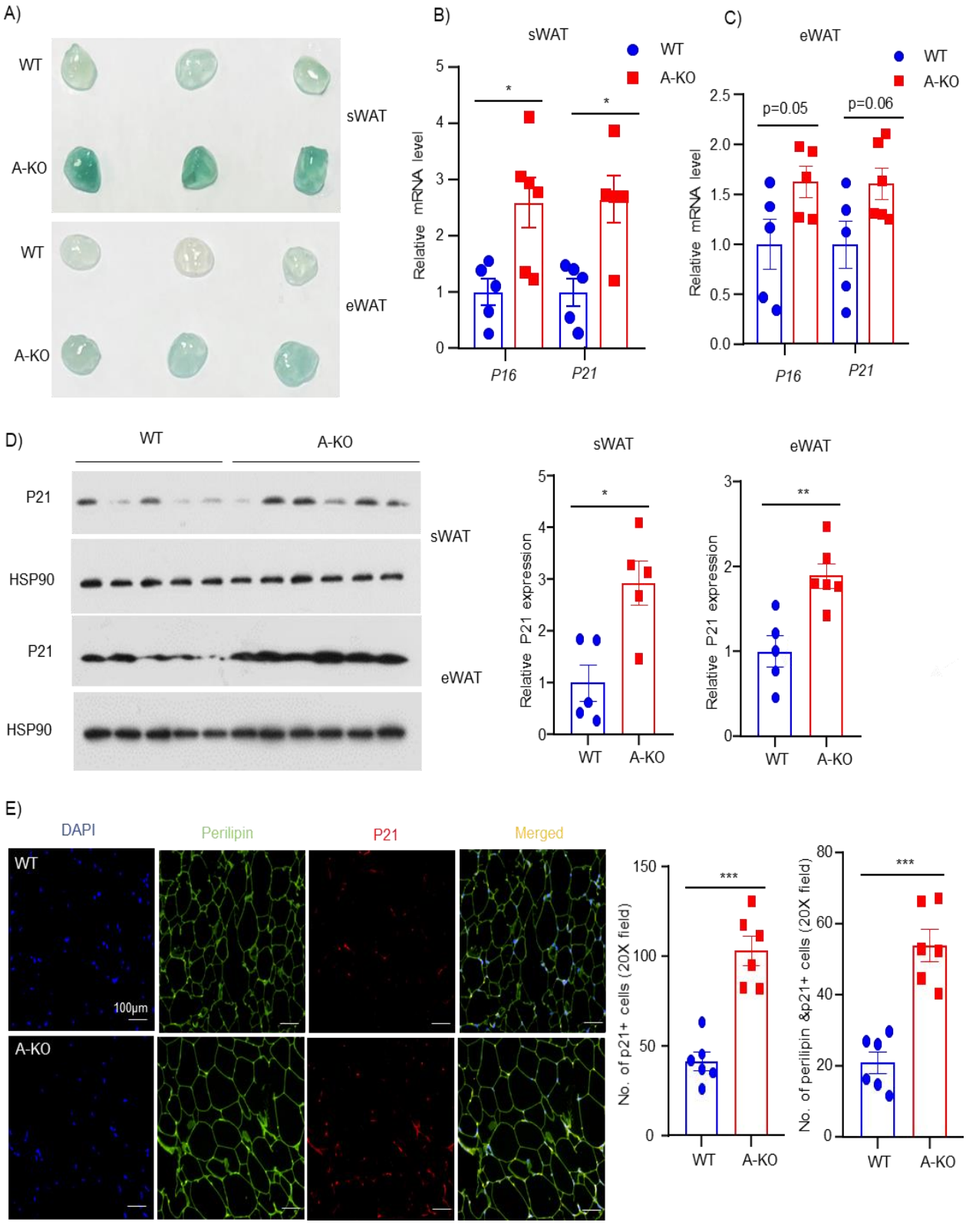
A)
WT
A-KO
sWAT
WT
A-KO
eWAT
B)
sWAT
WT
A-KO
Relative mRNA level
P16
P21
C)
eWAT
WT
A-KO
p=0.05
p=0.06
Relative mRNA level
P16
P21
D)
WT
A-KO
P21
HSP90
P21
HSP90
sWAT
eWAT
sWAT
Relative P21 expression
WT
A-KO
eWAT
Relative P21 expression
WT
A-KO
E)
DAPI
Perilipin
P21
Merged
WT
100μm
A-KO
No. of p21+ cells (20X field)
WT
A-KO
No. of perilipin &p21+ cells (20X field)
WT
A-KO

Figure 5.2: Loss of adipocyte PPM1K induces senescence in WAT. A) β-Galactosidase staining in sWAT and eWAT. B-C) mRNA expression of senescence markers *P16* and *P21* in B) sWAT and C) eWAT in WT and A-KO mice. D) P21 protein levels in sWAT and eWAT of WT and A-KO mice. E) IF co-staining of perilipin and P21 and their quantification data in sWAT of WT and A-KO mice (n=5-6). All data are presented as mean ± SEM. *$p < 0.05$ and **$p < 0.01$.

5.2.3. Adipocyte PPM1K deficiency causes inflammation in adipose tissue.

Adipose tissue acts as an endocrine and secretes a variety of pro-inflammatory and anti-inflammatory cytokines. Most of the pro-inflammatory cytokines are increased in obese conditions including leptin, retinol-binding protein 4 (RBP4), IL-6, IL-18, TNF, and Monocyte Chemoattractant Protein-1 (MCP-1) [13]. Firstly, the levels of pro-inflammatory cytokines IL-1β and MCP-1 were checked in serum samples of WT and A-KO mice. Both IL-1β and MCP-1 serum levels were elevated in A-KO mice and these cytokines are considered as common SASPs. Further, the mRNA expression of pro-inflammatory genes *Mcp1, Il1b,* and *F4/80* was also upregulated in eWAT and sWAT of A-KO mice (Figure 5.3C&D). IL-1β is primarily produced by macrophages and the active form of IL-1β (cleaved IL-1β) is formed by the cleavage of pro-IL-1β by caspase-1 [142]. The protein expression levels of both total and cleaved IL-1β were measured in sWAT. The protein levels of cleaved IL-1β were increased in A-KO samples whereas a reduced level of total IL-1β was observed (although the changes are not significant due to large variations within the group). This suggests that there is more conversion of total IL-1β to cleaved IL-1β in A-KO samples in comparison with WT. However, the protein levels of caspase 1 (cleaves pro-IL-1β to generate cleaved IL-1β) were not checked in these samples.

Collectively, these data suggest that adipocyte PPM1K deficiency induces inflammatory response in adipose tissue.

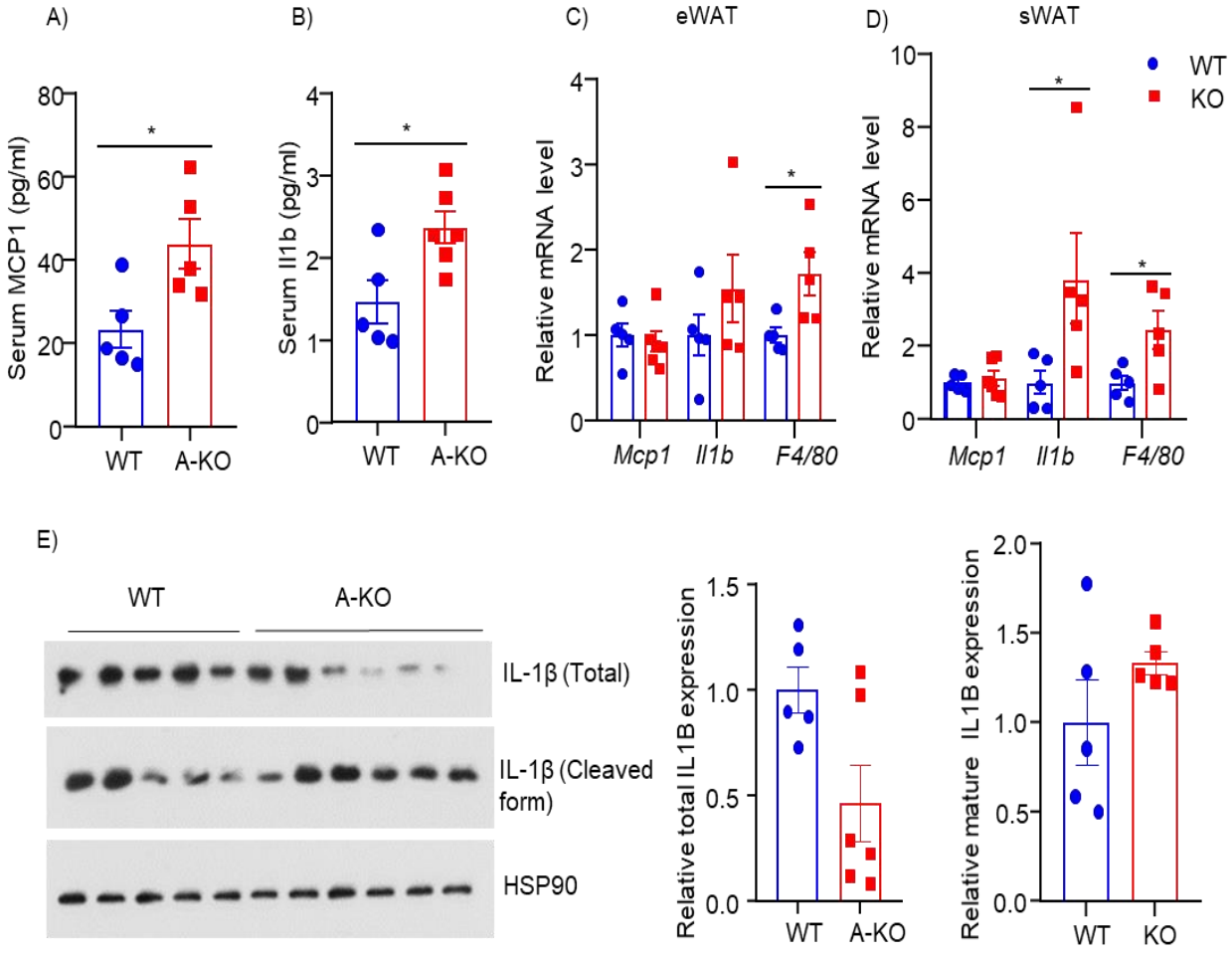

Figure 5.3: Adipocyte PPM1K deficiency causes inflammation. A) Serum MCP-1, and B) IL1B levels in WT and A-KO mice post-cull (age-6 months). mRNA expression of pro-inflammatory cytokines in C) eWAT, D) sWAT, and E) Protein levels of total and cleaved IL-1β and HSP90 (as internal control) in sWAT of WT and A-KO samples (n=5-6). All data are presented as mean ± SEM. *p < 0.05 and **p < 0.01.

5.2.4. A-KO mice showed higher infiltration of immune cells (M1 macrophages) in eWAT.

Fibrosis and inflammation are the characteristic features of adipose tissue dysfunction and are linked to insulin resistance and T2D [118]. Adipocyte hypertrophy and increased infiltration of M1 macrophage happen in adipose tissue during obesity. A-KO mice displayed increased adipose tissue fibrosis and increased serum pro-inflammatory cytokines levels as compared to WT. Further histological analysis was performed on eWAT and sWAT to further examine the biology of adipose tissue. Firstly, the infiltration of immune cells in WAT was evaluated using H&E staining. The data showed more infiltration of immune-like cells and more enriched crown-like structure (CLS) in A-KO samples as compared to WT (Figure 5.4A). The CLS primarily consists of pro-inflammatory adipose tissue macrophages (ATMs) and is reported to correlate with insulin resistance in obese human subjects [143]. Consistently, the IF co-staining of F4/80 (macrophage marker) and iNOS (M1 macrophage marker) showed a higher number of inflammatory ATMs (F4/80+ iNOS+) in A-KO mice, suggesting that adipocyte PPM1K deficiency promotes infiltration of pro-inflammatory ATMs (M1 macrophages) in eWAT. Collectively, these data indicated that deletion of adipocyte PPM1K can mediate a shift in ATMs to more toward pro-inflammatory M1 macrophages.

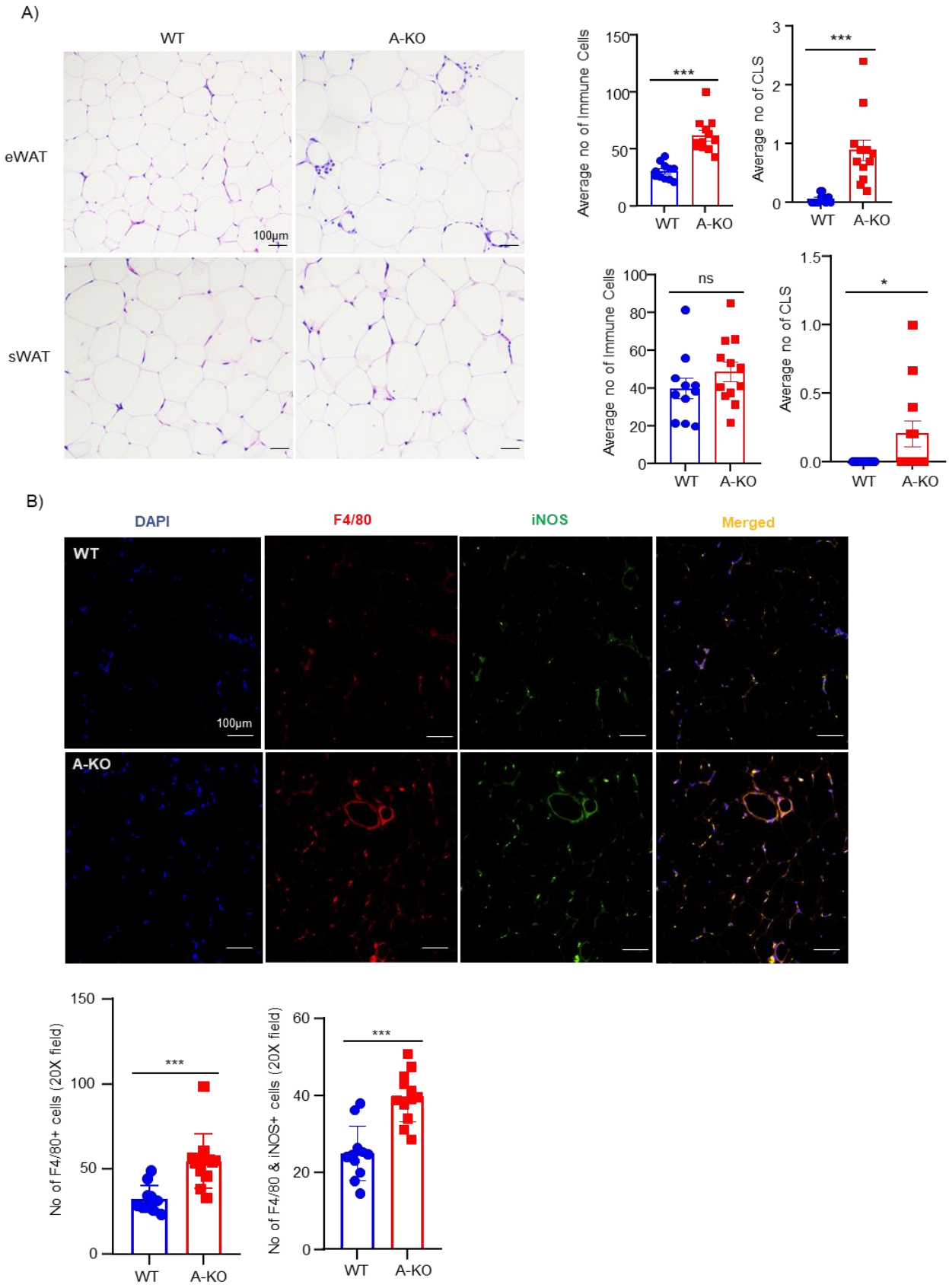
A)
WT
A-KO
eWAT
sWAT
100μm
Average no of Immune Cells
Average no of CLS
***
ns
*
B)
DAPI
F4/80
iNOS
Merged
WT
A-KO
100μm
No of F4/80+ cells (20X field)
No of F4/80 & iNOS+ cells (20X field)

Figure 5.4: A-KO mice showed higher infiltration of immune cells (M1 macrophages) in eWAT. A) Representative images and quantification data (immune cells and crown-like structure) of H&E staining in eWAT and sWAT of WT and A-KO mice (n=10); scale bar, 100um. B) Representative images and quantification data of immunofluorescence staining of F4/80 and iNOS in eWAT of WT and A-KO mice (n=10); scale bar, 100um. All data are presented as mean ± SEM. *$p < 0.05$ and **$p < 0.01$.

5.2.5. Loss of adipocyte PPM1K induces BAT whitening.

The primary function of BAT is non-shivering thermogenesis. It's worth mentioning that BCAAs were recently identified as thermogenic substrates in BAT by Yoneshiro et. al [84]. The defective BCAA catabolism was observed in BAT as evidenced by the higher levels of BCAAs/BCKAs (shown in Chapter 4) in A-KO mice. So, H&E staining was performed to see any histological abnormalities in BAT of WT and A-KO mice. Interestingly, the histological analysis data showed more lipid content and less cellularity in A-KO mice in comparison with WT (Figure 5.5A). In addition, the mRNA expression of thermogenesis genes *Cidea* and *Dio2* was also reduced in BAT of A-KO (Figure 5.5B). These data highlight the importance of adipocyte PPM1K in the regulation of thermogenesis and whitening in BAT. However, more experimental evidence such as UCP1 staining and cold-induced thermogenesis is needed to further support the findings.

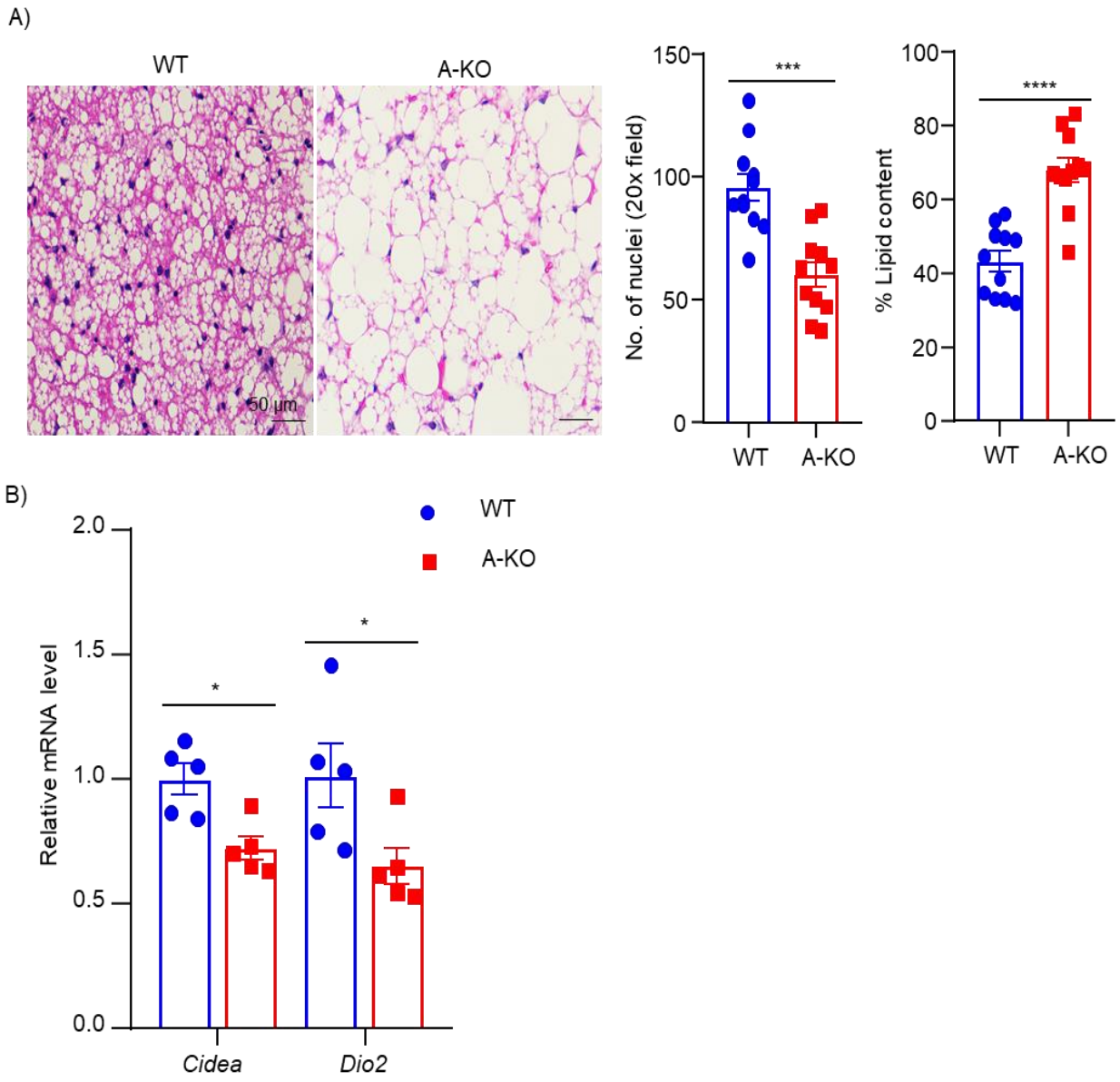

Figure 5.5: Loss of adipocyte PPM1K induces BAT whitening. A) Representative images and quantification data (nuclei count and lipid content) of H&E staining in BAT of WT and A-KO mice (n=10); scale bar, 100um. B) mRNA expression of thermogenesis genes *Cidea* and *Dio2* in BAT of WT and A-KO mice (n=5-6); scale bar, 50um. All data are presented as mean ± SEM. *p < 0.05 and **p < 0.01.

5.2.6. Adipocyte-specific deletion of PPM1K led to hepatic steatosis, fibrosis, and inflammation.

Increased fibrosis leads to higher rigidity or reduced plasticity in adipose tissue, restricting its expendability and thus resulting in ectopic lipid accumulation [119]. A higher degree of fibrosis is observed in adipose tissue of A-KO mice in comparison with WT. The effect of adipocyte-specific PPM1K deletion in inducing liver dysfunction was assessed. The H&E and ORO staining data showed higher lipid deposition (liver steatosis) in A-KO liver as compared to WT (Figure 5.6A). In addition, increased fibrosis was observed as evidenced by the increase in the area of fibrosis in Sirius red staining (Figure 5.6A) and upregulation of pro-fibrosis gene markers including *Col1a1*, *Col3a1,* and *Col6a3* in liver samples of A-KO mice. Increased inflammation is also observed as revealed by the higher expression of pro-inflammatory cytokines *A-fabp, F4/80, Mcp-1,* and *Il-1β* in A-KO liver samples than in the WT control. These data suggest the deletion of adipocyte PPM1K causes adipose tissue dysfunction such as increased fibrosis and inflammation, and decreased TG- clearance, thus putting more metabolic stress on liver tissue. This led to increased steatosis, fibrosis, and inflammation in the liver.

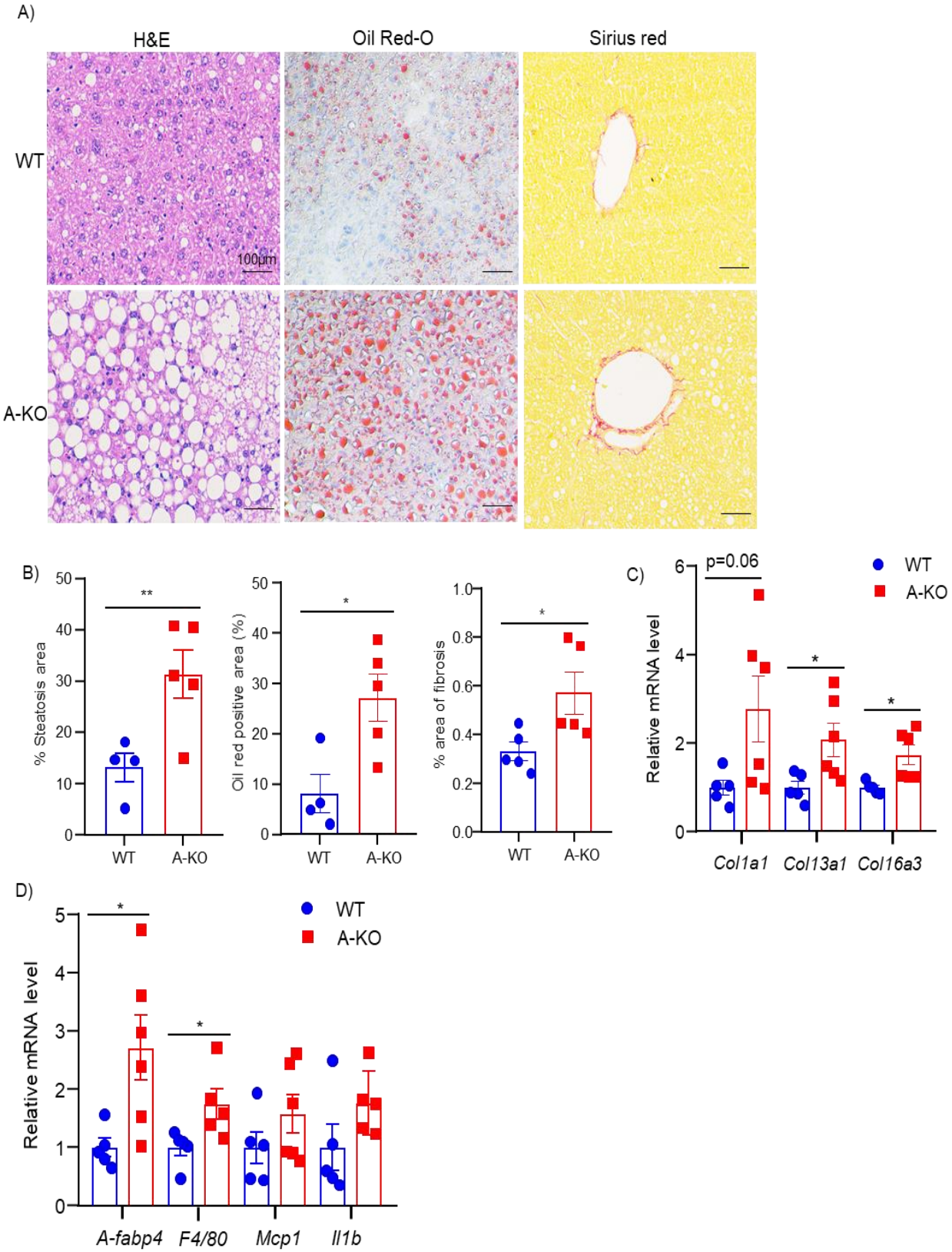
A)
H&E
Oil Red-O
Sirius red
WT
A-KO
100μm
B)
% Steatosis area
Oil red positive area (%)
% area of fibrosis
WT
A-KO
C)
p=0.06
Relative mRNA level
Col1a1
Col13a1
Col16a3
D)
Relative mRNA level
A-fabp4
F4/80
Mcp1
Il1b

Figure 5.6: Adipocyte-specific deletion of PPM1K led to hepatic steatosis, fibrosis, and inflammation. A) Representative images of H&E staining, Oil red staining, and picrosirius red staining of liver section (scale bar, 100um) and their B) quantification data in WT and A-KO mice (n=5-6). C-D) relative mRNA expression levels of C) *Col1a1*, *Col3a1*, and *Col6a3* and D) *A-fabp, F4/80*, *Mcp*-1, and Il-*1β* (normalized with 18s) in WT and A-KO livers (n=5-6). All data are presented as mean ± SEM. *p < 0.05 and **p < 0.01.

5.2.7. Gene Set Enrichment Analysis (GSEA) from RNA sequencing data showed downregulation of the TCA cycle and mitochondrial respiration pathways in eWAT.

The RNA sequencing was performed to observe the overall changes at mRNA levels in adipose tissue upon deletion of PPM1K. The GSEA data showed the downregulation of pathways involved in the TCA cycle and mitochondrial respiration (Figure 5.7A, B) in A-KO compared to WT, thus indicating deletion of PPM1K blunted the cellular respiration and further energy generation through electron transport chain (ETC). Consistent with these findings, the seahorse analysis showed the reduced oxygen consumption rate (OCR) in eWAT of A-KO (Figure 5.7E), thus suggesting the attenuated rate of mitochondrial respiration in A-KO.

In addition, the downregulation of adipogenesis pathways was also observed in A-KO (Figure 5.7C) (LI_ADIPOGENESIS_BY_ACTIVATED_PPARG). It suggests deletion of adipocyte PPM1K may affect adipogenesis however further evidence is needed. The top downregulated pathways with normalized enrichment score (NES) are shown in Figure 5.7D.

Altogether, these data discovered the new role of PPM1K in the regulation of cellular respiration and adipogenesis.

A)

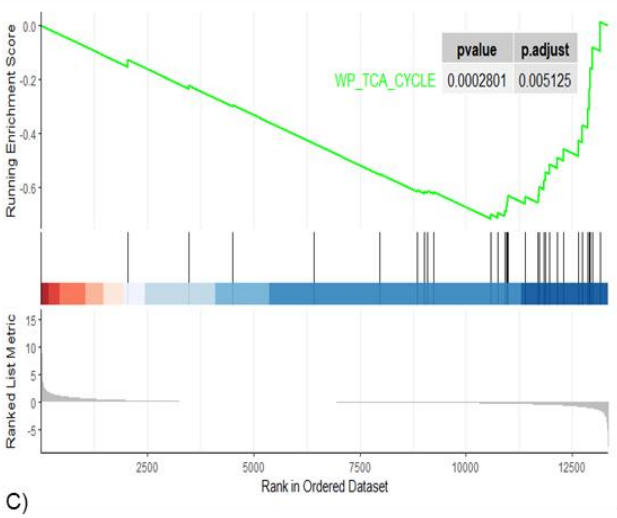

B)

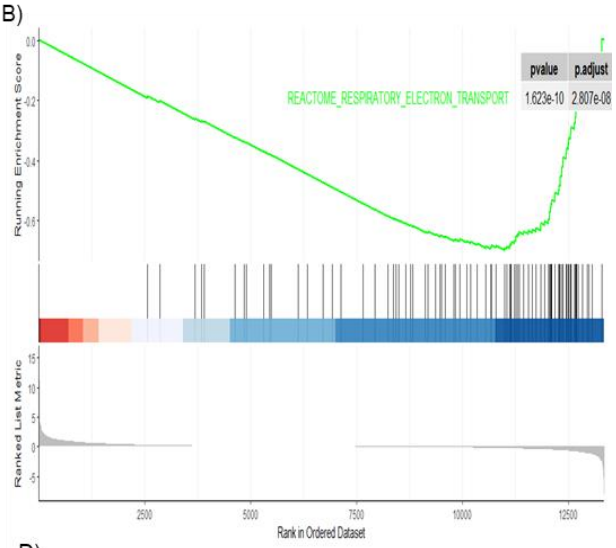

C)

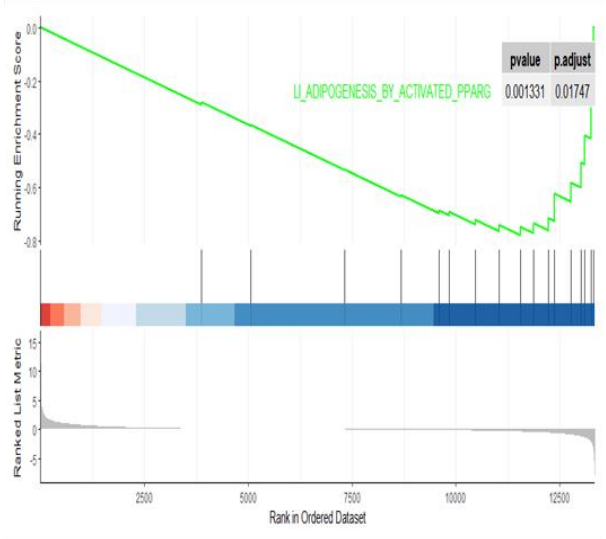

D)

Top downregulated pathways	NES-score	P-adj value
REACTOME_THE_CITRIC_ACID_TCA_CYCLE_AND_RESPIRATORY_ELECTRON_TRANSPORT	-2.33	1.90E-08
REACTOME_RESPIRATORY_ELECTRON_TRANSPORT	-2.26	6.21E-08
LI_ADIPOGENESIS_BY_ACTIVATED_PPARG	-1.81	0.005

E)

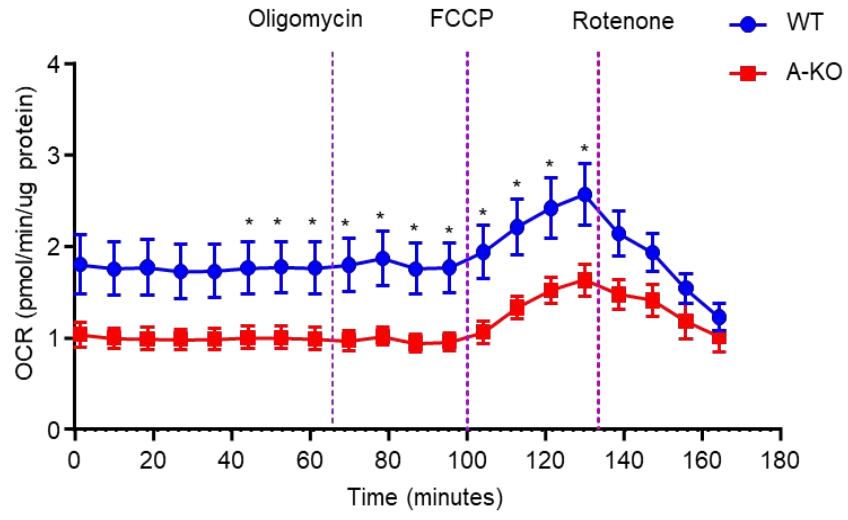

Figure 5.7: GSEA showed downregulation of the TCA cycle and mitochondrial respiration pathways in eWAT. GESA plot in eWAT for A) Reactome _citric acid cycle. B) reactome_respiratory electron transport. C) reactome_BCAA catabolism. D) reactome_adipogenesis by activated PPARγ (n=4-5). E) Seahorse analysis showing OCR in eWAT tissue explant (n=3-4) and data are presented as mean ± SEM. *$p < 0.05$ and **$p < 0.01$.

5.2.8. RNA sequencing data corroborated the findings of increased fibrosis in WAT and senescence in eWAT in A-KO mice.

Histological analysis and qPCR data showed increased fibrosis in WAT. Consistently, the GSEA analysis showed the enrichment of pathways involved in the synthesis or organization of ECM proteins including collagen.

In eWAT, the Reactome of extracellular matrix organization was one of the most pathways (upregulated) in GSEA analysis (Figure 5.8A, B) in A-KO samples. Additionally, P53 signaling pathways are significantly upregulated in A-KO mice (Figure 5.8C, D), thus supporting the phenomena of senescence in eWAT.

Similarly, in sWAT the pathways of collagen formation/synthesis and the reactome of extracellular matrix organisation were the most enriched pathways and are upregulated in A-KO samples (Figure 5.8E, F). Interestingly, the phenomenon of fibrosis was more prominent in sWAT as compared with eWAT.

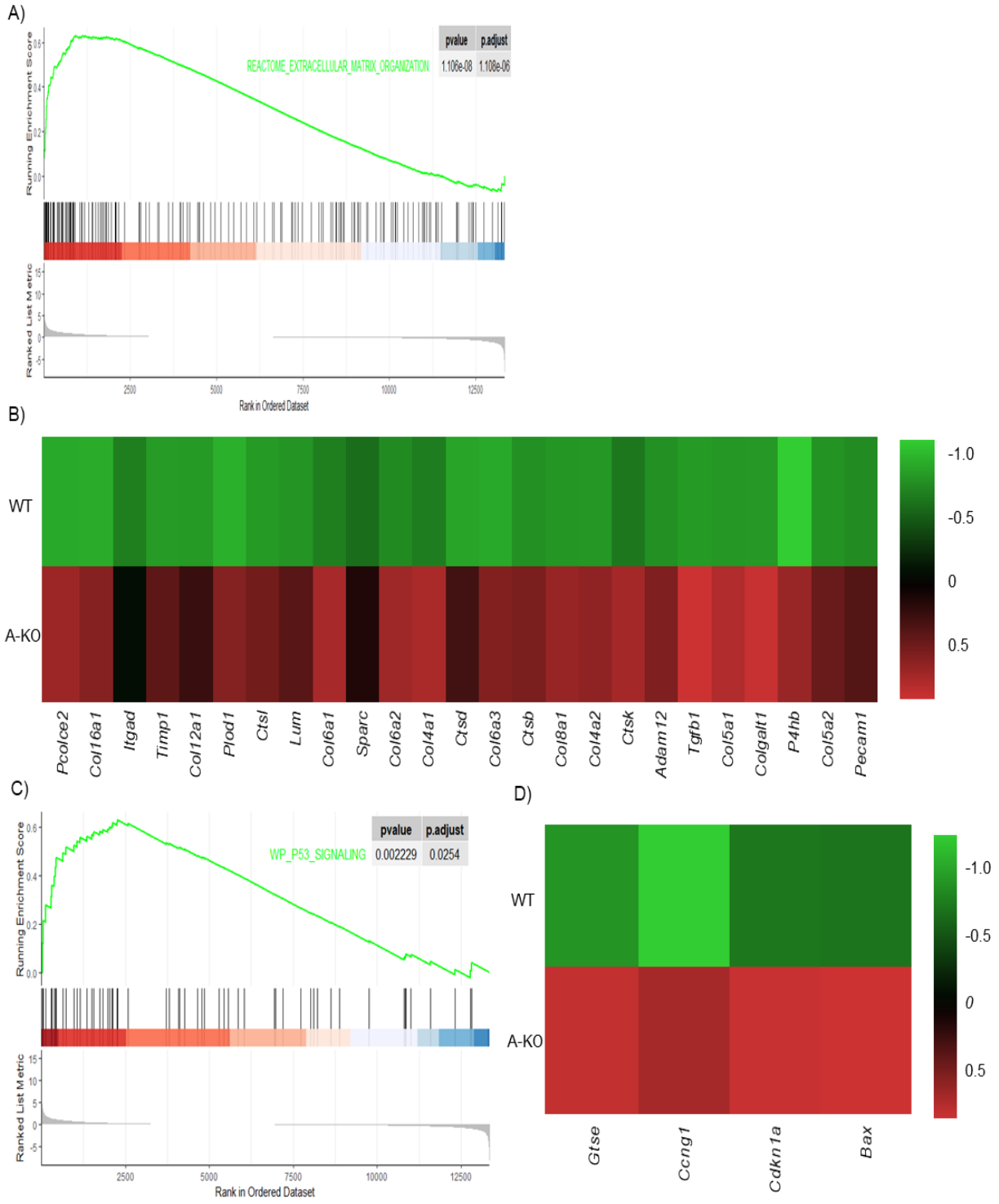
A)
pvalue
p.adjust
REACTOME_EXTRACELLULAR_MATRIX_ORGANIZATION
1.106e-08
1.108e-06
Running Enrichment Score
Ranked List Metric
Rank in Ordered Dataset
B)
WT
A-KO
Pcolce2
Col16a1
Itgad
Timp1
Col12a1
Plod1
Ctsl
Lum
Col6a1
Sparc
Col6a2
Col4a1
Ctsd
Col6a3
Ctsb
Col8a1
Col4a2
Ctsk
Adam12
Tgfb1
Col5a1
Colgalt1
P4hb
Col5a2
Pecam1
-1.0
-0.5
0
0.5
C)
pvalue
p.adjust
WP_P53_SIGNALING
0.002229
0.0254
Running Enrichment Score
Ranked List Metric
Rank in Ordered Dataset
D)
WT
A-KO
Gtse
Ccng1
Cdkn1a
Bax
-1.0
-0.5
0
0.5

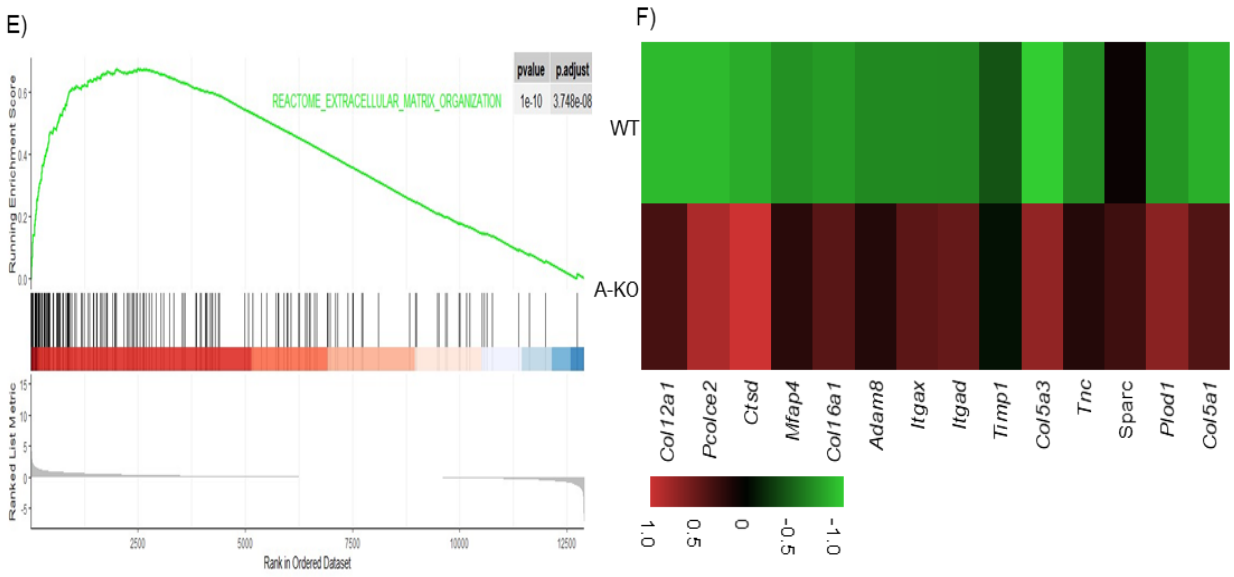

Figure 5.8: RNA sequencing data corroborated the findings of increased fibrosis in WAT and senescence in eWAT in A-KO mice. GESA plot in eWAT **A**) GSEA plot of Reactome of extracellular matrix organization and B) heat map of differentially expressed genes in respective pathway (ECM) in eWAT. C) GSEA plot of P53 signaling and D) heat map of differentially expressed genes in the respective pathway in eWAT. E) GSEA plot reactome_collagen formation, and F) heat map of differentially expressed genes in the respective pathway in sWAT.

5.2.9. The adipose tissue dysfunction in A-KO mice is likely to mediate through activation of Rho-pathway.

Different experimental evidence including metabolic characterization, histological analysis, mRNA expression profile using qPCR, and RNA-sequencing showed defects in adipose tissue functions in A-KO mice. However, the underlying mechanism remains elusive.

The deep insights into RNA-sequencing data showed some overlapped and highly enriched pathways in eWAT and sWAT. Among these highly enriched pathways, the extracellular matrix organization and Rho GTPase effectors pathways were important in terms of their relevance to adipose tissue function. Activation of Rho pathways (such as Rho kinase) resulted in insulin resistance and higher body weight in HFD mice [144]. In adipocytes, mechanical stress causes the activation of Rho pathways and the formation of stress fibers. Additionally RND3, a Rho-related GTP-binding protein showed elevated expression in obesity and was associated with insulin resistance in humans, and also regulated adipocyte lipolysis [145]. Based on the literature, it was speculated that upregulated expression of Rho GTPase effectors pathways might be involved in inducing the adipose tissue dysfunction in A-KO mice in WAT. The Rho GTPase is the regulator of actin cytoskeleton rearrangement, so for further assessment, the F-staining was performed. Consistently, the A-KO showed a higher % area of F-actin staining (due to the small sample size couldn't reach the statistical significance) indicating the activation of Rho GTPase. To support the role of the Rho GTPase pathway in adipose tissue dysfunction in the A-KO mice model warrants further experimental validation.

A)

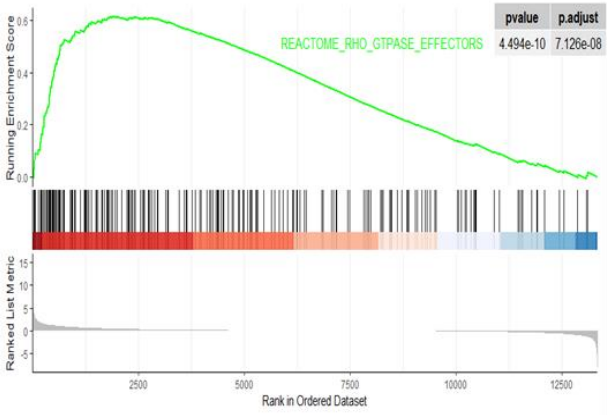

B)

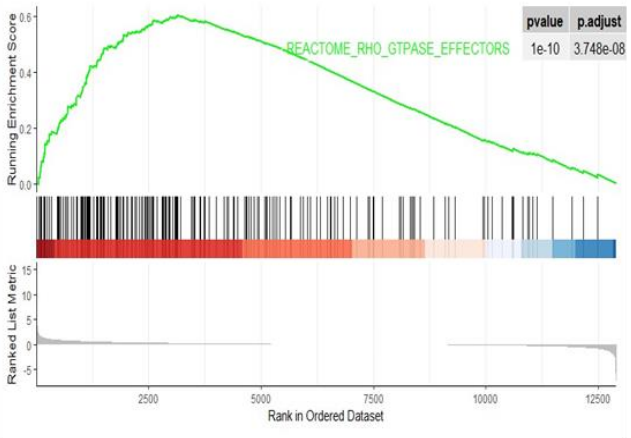

C)

Top upregulated pathways	NES-score	P-adj value
EXTRACELLULA_MATRIX_ORGANIZATION	2.44	3.75E-08
	2.03	4.72E-07
RHO_GTPASE_EFFECTORS	2.25	3.75E-08
	2.03	9.03E-08
GOLDRATH_ANTIGEN_RESPONSE	2.18	3.75E-08
	2.10	1.90E-08

D)

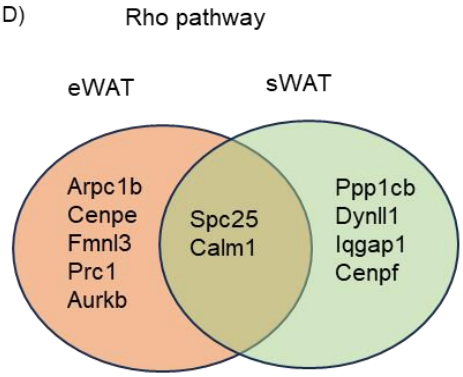

E)

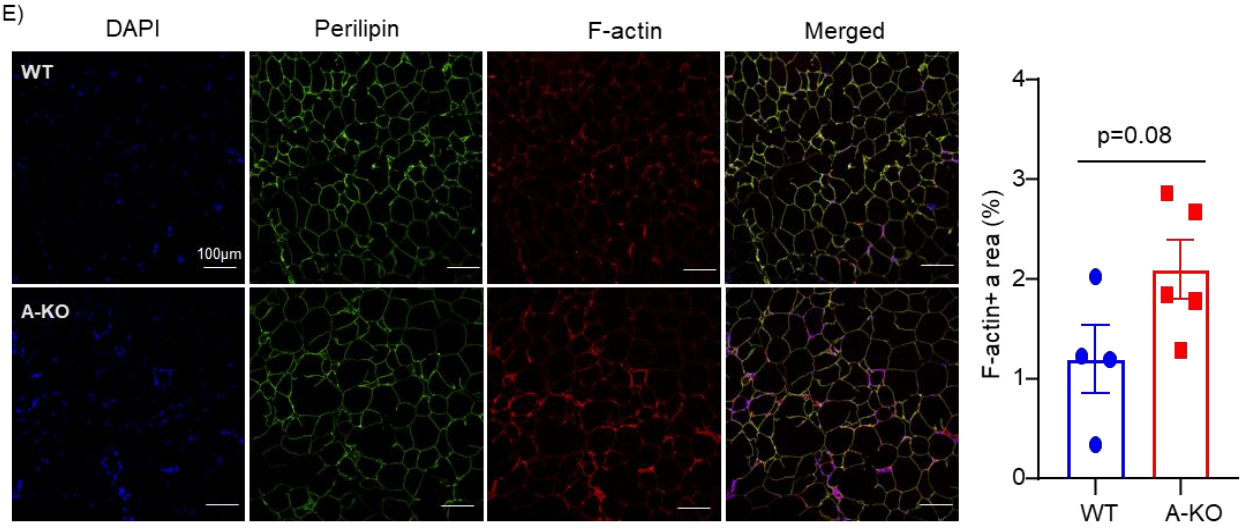

Figure 5.9: The adipose tissue dysfunction in A-KO mice likely to mediate through activation of Rho-pathway. GESA enrichment plot (A-B) of reactome GTPase effectors in A) eWAT, and B) sWAT. C) Overlapped and highly enriched pathways in sWAT (red color) and eWAT (black color) with enrichment score (NES) score. D)Venn diagram showing the most significantly expressed genes of Rho-GTPase effectors reactome in eWAT, and sWAT and overlapped in both eWAT and sWAT (sample size, n=5-6). E) Representative images and quantification data of F-actin (using phalloidin-iFluor 555 Reagent) and Perilipin co-staining in eWAT (n=4-5) and data are presented as mean ± SEM. *$p < 0.05$ and **$p < 0.01$.

5.3: Conclusion:

A-KO mice displayed an obvious increase in fibrosis, inflammation, and senescence in adipose tissue. These findings were further corroborated by mRNA expression by qPCR and RNA sequencing analysis. The RNA sequencing data also revealed the role of adipocyte PPM1K in regulating cellular respiration (TCA cycle and electron transport chain). From the RNA sequencing data, the Rho GTPase pathway is speculated as one of the pathways responsible for inducing adipose tissue dysfunction, and further study is needed to investigate the detailed mechanism. In addition to adipose tissue dysfunction, adipocyte PPM1K deletion also altered the liver function profile including increased fibrosis, inflammation, and steatosis.

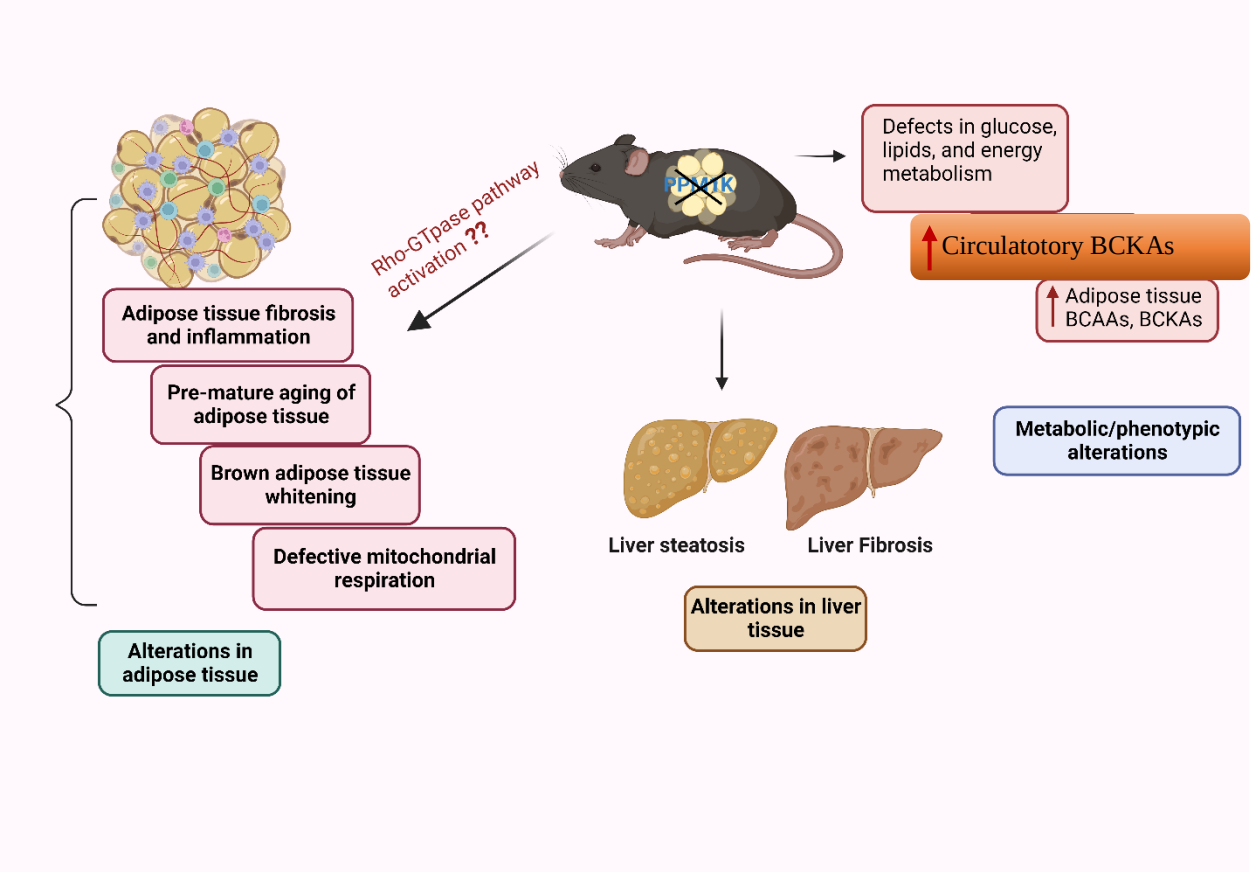

Figure 5.10: Summary figure showing adipocyte PPM1K deficiency induces adipose tissue dysfunction (fibrosis, inflammation, senescence) and liver steatosis.

Chapter 6: Discussion and future directions

6.1 Global genetic deletion of BCAA catabolic gene PPM1K causes adipose tissue dysfunction in a mouse model

Elevated levels of plasma BCAAs/BCKAs have been reported long back in different obese/diabetic rodent models. Adipose tissue can catabolize BCAAs as shown by *in-vitro* and *ex-vivo* studies and can modulate the circulatory BCAAs levels [78]. The disrupted BCAA catabolism causes impaired differentiation of pre-adipocytes to mature adipocytes [81]. Both in obese and diabetic mouse models, the attenuated expression of BCAA catabolic genes such as BCKDHA and PPM1K is reported in adipose tissue [89]. In line with previous findings, analysis using human datasets GSE152991 and GSE159924 showed a decrease in the expression of genes involved in the BCAA catabolic pathway in sWAT (as presented in Chapter 3). Thus, these studies suggest the defective BCAA catabolism in adipose tissue during obesity/T2D. However, how defects in BCAA catabolic pathways alter adipose tissue functions remains elusive. Based on these findings from literature and analysis of different datasets, the role of PPM1K is investigated in the regulation of metabolism and adipose tissue functions.

In the current study, the deletion of PPM1K resulted in the accumulation of BCAAs/BCKAs in circulation and adipose tissue. The obvious increase in BCAAs/BCKAs levels was expected as PPM1K controls the key rate-limiting enzyme BCKDH complex and is also consistent with previous findings [146]. Further metabolic characterization revealed PPM1K global KO displayed modest changes in glucose intolerance and insulin sensitivity however the different studies from the literature either showed beneficial effects on glucose tolerance [147] or no significant changes in glucose tolerance and insulin sensitivity in PPM1K KO mice [146]. In addition, despite higher BCAAs/BCKAs levels, PPM1K KO mice showed either no changes

or modest changes in glucose tolerance since these mice have impaired gluconeogenesis as reported previously [146]. The differences in changes in glucose tolerance from different studies might be due to differences in the timeline of experiments performed. On the other hand, inhibition of BCKDK (a negative regulator of BCKDH) using BT2 reduces BCAAS/BCKAs levels and shows improvement in glucose tolerance in Zucker fatty rats [40].

A study (RNA sequencing) by Cifarelli et al; gave a clue about the involvement of the BCAA catabolic pathway in adipose tissue fibrosis and inflammation in obese human subjects [98]. Consistently, increased fibrosis and inflammation were observed in PPM1K KO mice (these mice have defective BCAA catabolism as data shown in Figure 3.3B) in WAT but no changes in BAT and liver. These findings were substantiated by the analyses of different human databases showing a negative correlation between PPM1K and pro-fibrotic gene expression (Figure 3.6B).

A seminal work by Yoneshiro *et al;* showed defects in BCAA catabolic pathways lead to reduced systemic clearance of BCAA, less tolerance to cold temperature, and thermogenesis in BAT-specific-BCKDHA-KO mice [84]. Consistently, the PPM1K KO showed less tolerance to cold, increased BAT whitening, and reduced energy expenditure.

In adipose tissue, different cell types produce ECM proteins including mature adipocytes, progenitor cells, and fibroblasts. In the present study, the SVF (heterogeneous mixture of cells) was identified as an inducer of fibrosis as no changes were observed in mature adipocyte fractions. In the previous study, the mature adipocytes were reported to acquire the phenotype of fibroblast, including higher expression of ECM genes in mature adipocyte fractions isolated from eWAT of HFD-mice [121]. The ambiguity in results may be due to differences in dietary intervention as the present study utilized the STC diet instead of HFD.

Among SVF, which cell type is specifically inducing the fibrosis was not clarified given the fact that eWAT and sWAT have different cell populations exhibiting pro-fibrotic potential. Both PDGFRα and β cells were identified to induce fibrotic response in WAT. For example, in eWAT, fibro-inflammatory progenitors (LYC6+ PDGFRβ+ cells), or ‘‘FIPs,’’ are reported to exert strong pro-inflammatory, pro-fibrotic, and anti-adipogenic responses. On the other hand, LYC6-, CD9- subpopulations of PDGFRβ+ were identified as adipocyte precursor cells (APCs) with an increased abundance of genes involved in adipogenesis [148,149]. In addition, activation of PDGFRα signaling induces fibrosis by transitioning the perivascular cells to ECM-producing pro-fibrotic cells [150]. The expression of CD9 differentiates between two subsets of PDGFRα+ cells in adipose tissue (eWAT). The PDGFRα+ cells with higher expression of CD9 (CD9 high) showed fibrotic potential and induced fibrosis in eWAT [125].

In sWAT, expression of LYC6 did not discriminate between different clusters of PDGFRβ+ cells but they can be separated based on expression of marker DPP4. Single-cell RNA sequencing (scRNA-seq) analysis suggests that sWAT DPP4+ PDGFRβ+ cells and DPP4- PDGFRβ+ cells bear molecular resemblance to eWAT FIPs and APCs, respectively. However, functional analysis highlighted differences in progenitor cell heterogeneity (but it was not uncovered by transcriptomic profiling) [149] [148]. Based on the following literature further investigation is needed to identify the cell type present in SVF responsible for inducing fibrosis in PPM1K KO mice. The flow cytometry analysis of these cell populations showed no difference in their percentage or total number, yet their functionality has not been determined. For future studies, the different populations responsible for the induction of fibrosis will be isolated (and cultured) from PPM1K WT and KO mice. Both the adipogenic and fibrogenic potential of these cells will be checked by evaluating the expression profile of

pro-fibrotic and adipogenesis genes in different cell populations from PPM1K WT and KO mice.

Hypoxia not only causes inflammation but also contributes to angiogenesis and tissue fibrosis [96]. The hypoxic environment raises the level of HIF-1α and activates HIF target genes such as COL1A1, COL3A1, and lysyl oxidase, an enzyme that promotes collagen cross-linking [122,123]**.** Under hypoxic conditions, the rate of BCAA consumption is attenuated, which impacts the process of de novo lipogenesis in adipocytes [95]. It has been reported hypoxia is negatively associated with the expression of several BCAA catabolic genes (such as *BCKDHB*, *HIBDH*, *MMUT*, etc.) and positively correlated with pro-fibrosis genes (such as *COL3A1*, *COL6A2*, *LOXL1*, and *LOXL2*) in obese human subjects [98]. Consistently, *Hif-1α* expression is increased in sWAT of PPM1K global KO mice as evidenced by qPCR and IF data however the activity was HIF-1α still needs to be determined. On the other hand, in IF staining data of HIF-1α and perilipin (adipocyte marker), the perilipin signal didn't co-stained with HIF-1α (no perilipin+ and HIF-1α+ cells) (not shown in the thesis), suggesting the possibility that adipocytes may not be inducing HIF-1α production in PPM1K global KO mice. The literature studies and the data from the current study speculated the involvement of HIF-1α activation in the induction of fibrosis in PPM1K global KO mice.

For future studies, to further disseminate the role of HIF-1α in the induction of adipose tissue dysfunction will be evaluated by supplementing PPM1K WT and KO mice HIF-1α inhibitor and monitor the improvement in metabolic parameters. Further, alleviation in adipose tissue fibrosis and inflammation upon HIF-1α inhibition will be evaluated using histological and expression profiles of pro-fibrotic and inflammatory genes.

All PPM1K-regulated phosphosites had a "SxS" (5/7) or a "RxxS" (5/7) motif, with three of the seven phosphosites, including Ser454 of ACL, having both, i.e., "RxxSxS" [40]. It is crucial to know if any of these phosphosites are present in HIF-1α as these sites are reported to modulate by PPM1K. Among different phosphorylation target sites (serine residue) in HIF1A (mice) (using phosphoSiteplus), only one site matches with the reported phosphosites regulated by PPM1K (the list is given below).

Table 6.1: Different phosphorylation target site (serine residue) in HIF1A (mice): from phosphoSiteplus

1.	**DAARSRRSKESEVFY**
2.	RVKGFISSEQNGTEQ
3.	DAARSRRSKESEVFY
4.	VNAPIQGSRNLLQGE
5.	DGDMVYISDNVNKYM
6.	KTFLSRHSLDMKFSY
7.	LNINLAMSPLPSSET
8.	LAMSPLPSSETPKPL
9.	TPKPLRSSADPALNQ
10.	TEAKNPFSTQDTDLD
11.	DDDFQLRSFDQLSPL
12.	PLESNSPSPPSMSTV
13.	DIKILIASPsStQVP
14.	**GTHSRTASPDRAGKR: S679 (with "RxxS" (5/7) motif)**
15.	TDKAHPRSLNLSATL

16.	HPRSLNLSATLNQRN
17.	RKMEHDGSLFQAAGI
18.	ETTTAKASAYSGTHS
19.	KRVKGFISSEQNGTE

Based on this prediction data, there is the possibility that PPM1K can alter the phosphorylation status of HIF-1α. To disseminate how PPM1K controls HIF-1α, it is important to check if PPM1K can bind HIF-1α (*in-vitro* evidence) and modulate its activity by dephosphorylation or by some other mechanisms. *In-vitro*, the binding of HIF-1α and PPM1K can be evaluated using co-immunoprecipitation.

HIF-1α activity and stability is regulated by different post-translational modifications. Apart from hydroxylation, the transcriptional activity and stability of HIF-1α can also be regulated by SUMOylation, acetylation, and phosphorylation [151]. A set of protein kinases including GSK-3β and ERK1/2 can regulate the stability or transcriptional activity of HIF-1α by phosphorylating it (directly or indirectly) [151]. Thus, phosphorylation plays an important role in regulating HIF-1α activity/stability. Based on literature and prediction study from phosphoSiteplus, it is worth checking if the binding of PPM1K can alter the HIF-1α activity which in turn induces the adipose tissue dysfunction and metabolic alteration.

It has been shown in previous and current studies that PPM1K global KO has defective BCAA catabolism. However, it's not clear if the metabolic and adipose tissue alterations caused by PPM1K deletion are mediated via the accumulation of BCAAs/BCKAs (BCAA dependent). Given the fact even if PPM1K is absent in these mice, there is still a possibility of conversion of BCAAs/BCKAs to their downstream metabolites. Apart from PPM1K, BCKDK expression

also affects the activity of the BCKDH complex. In future studies, by using different approaches including knockdown of *Bckdha*, inhibition of BCKDK by using BT2, and using BCAA-free media it can be identified if the metabolic alteration in PPM1K global KO mice is BCAA dependent or independent.

6.2 Adipocyte PPM1K deficiency induces adipose tissue dysfunction (fibrosis, inflammation, senescence) and liver steatosis.

To study the role of PPM1K in adipose tissue biology, exploiting a global KO won't be a good choice. In global KO, BCAA catabolism is defective in all tissue, in this case, it's difficult to identify in which tissue defective BCAA catabolism is contributing to adipose tissue dysfunction. To specifically evaluate the role of adipocyte PPM1K, an adipocyte-specific PPM1K KO (A-KO) mouse model was generated. Even though A-KO mice lack PPM1K only in adipocytes, still they showed increased circulatory BCAAs/BCKAs levels. A previous study reported adipose tissue can modulate the circulatory BCAAs levels [78] however adipocytes were not reported as contributor cell types for the phenomena. The current study has pointed adipocytes are important for maintaining circulatory BCAAs levels. A-KO mice showed an alteration in glucose, lipid, and energy metabolism and the effect is more pronounced as compared to global KO mice.

Despite the fact, that in PPM1K-global KO mice, there were no changes observed in fibrosis in mature adipocyte fractions, adipocyte-specific deletion of PPM1K led to elevated fibrosis and infiltration of M1 macrophages in WAT. It might be due to masking effects from other tissues in the PPM1K global KO mouse model. In a previous study, the knockdown of Bckdha led to a decrease in the expression of adipogenic genes including *Pparg, Glut4, Plin4, Adipoq,* and *Lep,* and attenuated lipid droplets in mature adipocytes [81]. These findings highlight the importance of adipocyte BCAA catabolism in the regulation of adipose tissue function.

In recent years, elevated circulatory BCAAs levels have been observed in aged mice. Additionally, the expression of BCAA catabolic genes *Bckdha, Bckdhb, Pcca, and Pccb* is reduced in aging adipose tissue [67]. In a different study role of Bcat1 is reported in the

regulation of physiological aging in various experimental model organisms including *C. elegans*, Zebrafish, and mice [68]. Similar to these observations, the sign of pre-mature aging of adipose tissue was observed in A-KO mice as evidenced by the increase in β-Gal staining, and higher expression of senescent markers P21. However, the mechanism of how deletion of adipocyte PPM1K induces pre-mature aging remains elusive.

Previous reports showed defects in thermogenesis, energy expenditure, and BCAA oxidation in BAT-specific BCKDHA-KO mice [84]. Consistently, the absence of adipocyte PPM1K led to defective thermogenesis, energy expenditure, and altered BCAA catabolism in BAT of A-KO mice. These studies highlight the significance of intact BCAA catabolic machinery in the maintenance of BAT functions.

Adipose tissue dysfunction promotes the pathophysiology of NAFLD by enhancing the supply of lipids and adipokines to the liver, which can elevate hepatic steatosis and inflammation [152]. In line with literature studies, the A-KO mice showed increased hepatic steatosis, fibrosis, and inflammation possibly due to adipose tissue dysfunction in these mice. On the other hand, a positive correlation has been observed between plasma BCAA and steatosis stages and fat content in the liver in NAFLD subjects with severe obesity [153]. Similar to this, an increased serum BCKAs was observed in adipocyte-PPM1K KO mice and partly this can also contribute to alteration in liver steatosis.

The primary role of mitochondria in adipocytes is to generate ATP for various biological processes including lipogenesis, re-esterification of fatty acids, and gluconeogenesis [154]. In addition to increased fibrosis and inflammation, RNA seq analysis revealed the role of adipocyte-PPM1K in mitochondrial respiration in eWAT. In support of this observation, the BCAA catabolic defect/BCKA accumulation can diminish the mitochondrial function, and

lead to the production of ROS in cardiac tissue [47]. In another mouse model (3-MST KO mice), an increase in BCAAs is associated with decreased mitochondrial respiration and production of ATP in the myocardium [155].

An induction of Rho pathways (such as Rho kinase) resulted in insulin resistance and higher body weight in HFD mice [144]. In adipocytes, mechanical stress causes the activation of Rho pathways and the formation of stress fibers and the Rho GTPase is the regulator of actin cytoskeleton rearrangement. Additionally RND3, a Rho-related GTP-binding protein showed elevated expression in obesity and was associated with insulin resistance in humans, and also regulates adipocyte lipolysis [145]. In the current study, Rho GTPase effectors pathways were identified as one of the highly enriched pathways both in eWAT and sWAT. Based on the literature and current findings, it was speculated that upregulated expression of Rho GTPase effectors pathways might be involved in the induction of adipose tissue dysfunction in A-KO mice in WAT. Nevertheless, further investigation is needed to validate this speculation. For future studies, the role of the Rho GTPase effectors pathway in the induction of adipose tissue dysfunction will be investigated in adipocyte-PPM1K KO mice. This is one of the promising target pathways to be evaluated. In contrast to PPM1K-global KO mice, the HIF-1α activation pathway was not targeted, as it was not an overlapped and enriched pathway in RNA sequencing data.

6.3 Limitations of the study

This study revealed the unprecedented role of PPM1K in adipose tissue functions including remodeling, adipogenesis, and senescence. In addition, the deleterious effects of adipocyte PPM1K deletion were observed on liver tissue biology. Despite the novel findings, this study has several limitations including

1) Gut microbiota is identified as one of the factors affecting the BCAA levels. Some gut bacteria including *Prevotella copri* and *Bacteroides vulgatus* can biosynthesize BCAA and are positively correlated with circulating BCAAs levels in human subjects with insulin resistance [156]. In both mouse models including PPM1K-global KO and adipocyte-specific PPM1K KO, higher BCAAs levels and insulin resistance in observed. However, is there any change in gut microbiota abundance in these mice models was not investigated. Additionally, the possibility of the involvement of gut microbiota in the induction of metabolic alterations is not studied.
2) For studying the role of adipocyte PPM1K only HFHC-fed mice were considered for the study. However, the functions of adipocyte PPM1K under the STC- diet (which serves as a control diet) are not explored.
3) In addition, the effect of adipocyte PPM1K deletion on BAT and liver tissue biology is not investigated in depth.

Most importantly, the underlying mechanism of how PPM1K controls adipose tissue functions needs further investigation in both mouse models including global KO and adipocyte-PPM1K KO.

References

1. WHO. World Health Organization (WHO) - Expert Consultation;appropriate body-mass index for Asian populations and its implications for policy and intervention strategies. Lancet.
2. Chatterjee A, Gerdes MW, Martinez SG. Identification of risk factors associated with obesity and overweight—a machine learning overview. *Sensors (Switzerland)*. Published online 2020. doi:10.3390/s20092734
3. Sattar N, McInnes IB, McMurray JJV. Obesity Is a Risk Factor for Severe COVID-19 Infection: Multiple Potential Mechanisms. *Circulation*. Published online 2020. doi:10.1161/CIRCULATIONAHA.120.047659
4. Vishvanath L, Gupta RK. Contribution of adipogenesis to healthy adipose tissue expansion in obesity. *J Clin Invest*. Published online 2019. doi:10.1172/JCI129191
5. Richard AJ, White U, Elks CM, Stephens JM. *Adipose Tissue: Physiology to Metabolic Dysfunction*.; 2000.
6. Choe SS, Huh JY, Hwang IJ, Kim JI, Kim JB. Adipose tissue remodeling: Its role in energy metabolism and metabolic disorders. *Front Endocrinol (Lausanne)*. Published online 2016. doi:10.3389/fendo.2016.00030
7. Kersten S. Physiological regulation of lipoprotein lipase. *Biochim Biophys Acta - Mol Cell Biol Lipids*. Published online 2014. doi:10.1016/j.bbalip.2014.03.013
8. Song Z, Xiaoli AM, Yang F. Regulation and metabolic significance of De Novo lipogenesis in adipose tissues. *Nutrients*. Published online 2018. doi:10.3390/nu10101383
9. Rondinone CM. Adipocyte-derived hormones, cytokines, and mediators. *Endocrine*.

Published online 2006. doi:10.1385/ENDO:29:1:81

10. Fasshauer M, Blüher M. Adipokines in health and disease. *Trends Pharmacol Sci*. Published online 2015. doi:10.1016/j.tips.2015.04.014

11. Blüher M. Importance of adipokines in glucose homeostasis. *Diabetes Manag*. Published online 2013. doi:10.2217/dmt.13.35

12. Blüher M. Adipose tissue dysfunction contributes to obesity related metabolic diseases. *Best Pract Res Clin Endocrinol Metab*. Published online 2013. doi:10.1016/j.beem.2013.02.005

13. Ouchi N, Parker JL, Lugus JJ, Walsh K. Adipokines in inflammation and metabolic disease. *Nat Rev Immunol*. Published online 2011. doi:10.1038/nri2921

14. Maffei M, Halaas J, Ravussin E, et al. Leptin levels in human and rodent: Measurement of plasma leptin and ob RNA in obese and weight-reduced subjects. *Nat Med*. Published online 1995. doi:10.1038/nm1195-1155

15. Diep Nguyen T. Adiponectin: Role in physiology and pathophysiology. *Int J Prev Med*. Published online 2020. doi:10.4103/ijpvm.ijpvm_193_20

16. Yamauchi T, Kamon J, Waki H, et al. The fat-derived hormone adiponectin reverses insulin resistance associated with both lipoatrophy and obesity. *Nat Med*. Published online 2001. doi:10.1038/90984

17. Xu A, Wang Y, Keshaw H, Xu LY, Lam KSL, Cooper GJS. The fat-derived hormone adiponectin alleviates alcoholic and nonalcoholic fatty liver diseases in mice. *J Clin Invest*. Published online 2003. doi:10.1172/JCI200317797

18. Kara K, Boutin P, Mori Y, et al. Genetic variation in the gene encoding adiponectin is associated with an increased risk of type 2 diabetes in the Japanese population. *Diabetes*.

Published online 2002. doi:10.2337/diabetes.51.2.536

19. Ouchi N, Higuchi A, Ohashi K, et al. Sfrp5 is an anti-inflammatory adipokine that modulates metabolic dysfunction in obesity. *Science (80-).* Published online 2010. doi:10.1126/science.1188280

20. Cannon B, Nedergaard J. Brown Adipose Tissue: Function and Physiological Significance. *Physiol Rev*. Published online 2004. doi:10.1152/physrev.00015.2003

21. Puigserver P, Wu Z, Park CW, Graves R, Wright M, Spiegelman BM. A cold-inducible coactivator of nuclear receptors linked to adaptive thermogenesis. *Cell*. Published online 1998. doi:10.1016/S0092-8674(00)81410-5

22. Herold J, Kalucka J. Angiogenesis in Adipose Tissue: The Interplay Between Adipose and Endothelial Cells. *Front Physiol*. Published online 2021. doi:10.3389/fphys.2020.624903

23. Chung S, LaPoint K, Martinez K, Kennedy A, Sandberg MB, McIntosh MK. Preadipocytes mediate lipopolysaccharide-induced inflammation and insulin resistance in primary cultures of newly differentiated human adipocytes. *Endocrinology*. Published online 2006. doi:10.1210/en.2006-0536

24. Rosen ED, MacDougald OA. Adipocyte differentiation from the inside out. *Nat Rev Mol Cell Biol*. Published online 2006. doi:10.1038/nrm2066

25. Rodeheffer MS, Birsoy K, Friedman JM. Identification of White Adipocyte Progenitor Cells In Vivo. *Cell*. Published online 2008. doi:10.1016/j.cell.2008.09.036

26. Hepler C, Shan B, Zhang Q, et al. Identification of functionally distinct fibro-inflammatory and adipogenic stromal subpopulations in visceral adipose tissue of adult mice. *Elife*. Published online 2018. doi:10.7554/eLife.39636

27. Layman DK. The role of leucine in weight loss diets and glucose homeostasis. In: *Journal of Nutrition*. ; 2003. doi:10.1093/jn/133.1.261s

28. Biswas D, Duffley L, Pulinilkunnil T. Role of branched-chain amino acid–catabolizing enzymes in intertissue signaling, metabolic remodeling, and energy homeostasis. *FASEB J*. 2019;33(8):8711-8731. doi:10.1096/fj.201802842RR

29. Hutson SM, Wallin R, Hall TR. Identification of mitochondrial branched chain aminotransferase and its isoforms in rat tissues. *J Biol Chem*. Published online 1992. doi:10.1016/s0021-9258(19)49589-6

30. Ding C, Li Y, Guo F, et al. A cell-type-resolved liver proteome. *Mol Cell Proteomics*. Published online 2016. doi:10.1074/mcp.M116.060145

31. Neinast MD, Jang C, Hui S, et al. Quantitative Analysis of the Whole-Body Metabolic Fate of Branched-Chain Amino Acids. *Cell Metab*. Published online 2019. doi:10.1016/j.cmet.2018.10.013

32. Hutson SM, Sweatt AJ, LaNoue KF. Brached-chain amino acid metabolism: Implications for establishing safe intakes. In: *Journal of Nutrition*. ; 2005. doi:10.1093/jn/135.6.1557s

33. Yudkoff M, Daikhin Y, Nissim I, et al. Brain amino acid requirements and toxicity: The example of leucine. In: *Journal of Nutrition*. ; 2005. doi:10.1093/jn/135.6.1531s

34. Brosnan JT, Brosnan ME. Branched-chain amino acids: Enzyme and substrate regulation. In: *Journal of Nutrition*. ; 2006. doi:10.1093/jn/136.1.207s

35. Vanweert F, Schrauwen P, Phielix E. Role of branched-chain amino acid metabolism in the pathogenesis of obesity and type 2 diabetes-related metabolic disturbances BCAA metabolism in type 2 diabetes. *Nutr Diabetes*. Published online 2022.

doi:10.1038/s41387-022-00213-3

36. Ævarsson A, Chuang JL, Max Wynn R, Turley S, Chuang DT, Hol WGJ. Crystal structure of human branched-chain α-ketoacid dehydrogenase and the molecular basis of multienzyme complex deficiency in maple syrup urine disease. *Structure*. Published online 2000. doi:10.1016/S0969-2126(00)00105-2

37. Lu G, Sun H, She P, et al. Protein phosphatase 2Cm is a critical regulator of branched-chain amino acid catabolism in mice and cultured cells. *J Clin Invest*. Published online 2009. doi:10.1172/JCI38151

38. Shimomura Y, Nanaumi N, Suzuki M, Popov KM, Harris RA. Purification and partial characterization of branched-chain α-ketoacid dehydrogenase kinase from rat liver and rat heart. *Arch Biochem Biophys*. Published online 1990. doi:10.1016/0003-9861(90)90645-F

39. Jang C, Oh SF, Wada S, et al. A branched-chain amino acid metabolite drives vascular fatty acid transport and causes insulin resistance. *Nat Med*. Published online 2016. doi:10.1038/nm.4057

40. White PJ, McGarrah RW, Grimsrud PA, et al. The BCKDH Kinase and Phosphatase Integrate BCAA and Lipid Metabolism via Regulation of ATP-Citrate Lyase. *Cell Metab*. 2018;27(6):1281-1293.e7. doi:10.1016/j.cmet.2018.04.015

41. Li T, Zhang Z, Kolwicz SC, et al. Defective Branched-Chain Amino Acid Catabolism Disrupts Glucose Metabolism and Sensitizes the Heart to Ischemia-Reperfusion Injury. *Cell Metab*. Published online 2017. doi:10.1016/j.cmet.2016.11.005

42. Newgard CB, An J, Bain JR, et al. A Branched-Chain Amino Acid-Related Metabolic Signature that Differentiates Obese and Lean Humans and Contributes to Insulin

Resistance. *Cell Metab*. Published online 2009. doi:10.1016/j.cmet.2009.02.002

43. Anthony JC, Yoshizawa F, Anthony TG, Vary TC, Jefferson LS, Kimball SR. Leucine stimulates translation initiation skeletal muscle of postabsorptive rats via a rapamycin-sensitive pathway. *J Nutr*. Published online 2000. doi:10.1093/jn/130.10.2413

44. Saha AK, Xu XJ, Lawson E, et al. Downregulation of AMPK accompanies leucine- and glucose-induced increases in protein synthesis and insulin resistance in rat skeletal muscle. *Diabetes*. 2010;59(10):2426-2434. doi:10.2337/db09-1870

45. Xiao F, Huang Z, Li H, et al. Leucine deprivation increases hepatic insulin sensitivity via GCN2/mTOR/S6K1 and AMPK pathways. *Diabetes*. Published online 2011. doi:10.2337/db10-1246

46. Giesbertz P, Padberg I, Rein D, et al. Metabolite profiling in plasma and tissues of ob/ob and db/db mice identifies novel markers of obesity and type 2 diabetes. *Diabetologia*. Published online 2015. doi:10.1007/s00125-015-3656-y

47. Sun H, Olson KC, Gao C, et al. Catabolic defect of branched-chain amino acids promotes heart failure. *Circulation*. Published online 2016. doi:10.1161/CIRCULATIONAHA.115.020226

48. Tobias DK, Lawler PR, Harada PH, et al. Circulating Branched-Chain Amino Acids and Incident Cardiovascular Disease in a Prospective Cohort of US Women. *Circ Genomic Precis Med*. Published online 2018. doi:10.1161/CIRCGEN.118.002157

49. Wang TJ, Larson MG, Vasan RS, et al. Metabolite profiles and the risk of developing diabetes. *Nat Med*. Published online 2011. doi:10.1038/nm.2307

50. Newgard CB. Interplay between lipids and branched-chain amino acids in development of insulin resistance. *Cell Metab*. 2012;15(5):606-614. doi:10.1016/j.cmet.2012.01.024

51. She P, Olson KC, Kadota Y, et al. Leucine and Protein Metabolism in Obese Zucker Rats. *PLoS One*. Published online 2013. doi:10.1371/journal.pone.0059443

52. Ramzan I, Ardavani A, Vanweert F, Mellett A, Atherton PJ, Idris I. The Association between Circulating Branched Chain Amino Acids and the Temporal Risk of Developing Type 2 Diabetes Mellitus: A Systematic Review & Meta-Analysis. *Nutrients*. Published online 2022. doi:10.3390/nu14204411

53. Lynch CJ, Adams SH. Branched-chain amino acids in metabolic signalling and insulin resistance. *Nat Rev Endocrinol*. 2014;10(12):723-736. doi:10.1038/nrendo.2014.171

54. Vargas-Morales JM, Guizar-Heredia R, Méndez-García AL, et al. Association of BCAT2 and BCKDH polymorphisms with clinical, anthropometric and biochemical parameters in young adults. *Nutr Metab Cardiovasc Dis*. Published online 2021. doi:10.1016/j.numecd.2021.07.011

55. Hu W, Liu Z, Yu W, et al. Effects of PPM1K rs1440581 and rs7678928 on serum branched-chain amino acid levels and risk of cardiovascular disease. *Ann Med*. Published online 2021. doi:10.1080/07853890.2021.1965204

56. Lotta LA, Scott RA, Sharp SJ, et al. Genetic Predisposition to an Impaired Metabolism of the Branched-Chain Amino Acids and Risk of Type 2 Diabetes: A Mendelian Randomisation Analysis. *PLoS Med*. Published online 2016. doi:10.1371/journal.pmed.1002179

57. Grenier-Larouche T, Coulter Kwee L, Deleye Y, et al. Altered branched-chain α-keto acid metabolism is a feature of NAFLD in individuals with severe obesity. *JCI insight*. Published online 2022. doi:10.1172/jci.insight.159204

58. C. M, E. F, I. E, et al. Biomarkers for type 2 diabetes and impaired fasting glucose using

a nontargeted metabolomics approach. *Diabetes*. Published online 2013.

59. Nilsen MS, Jersin RÅ, Ulvik A, et al. 3-Hydroxyisobutyrate, A Strong Marker of Insulin Resistance in Type 2 Diabetes and Obesity That Modulates White and Brown Adipocyte Metabolism. *Diabetes*. Published online 2020. doi:10.2337/db19-1174

60. Mardinoglu A, Gogg S, Lotta LA, et al. Elevated Plasma Levels of 3-Hydroxyisobutyric Acid Are Associated With Incident Type 2 Diabetes. *EBioMedicine*. 2018;27:151-155. doi:10.1016/j.ebiom.2017.12.008

61. Bjune MS, Lawrence-Archer L, Laupsa-Borge J, et al. Metabolic role of the hepatic valine/3-hydroxyisobutyrate (3-HIB) pathway in fatty liver disease. *eBioMedicine*. 2023;91:104569. doi:10.1016/j.ebiom.2023.104569

62. Fontana L, Cummings NE, Arriola Apelo SI, et al. Decreased Consumption of Branched-Chain Amino Acids Improves Metabolic Health. *Cell Rep*. Published online 2016. doi:10.1016/j.celrep.2016.05.092

63. Cummings NE, Williams EM, Kasza I, et al. Restoration of metabolic health by decreased consumption of branched-chain amino acids. *J Physiol*. 2018;596(4):623-645. doi:10.1113/JP275075

64. Cheng Y, Meng Q, Wang C, et al. Leucine deprivation decreases fat mass by stimulation of lipolysis in white adipose tissue and upregulation of uncoupling protein 1 (UCP1) in brown adipose tissue. *Diabetes*. Published online 2010. doi:10.2337/db09-0929

65. Yoon MS. The emerging role of branched-chain amino acids in insulin resistance and metabolism. *Nutrients*. 2016;8(7). doi:10.3390/nu8070405

66. Zhou M, Shao J, Wu CY, et al. Targeting BCAA catabolism to treat obesity-associated insulin resistance. *Diabetes*. 2019;68(9):1730-1746. doi:10.2337/db18-0927

67. Han H-S, Ahn E, Park ES, et al. Impaired BCAA catabolism in adipose tissues promotes age-associated metabolic derangement. . *Nat Aging*. 2023;vol:XXX-XXX. doi:10.1038/s43587-023-00460-8

68. Mansfeld J, Urban N, Priebe S, et al. Branched-chain amino acid catabolism is a conserved regulator of physiological ageing. *Nat Commun*. Published online 2015. doi:10.1038/ncomms10043

69. Richardson NE, Konon EN, Schuster HS, et al. Lifelong restriction of dietary branched-chain amino acids has sex-specific benefits for frailty and life span in mice. *Nat Aging*. Published online 2021. doi:10.1038/s43587-020-00006-2

70. Scherer PE. Adipose tissue: From lipid storage compartment to endocrine organ. In: *Diabetes*. ; 2006. doi:10.2337/db06-0263

71. Rosen ED, Spiegelman BM. What we talk about when we talk about fat. *Cell*. Published online 2014. doi:10.1016/j.cell.2013.12.012

72. Kusminski CM, Bickel PE, Scherer PE. Targeting adipose tissue in the treatment of obesity-associated diabetes. *Nat Rev Drug Discov*. Published online 2016. doi:10.1038/nrd.2016.75

73. Burrill JS, Long EK, Reilly B, et al. Inflammation and ER stress regulate branched-chain amino acid uptake and metabolism in adipocytes. *Mol Endocrinol*. Published online 2015. doi:10.1210/me.2014-1275

74. Segawa H, Fukasawa Y, Miyamoto KI, Takeda E, Endou H, Kanai Y. Identification and functional characterization of a Na+-independent neutral amino acid transporter with broad substrate selectivity. *J Biol Chem*. Published online 1999. doi:10.1074/jbc.274.28.19745

75. Utsunomiya-Tate N, Endou H, Kanai Y. Cloning and functional characterization of a system ASC-like Na+-dependent neutral amino acid transporter. *J Biol Chem*. Published online 1996. doi:10.1074/jbc.271.25.14883

76. Kanai Y, Segawa H, Miyamoto KI, Uchino H, Takeda E, Endou H. Expression cloning and characterization of a transporter for large neutral amino acids activated by the heavy chain of 4F2 antigen (CD98). *J Biol Chem*. Published online 1998. doi:10.1074/jbc.273.37.23629

77. Wallace M, Green CR, Roberts LS, et al. Enzyme promiscuity drives branched-chain fatty acid synthesis in adipose tissues. *Nat Chem Biol*. Published online 2018. doi:10.1038/s41589-018-0132-2

78. Herman MA, She P, Peroni OD, Lynch CJ, Kahn BB. Adipose tissue Branched Chain Amino Acid (BCAA) metabolism modulates circulating BCAA levels. *J Biol Chem*. Published online 2010. doi:10.1074/jbc.M109.075184

79. Tischler ME, Goldberg AL. Leucine degradation and release of glutamine and alanine by adipose tissue. *J Biol Chem*. Published online 1980. doi:10.1016/s0021-9258(19)70609-7

80. Rosenthal J, Angel A, Farkas J. Metabolic fate of leucine: a significant sterol precursor in adipose tissue and muscle. *Am J Physiol*. Published online 1974. doi:10.1152/ajplegacy.1974.226.2.411

81. Green CR, Wallace M, Divakaruni AS, et al. Branched-chain amino acid catabolism fuels adipocyte differentiation and lipogenesis. *Nat Chem Biol*. Published online 2016. doi:10.1038/nchembio.1961

82. Fenzl A, Kiefer FW. Brown adipose tissue and thermogenesis. *Horm Mol Biol Clin*

Investig. Published online 2014. doi:10.1515/hmbci-2014-0022

83. Sun H, Wang Y. A new branch connecting thermogenesis and diabetes. *Nat Metab*. Published online 2019. doi:10.1038/s42255-019-0112-1

84. Yoneshiro T, Wang Q, Tajima K, et al. BCAA catabolism in brown fat controls energy homeostasis through SLC25A44. *Nature*. Published online 2019. doi:10.1038/s41586-019-1503-x

85. Turer AT, Scherer PE. Adiponectin: Mechanistic insights and clinical implications. *Diabetologia*. Published online 2012. doi:10.1007/s00125-012-2598-x

86. Yamauchi T, Kamon J, Minokoshi Y, et al. Adiponectin stimulates glucose utilization and fatty-acid oxidation by activating AMP-activated protein kinase. *Nat Med*. Published online 2002. doi:10.1038/nm788

87. Li S, Shin HJ, Ding EL, Van Dam RM. Adiponectin levels and risk of type 2 diabetes: A systematic review and meta-analysis. *JAMA - J Am Med Assoc*. Published online 2009. doi:10.1001/jama.2009.976

88. Weyer C, Funahashi T, Tanaka S, et al. Hypoadiponectinemia in obesity and type 2 diabetes: Close association with insulin resistance and hyperinsulinemia. *J Clin Endocrinol Metab*. Published online 2001. doi:10.1210/jcem.86.5.7463

89. Lian K, Du C, Liu Y, et al. Impaired adiponectin signaling contributes to disturbed catabolism of branched-chain amino acids in diabetic mice. *Diabetes*. Published online 2015. doi:10.2337/db14-0312

90. Liu Y, Turdi S, Park T, et al. Adiponectin corrects high-fat diet-induced disturbances in muscle metabolomic profile and whole-body glucose homeostasis. *Diabetes*. Published online 2013. doi:10.2337/db12-0687

91. Kilroy GE, Zhang X, Floyd ZE. PPAR-γ AF-2 domain functions as a component of a ubiquitin-dependent degradation signal. *Obesity*. Published online 2009. doi:10.1038/oby.2008.616

92. Anghel SI, Wahli W. Fat poetry: A kingdom for PPARγ. *Cell Res*. Published online 2007. doi:10.1038/cr.2007.48

93. Hsiao G, Chapman J, Ofrecio JM, et al. Multi-tissue, selective PPARγ modulation of insulin sensitivity and metabolic pathways in obese rats. *Am J Physiol - Endocrinol Metab*. Published online 2011. doi:10.1152/ajpendo.00219.2010

94. Blanchard PG, Moreira RJ, Castro É, et al. PPARγ is a major regulator of branched-chain amino acid blood levels and catabolism in white and brown adipose tissues. *Metabolism*. Published online 2018. doi:10.1016/j.metabol.2018.09.007

95. Oates EH, Antoniewicz MR. 13C-Metabolic flux analysis of 3T3-L1 adipocytes illuminates its core metabolism under hypoxia. *Metab Eng*. Published online 2023. doi:10.1016/j.ymben.2023.02.002

96. Andrei AM, Berbecaru-Iovan A, Din-Anghel FRI, et al. Interplay between Hypoxia, Inflammation and Adipocyte Remodeling in the Metabolic Syndrome. In: *Hypoxia and Human Diseases*. ; 2017. doi:10.5772/65491

97. Crewe C, An YA, Scherer PE. The ominous triad of adipose tissue dysfunction: Inflammation, fibrosis, and impaired angiogenesis. *J Clin Invest*. Published online 2017. doi:10.1172/JCI88883

98. Cifarelli V, Beeman SC, Smith GI, et al. Decreased adipose tissue oxygenation associates with insulin resistance in individuals with obesity. *J Clin Invest*. 2020;130(12):6688-6699. doi:10.1172/JCI141828

99. Seale P, Conroe HM, Estall J, et al. Prdm16 determines the thermogenic program of subcutaneous white adipose tissue in mice. *J Clin Invest*. Published online 2011. doi:10.1172/JCI44271

100. Ma QX, Zhu WY, Lu XC, et al. BCAA–BCKA axis regulates WAT browning through acetylation of PRDM16. *Nat Metab*. Published online 2022. doi:10.1038/s42255-021-00520-6

101. Zhao S, Zhou L, Wang Q, et al. Elevated branched-chain amino acid promotes atherosclerosis progression by enhancing mitochondrial-to-nuclear H2O2-disulfide HMGB1 in macrophages. *Redox Biol*. 2023;62(April):102696. doi:10.1016/j.redox.2023.102696

102. Son M, Porat A, He M, et al. C1q and HMGB1 reciprocally regulate human macrophage polarization. *Blood*. Published online 2016. doi:10.1182/blood-2016-05-719757

103. Liu S, Li L, Lou P, et al. Elevated branched-chain α-keto acids exacerbate macrophage oxidative stress and chronic inflammatory damage in type 2 diabetes mellitus. *Free Radic Biol Med*. Published online 2021. doi:10.1016/j.freeradbiomed.2021.08.240

104. Sam S, Mazzone T. Adipose tissue changes in obesity and the impact on metabolic function. *Transl Res*. Published online 2014. doi:10.1016/j.trsl.2014.05.008

105. Nerstedt A, Smith U. The impact of cellular senescence in human adipose tissue. *J Cell Commun Signal*. Published online 2023. doi:10.1007/s12079-023-00769-4

106. Desai M, Guang Han, Ferelli M, Kallichanda N, Lane RH. Programmed upregulation of adipogenic transcription factors in intrauterine growth-restricted offspring. *Reprod Sci*. Published online 2008. doi:10.1177/1933719108318597

107. Alligier M, Meugnier E, Debard C, et al. Subcutaneous adipose tissue remodeling during

the initial phase of weight gain induced by overfeeding in humans. *J Clin Endocrinol Metab*. Published online 2012. doi:10.1210/jc.2011-2314

108. Khan T, Muise ES, Iyengar P, et al. Metabolic Dysregulation and Adipose Tissue Fibrosis: Role of Collagen VI. *Mol Cell Biol*. Published online 2009. doi:10.1128/mcb.01300-08

109. Ye J, Gao Z, Yin J, He Q. Hypoxia is a potential risk factor for chronic inflammation and adiponectin reduction in adipose tissue of ob/ob and dietary obese mice. *Am J Physiol - Endocrinol Metab*. Published online 2007. doi:10.1152/ajpendo.00435.2007

110. Wang B, Wood IS, Trayhurn P. Dysregulation of the expression and secretion of inflammation-related adipokines by hypoxia in human adipocytes. *Pflugers Arch Eur J Physiol*. Published online 2007. doi:10.1007/s00424-007-0301-8

111. Hotamisligil GS. Endoplasmic Reticulum Stress and the Inflammatory Basis of Metabolic Disease. *Cell*. Published online 2010. doi:10.1016/j.cell.2010.02.034

112. Kosteli A, Sugaru E, Haemmerle G, et al. Weight loss and lipolysis promote a dynamic immune response in murine adipose tissue. *J Clin Invest*. Published online 2010. doi:10.1172/JCI42845

113. Xu H, Barnes GT, Yang Q, et al. Chronic inflammation in fat plays a crucial role in the development of obesity-related insulin resistance. *J Clin Invest*. Published online 2003. doi:10.1172/JCI200319451

114. Kamei N, Tobe K, Suzuki R, et al. Overexpression of monocyte chemoattractant protein-1 in adipose tissues causes macrophage recruitment and insulin resistance. *J Biol Chem*. Published online 2006. doi:10.1074/jbc.M601284200

115. Kanda H, Tateya S, Tamori Y, et al. MCP-1 contributes to macrophage infiltration into

adipose tissue, insulin resistance, and hepatic steatosis in obesity. *J Clin Invest*. Published online 2006. doi:10.1172/JCI26498

116. Bruun JM, Helge JW, Richelsen B, Stallknecht B. Diet and exercise reduce low-grade inflammation and macrophage infiltration in adipose tissue but not in skeletal muscle in severely obese subjects. *Am J Physiol - Endocrinol Metab*. Published online 2006. doi:10.1152/ajpendo.00506.2005

117. Kamei N, Tobe K, Suzuki R, et al. Overexpression of MCP-1 in adipose tissues causes macrophage recruitment and insulin resistance. *J Biol Chem*. Published online 2006.

118. Hasegawa Y, Ikeda K, Chen Y, et al. Repression of Adipose Tissue Fibrosis through a PRDM16-GTF2IRD1 Complex Improves Systemic Glucose Homeostasis. *Cell Metab*. Published online 2018. doi:10.1016/j.cmet.2017.12.005

119. Savage DB, Petersen KF, Shulman GI. Disordered lipid metabolism and the pathogenesis of insulin resistance. *Physiol Rev*. Published online 2007. doi:10.1152/physrev.00024.2006

120. Sun K, Park J, Gupta OT, et al. Endotrophin triggers adipose tissue fibrosis and metabolic dysfunction. *Nat Commun*. Published online 2014. doi:10.1038/ncomms4485

121. Jones JEC, Rabhi N, Orofino J, et al. The Adipocyte Acquires a Fibroblast-Like Transcriptional Signature in Response to a High Fat Diet. *Sci Rep*. Published online 2020. doi:10.1038/s41598-020-59284-w

122. Sun K, Tordjman J, Clément K, Scherer PE. Fibrosis and adipose tissue dysfunction. *Cell Metab*. Published online 2013. doi:10.1016/j.cmet.2013.06.016

123. Halberg N, Khan T, Trujillo ME, et al. Hypoxia-Inducible Factor 1α Induces Fibrosis and Insulin Resistance in White Adipose Tissue. *Mol Cell Biol*. 2009;29(16):4467-4483.

doi:10.1128/mcb.00192-09

124. Datta R, Podolsky MJ, Atabai K. Fat fibrosis: friend or foe? *JCI insight*. Published online 2018. doi:10.1172/jci.insight.122289

125. Marcelin G, Ferreira A, Liu Y, et al. A PDGFRα-Mediated Switch toward CD9high Adipocyte Progenitors Controls Obesity-Induced Adipose Tissue Fibrosis. *Cell Metab*. Published online 2017. doi:10.1016/j.cmet.2017.01.010

126. Keophiphath M, Achard V, Henegar C, Rouault C, Clément K, Lacasa D Le. Macrophage-secreted factors promote a profibrotic phenotype in human preadipocytes. *Mol Endocrinol*. Published online 2009. doi:10.1210/me.2008-0183

127. Vila IK, Badin PM, Marques MA, et al. Immune cell toll-like receptor 4 mediates the development of obesity- and endotoxemia-associated adipose tissue fibrosis. *Cell Rep*. Published online 2014. doi:10.1016/j.celrep.2014.03.062

128. Kaluz S, Kaluzová M, Stanbridge EJ. Regulation of gene expression by hypoxia: Integration of the HIF-transduced hypoxic signal at the hypoxia-responsive element. *Clin Chim Acta*. Published online 2008. doi:10.1016/j.cca.2008.05.002

129. Debari MK, Abbott RD. Adipose tissue fibrosis: Mechanisms, models, and importance. *Int J Mol Sci*. Published online 2020. doi:10.3390/ijms21176030

130. Mariman ECM, Wang P. Adipocyte extracellular matrix composition, dynamics and role in obesity. *Cell Mol Life Sci*. Published online 2010. doi:10.1007/s00018-010-0263-4

131. Sun K, Halberg N, Khan M, Magalang UJ, Scherer PE. Selective Inhibition of Hypoxia-Inducible Factor 1α Ameliorates Adipose Tissue Dysfunction. *Mol Cell Biol*. Published online 2013. doi:10.1128/mcb.00951-12

132. Budi EH, Duan D, Derynck R. Transforming Growth Factor-β Receptors and Smads:

Regulatory Complexity and Functional Versatility. *Trends Cell Biol*. Published online 2017. doi:10.1016/j.tcb.2017.04.005

133. Lee MJ. Transforming growth factor beta superfamily regulation of adipose tissue biology in obesity. *Biochim Biophys Acta - Mol Basis Dis*. Published online 2018. doi:10.1016/j.bbadis.2018.01.025

134. Bourlier V, Sengenès C, Zakaroff-Girard A, et al. TGFbeta family members are key mediators in the induction of myofibroblast phenotype of human adipose tissue progenitor cells by macrophages. *PLoS One*. Published online 2012. doi:10.1371/journal.pone.0031274

135. Holley RJ, Tai G, Williamson AJK, et al. Comparative quantification of the surfaceome of human multipotent mesenchymal progenitor cells. *Stem Cell Reports*. Published online 2015. doi:10.1016/j.stemcr.2015.01.007

136. Smith U, Li Q, Rydén M, Spalding KL. Cellular senescence and its role in white adipose tissue. *Int J Obes*. Published online 2021. doi:10.1038/s41366-021-00757-x

137. Palmer AK, Tchkonia T, Kirkland JL. Targeting cellular senescence in metabolic disease. *Mol Metab*. Published online 2022. doi:10.1016/j.molmet.2022.101601

138. Conley SM, Hickson LTJ, Kellogg TA, et al. Human Obesity Induces Dysfunction and Early Senescence in Adipose Tissue-Derived Mesenchymal Stromal/Stem Cells. *Front Cell Dev Biol*. Published online 2020. doi:10.3389/fcell.2020.00197

139. Gustafson B, Nerstedt A, Smith U. Reduced subcutaneous adipogenesis in human hypertrophic obesity is linked to senescent precursor cells. *Nat Commun*. Published online 2019. doi:10.1038/s41467-019-10688-x

140. Vergoni B, Cornejo PJ, Gilleron J, et al. DNA damage and the activation of the p53

pathway mediate alterations in metabolic and secretory functions of adipocytes. *Diabetes*. Published online 2016. doi:10.2337/db16-0014

141. Chen YW, Harris RA, Hatahet Z, Chou KM. Ablation of XP-V gene causes adipose tissue senescence and metabolic abnormalities. *Proc Natl Acad Sci U S A*. Published online 2015. doi:10.1073/pnas.1506954112

142. Bing C. Is interleukin-1β a culprit in macrophage-adipocyte crosstalk in obesity? *Adipocyte*. Published online 2015. doi:10.4161/21623945.2014.979661

143. Wentworth JM, Naselli G, Brown WA, et al. Pro-inflammatory CD11c+CD206+ adipose tissue macrophages are associated with insulin resistance in human obesity. *Diabetes*. Published online 2010. doi:10.2337/db09-0287

144. Hara Y, Wakino S, Tanabe Y, et al. Rho and Rho-kinase activity in adipocytes contributes to a vicious cycle in obesity that may involve mechanical stretch. *Sci Signal*. Published online 2011. doi:10.1126/scisignal.2001227

145. Dankel SN, Røst TH, Kulyté A, et al. The Rho GTPase RND3 regulates adipocyte lipolysis. *Metabolism*. Published online 2019. doi:10.1016/j.metabol.2019.153999

146. Nishi K, Yoshii A, Abell L, et al. Branched-chain keto acids inhibit mitochondrial pyruvate carrier and suppress gluconeogenesis in hepatocytes. *Cell Rep*. Published online 2023. doi:10.1016/j.celrep.2023.112641

147. Wang J, Liu Y, Lian K, et al. BCAA Catabolic Defect Alters Glucose Metabolism in Lean Mice. *Front Physiol*. 2019;10(September):1-14. doi:10.3389/fphys.2019.01140

148. Joffin N, Paschoal VA, Gliniak CM, et al. Mitochondrial metabolism is a key regulator of the fibro-inflammatory and adipogenic stromal subpopulations in white adipose tissue. *Cell Stem Cell*. Published online 2021. doi:10.1016/j.stem.2021.01.002

149. Shao M, Hepler C, Zhang Q, et al. Pathologic HIF1α signaling drives adipose progenitor dysfunction in obesity. *Cell Stem Cell*. Published online 2021. doi:10.1016/j.stem.2020.12.008

150. Iwayama T, Steele C, Yao L, et al. PDGFRα signaling drives adipose tissue fibrosis by targeting progenitor cell plasticity. *Genes Dev*. Published online 2015. doi:10.1101/gad.260554.115

151. Mennerich D, Dimova E, Kietzmann T. Direct phosphorylation events involved in HIF-α regulation: the role of GSK-3β *Hypoxia*. Published online 2014. doi:10.2147/hp.s60703

152. Wang X, Rao H, Liu F, Wei L, Li H, Wu C. Recent advances in adipose tissue dysfunction and its role in the pathogenesis of non-alcoholic fatty liver disease. *Cells*. Published online 2021. doi:10.3390/cells10123300

153. Lischka J, Schanzer A, Hojreh A, et al. A branched-chain amino acid-based metabolic score can predict liver fat in children and adolescents with severe obesity. *Pediatr Obes*. Published online 2021. doi:10.1111/ijpo.12739

154. Lee JH, Park A, Oh KJ, Lee SC, Kim WK, Bae KH. The role of adipose tissue mitochondria: Regulation of mitochondrial function for the treatment of metabolic diseases. *Int J Mol Sci*. Published online 2019. doi:10.3390/ijms20194924

155. Li Z, Xia H, Sharp TE, et al. Mitochondrial H2S Regulates BCAA Catabolism in Heart Failure. *Circ Res*. Published online 2022. doi:10.1161/CIRCRESAHA.121.319817

156. Pedersen HK, Gudmundsdottir V, Nielsen HB, et al. Human gut microbes impact host serum metabolome and insulin sensitivity. *Nature*. Published online 2016. doi:10.1038/nature18646